Online Neutral Line Fault Locator for Point-to-Point HVdc Transmission for Line to Ground Faults

By

Dexter M. T. J. Williams

A Thesis submitted to the faculty of Graduate Studies of

The University of Manitoba

In partial fulfilment of the requirement of the degree of

DOCTOR OF PHILOSOPHY

Department Of Electrical and Computer Engineering

University of Manitoba

Winnipeg

Abstract

High Voltage Direct Current (HVdc) transmission is seeing an increasing use as an efficient method for delivering renewable energy from remote areas to the load center(s). Maintaining the integrity of the HVdc transmission line is paramount to insuring the reliability and the sustainability of the supply. An important component, to this reliability and sustainability, is the rapid detection and repair of faults on the HVdc transmission line.

Modern point-to-point HVdc transmission systems utilize a neutral conductor in addition to the power carrying conductors for HVdc power transmission. The voltage of the neutral conductor is normally zero volts since the neutral conductor is grounded at one end. Online dc Line Fault Locator (dcLFL) systems, such as the dcLFL developed by Manitoba Hydro International (MHI), can reliably and rapidly detect the fault location on the main power carrying conductors of an HVdc transmission line. This is accomplished by detecting the arrival time of the traveling wave from the voltage at the station. However, the low voltage on the neutral conductor prevents the dcLFL from detecting fault locations on the neutral conductor.

The objective of this research is to design and implement a suitable method for reliably and rapidly detecting and locating faults on the neutral conductor. An online Neutral Line Fault Locator (nLFL) system which uses HVdc system measurements with regression analysis to derive the transmission line impedance to determine an accurate fault location is proposed. To surmount the low-voltage problem.

The proposed nLFL system was developed and tested, with a highly detailed Electromagnetic Transients (EMT) simulation model. The nLFL system was constructed in hardware and tested in real time using a real-time EMT simulator. After detailed EMT studies of various scenarios, the nLFL system was field tested on the East Alberta Transmission Line (EATL) HVdc system.

Acknowledgments

The author wishes to acknowledge the thesis Advisor Dr. Ani. Gole for his guidance and mentoring throughout the development of this thesis for the Doctor of Philosophy in Science.

The author would like to acknowledge Manitoba Hydro International for providing support, sponsorship and facilities for the development and testing of the thesis' proposition.

The author would like to acknowledge the support of Siemens AG in the development and testing of this thesis research.

The author would like to acknowledge the support of Atco Electric and its East Alberta Transmission Link team for their support in providing a commercial test environment for the thesis work equipment designed.

The author would like to acknowledge the support and advice of the Professors and the Support Staff of the Power System Group.

Dedication

This thesis is dedicated to my parents, who taught me to strive for excellence, to my godparents, to all my family and to my friends who have continuously supported me in my goals.

Table of Content

List of Figures

List of Tables

List of Acronyms

A	Station A (Heathfield)
ac	Alternating Current
ADC	Analog to Digital Converter
AIM2	Analog Interface Module 2
CSC	Current Source Convert
B	Station B (Newell)
C	Station C
dc	Direct Current
dcLFL	Online Direct Current Line Fault Locator
DMR	Dedicated Metallic Return
DCF	Direct Current Filters
EATL	East Alberta Transmission Link
EMT	Electromagnetic Transient
EMTDC	Electromagnetic Transient Direct Current
Flt	Fault
FPGA	Field Programmable Gate Array
GPS	Global Positioning System
GTAO	Gigabit Transfer Analog Output
GRTS	Ground Return Transfer Switch
HIL	Hardware In Loop
HVac	High Voltage Alternating Current
HVdc	High Voltage Direct Current
IGBT	Insulated Gate Bipolar Transistor
L	Inductor
LCC	Line Commutated Converters

LFL	Line Fault Locator
MRTB	Metallic Return Transfer Breaker
MMC	Modular Multilevel Converter
nLFL	Online Neutral Line Fault Locator
PSCAD	Power System Computer Aided Design
RTDS	Real-Time Digital Simulator
ROW	Right-Of-Way
SCR	Short Circuit Ratio
TDM	Transient Data Measurement
VSC	Voltage Sourced Converter

List of Symbols

$A\_U_{dx}{}^{1}$	Station A voltage for conductor x
A_U_{dH1}	Station A voltage for Pole 1
A_U_{dH2}	Station A voltage for Pole 2
A_U_{dN1}	Station A voltage for Neutral 1
A_U_{dN2}	Station A voltage for Neutral 2
$A\_I_{dx}{}^{1}$	Station A current for conductor x
A_I_{dLH1}	Station A current for Pole 1
A_I_{dLH2}	Station A current for Pole 2
A_I_{dLN1}	Station A current for Neutral 1
A_I_{dLN2}	Station A current for Neutral 2
A_I_{dDMR1}	Station A current for DMR 1
A_I_{dSG}	Station A current for ground electrode
A_I_{dSGHR}	Station A high resolution current for ground electrode
A_S_{BP1}	Station A bypass switch 1
A_S_{BP2}	Station A bypass switch 2
A_S_{H1}	Station A breaker for Pole 1
A_S_{H2}	Station A breaker for Pole 2
A_S_{N1}	Station A breaker for Neutral 1
$B\_U_{dx}{}^{1}$	Station B voltage for conductor x
B_U_{dH1}	Station B voltage for Pole 1
B_U_{dH2}	Station B voltage for Pole 2
B_U_{dN1}	Station B voltage for Neutral 1
B_U_{dN2}	Station B voltage for Neutral 2
$B\_I_{dx}{}^{1}$	Station B current for conductor x
B_I_{dLH1}	Station B current for Pole 1

B_I_{dLH2}	Station B current for Pole 2
B_I_{dLN1}	Station B current for Neutral 1
B_I_{dLN2}	Station B current for Neutral 2
B_I_{dDMR1}	Station B current for DMR 1
B_I_{dSG}	Station B current for ground electrode
B_I_{dSGHR}	Station B high resolution current for ground electrode
B_S_{BP1}	Station B bypass switch 1
B_S_{BP2}	Station B bypass switch 2
B_S_{H1}	Station B breaker for Pole 1
B_S_{H2}	Station B breaker for Pole 2
B_S_{N1}	Station B breaker for Neutral 1
$BP\_A\_S_{H1}$	Station A bypass switch for Pole 1
$BP\_A\_S_{H2}$	Station A bypass switch for Pole 2
$BP\_A\_S_{N1}$	Station A bypass switch for Neutral 1
$BP\_C\_S_{H1}$	Station C bypass switch for Pole 1
$BP\_C\_S_{H2}$	Station C bypass switch for Pole 2
$BP\_C\_S_{N1}$	Station C bypass switch for Neutral 1
C_U_{dx}[1]	Station C voltage for conductor x
C_U_{dH1}	Station C voltage for Pole 1
C_U_{dH2}	Station C voltage for Pole 2
C_U_{dN1}	Station C voltage for Neutral 1
C_U_{dN2}	Station C voltage for Neutral 2
C_I_{dx}[1]	Station C current for conductor x
C_I_{dLH1}	Station C current for Pole 1
C_I_{dLH2}	Station C current for Pole 2
C_I_{dLN1}	Station C current for Neutral 1
C_I_{dLN2}	Station C current for Neutral 2

C_I_{dDMR1}	Station C current for DMR 1
C_I_{dSG}	Station C current for ground electrode
C_I_{dSGHR}	Station C high resolution current for ground electrode
C_S_{BP1}	Station C bypass switch 1
C_S_{BP2}	Station C bypass switch 2
C_S_{H1}	Station C breaker for Pole 1
C_S_{H2}	Station C breaker for Pole 2
C_S_{N1}	Station C breaker for Neutral 1
c	Speed of light
D	Distance from the station to the fault location for the conductor under evaluation
$D_{A\_Flt\_x}$[1]	Distance from Station A to the fault location for conductor x
$D_{B\_Flt\_x}$[1]	Distance from Station B to the fault location for conductor x
I_d	Current for the conductor under evaluation
I_{Flt_x}[1]	Fault Current on conductor x
L	Total length for the conductor under evaluation
L_x[1]	Total length for conductor x
$R_{//}$	Resistance of Pole 2 and DMR 1 in parallel
R_D	Resistance from the station to the fault location for the conductor under evaluation
R_{D-L}	Resistance from the other station to the fault location for the conductor under evaluation
R_L	Total resistance for the conductor under evaluation
R_x[1]	Total resistance for conductor x
R_{GND}	Resistance of the ground electrode
R_{Flt}	Resistance of the fault on the conductor under evaluation
R_{Flt_x}[1]	Resistance of the fault on conductor x

[1] "x" represents a conductor Pole 1, Pole 2, DMR 1, DMR 2, Electrode 1 or Electrode 2

$R_{A\_Flt\_x}{}^{1}$	Resistance from Station A to the fault location for conductor x
$R_{B\_Flt\_x}{}^{1}$	Resistance from Station B to the fault location for conductor x
t	Time
T	Temperature current
t_0	Time of the fault event
T_0	Temperature ambient
t_A	Time of arrival of the first wave fronts at a Station A
t_{A2}	Time of arrival of the second wave fronts at a Station A
t_B	Time of arrival of the first wave fronts at a Station B
Δt	Total time delay of the event
$U_{//}$	Voltage across conductors Pole 2 and DMR 1 in parallel
$U_{Flt\_x}{}^{1}$	Fault voltage on conductor x
v	Propagation velocity for the conductor under evaluation
$V_{Inverter}$	Voltage across the equivalent source for the inverter converter station
$V_{Rectifier}$	Voltage across the equivalent source for the rectifier converter station
$X_{A\_Flt\_x}{}^{1}$	Percentage of total line length from Station A to the fault location for conductor x
$X_{B\_Flt\_x}{}^{1}$	Percentage of total line length from Station B to the fault location for conductor x
α	Temperature coefficient of resistivity
ρ	Conductor resistivity as a function of temperature
ρ_0	Conductor resistivity at ambient temperature T_0

Chapter 1: Introduction

This chapter discusses two important factors. Firstly, it discusses the growing use of High Voltage Direct Current (HVdc) for the transmission of renewable energy and the importance of maintaining the integrity of the network through accurate fault detection and fault location for the restoration of the system. Secondly, this chapter discusses the limitations of current HVdc line fault location techniques and the need for the development of new HVdc line fault location techniques to improve the reliability of the power grid. Thus, the focus of this thesis is the design and development of an online HVdc line fault locator for neutral or return conductors.

1.1 HVac versus HVdc Transmission for Renewable Power Transmission

Clean and sustainable power production is a fast-growing industry. Since this industry has grown rapidly, especially in the last several years, there is a need to combat the ever growing issues of climate change [1], [2], [3]. With the emergence of the climate change phenomena, incidents of wildfires have grown, and these are of particular concern to the power system, since wildfires can cause failure or damage to the power distribution system [4]. For instance, the smoke from a wildfire can lead to faults on the transmission line in the vicinity of the wildfire and also at great distances, since smoke from the fire can travel for great distances [4]. Furthermore, the heat from the wildfires can reduce the effective power carrying capacity of the transmission line and in addition the fire itself can destroy the physical transmission infrastructure itself. For example, investigations of the Chilean power system from January 2017 to June 2020 have shown that smoke has contributed to 16% of failures on the system, and that a combination of heat and smoke has caused 84% of failures on the system [4].

Therefore, the introduction of solutions to mitigate or reduce the impact of climate change will be of great benefit, both socially and economically, since both social and economical developments rely heavily on the health of the power system. The increased incidence of faults due to forest fires, stresses the need to develop improved fault detection and location mechanisms for these faults. One such application is the detection of faults on metallic return conductors in HVdc lines, which is the focus of this thesis.

The introduction of renewable energy into the power generation industry is one solution to the negative impact of the burning of fossil fuels for power generation [1], [5], [6]. Renewable energy generation does not produce the same amount of greenhouse gasses as the conventional burning of fossil fuels. The greenhouse gasses released from the burning of fossil fuels are held to be one of the leading contributors to climate change [5], [7].

There are many renewable energy sources that can be used for power generation. Some examples of renewable energy sources include the sun, the wind, the river flow and the sea tides and currents [5], [6]. However, many of the renewable energy stations are located in remote areas that are very far from the load centers that they serve. Therefore, since most renewable energy stations are often located in remote areas, the efficient transportation of the power from such renewable sources, back to the load centers, is very critical.

HVdc power transmission is a more efficient form of transporting power over long distances than High Voltage Alternating Current (HVac) power transmission [1], [8], [9]. One reason for this is that when the transmission line is transmitting HVdc power in the steady state, the inductive elements have zero impedance, and the capacitive components have zero admittance [10]. Hence the power factor of the line as is the case for ac does not come into the

picture, and so the current is much smaller in a dc transmission line than that in an ac transmission line, and as a result, so is the power loss. Additionally, the depth of penetration of the current in a conductor excited with a dc voltage is much larger than in the same conductor excited with an ac voltage. Consequently, the conductor resistance with dc excitation is much smaller than with ac excitation, which further reduces resistive power loss. HVdc has lower conduction losses than HVac [8]. Other advantages that HVdc systems have over HVac systems include a lower conductor insulation level for the same power rating, and an improved conductor utilization due to the absence of skin effect. In addition, because the converters feeding the line are power-electronic in nature, they are rapidly controllable. The result of the above factors is that HVdc systems have lower power losses and lower transient overvoltages than equivalent HVac systems [8]. Also, since the HVdc towers used to carry these conductors have smaller footprints than the HVac towers of similar voltages and power ratings, the width of the required transmission corridor is significantly reduced as seen in Figure 1-1 [11]. Furthermore, the construction of HVdc transmission systems is more cost effective than that of HVac transmission systems, for overhead transmission lines that are greater than 600.0 km and underground cable systems that are greater than 50.0 km [10], [8], [11]. Thus, in many projects there have been an increased use of HVdc power transmission systems, to tie remote renewable energy stations into the power grid or the load center [12], [13].

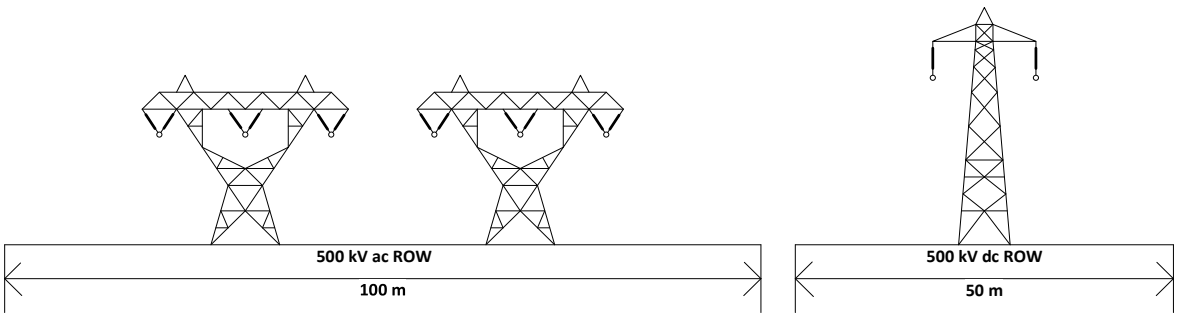

Figure 1-1: HVac vs HVdc Right Of Way (ROW) size comparison [10], [14].

1.2 HVac versus HVdc Fault Detection and Location

Faults on HVac systems are often triggered by natural events such as storms. Storms can cause lightning strikes on the transmission line or push debris against the transmission line, thereby causing the collapse of lines. Similarly, these events may also cause faults on HVdc systems. Fault detection and location is very important. It allows for the rapid dispatch and remediation of damaged power system infrastructure needed to maintain the reliability of the power grid and service to the public.

1.2.1 Ground Current Issues for Ground Faults on Power Transmission Lines

Faults on the transmission system can cause damage to the transmission lines. Line to ground faults are of particular concern, since they can have an impact on systems outside of the power system. Thus, it is important to identify and clear the line to ground fault on both HVac and HVdc systems, since the circulating ground current can cause issues in other areas than the power grid. For example, it is possible for this circulating ground current to cause damage to pipe coating or lead to corrosion of underground pipes [15]. This premature erosion of the pipes could lead to the failure of the pipe, and thereby cause an environmental incident if the pipe is transporting toxic or non-environmentally friendly substances (e.g., Oil, gas). In addition, this circulating ground current could lead to a rise in the voltage potential of the pipe. It would be dangerous to interact with such high voltage pipes. The pipe could become charged and would need to be safely discharged to prevent a dangerous or a hazardous shock potential on the pipe [15]. Furthermore, the greater the current magnitude, the greater is the impact on the piping system.

Additionally, these line to ground faults can produce a potential gradient in the vicinity of the downed conductor. This potential gradient is hazardous since the connection of the

different voltage potentials, (due to contact by animals or humans) could result in a hazardous shock potential. Under such conditions the current would flow through the body of the person or animal. Thus, it is critical to identify and remove these downed conductors before there is a chance to harm any person or animal. Thus, the HVdc system should not be operated with the downed conductor.

Such circulating ground currents could also impact other buried metallic structures, such as railways and telecommunication systems thereby causing corrosion [16]. Another issue is that ac wye grounded transformers can become saturated by these dc circulating currents. This saturation of the transformer can result in the creation of harmonics in the ac system and cause the vibration and the overheating of equipment or lead to the mal operation of protection systems [16]. Furthermore, these circulating ground currents, over a prolonged period of time can cause the heating of ground water in the area [16].

Both HVac and HVdc systems tend not to use the earth as a ground return path in the presence of key metallic infrastructure or underground resources, except for in emergency situations. Thus, HVac is usually transmitted using balanced power transmission and HVdc uses a balanced Bipolar transmission scheme or a Monopolar scheme with a neutral return or a Dedicated Metallic Return (DMR) path. However, it is important to note that a Monopolar HVdc scheme can operate with the earth as the return path even in the presence of a permanent fault on the return conductor path. In the presence of a permanent fault, in the return conductor path, the Monopolar HVdc scheme could continue to operate without any major performance issues. However, this would expose the underground metallic systems or resources to the risks previously discussed.

1.2.2 HVac Fault Mitigation Techniques Adapted for HVdc Fault Mitigation

For equivalent HVac and HVdc systems, HVac fault current magnitudes are usually smaller than HVdc fault current magnitudes, since HVac fault current magnitudes are limited by the ac transmission line impedance between the fault and the ac source. HVdc fault current magnitudes can be much larger than HVac fault current magnitudes. This is due to the much smaller dc transmission line impedance (resistance) between the fault and the dc converter. Hence, it is important to detect the fault and clear it before the current rises and causes damage to any system(s). Thus, the act of taking the transmission line out of service until the fault can be repaired is a very prudent action. It prevents further damage to the power system infrastructure.

A faulted HVac transmission line can be removed from service by opening the HVac breaker [10]. The zero crossing of the ac current aids in the opening of the HVac breaker. This provides a point of interruption in the power flow [11]. The opening of the breaker can be completed within several ac cycles of the system. However, the opening of the breakers on an HVdc system is more problematic since there is no zero crossing in the power flow of an HVdc system to open the breaker [10]. Thus, the current will continue to flow as there is no interruption in the current flow.

However, there are special HVdc breakers that can induce a zero crossing, and thereby allowing for the disruption in the current flow, required to facilitate the correct opening of the dc breaker [10], [17]. The opening of the breaker is usually the primary action required for clearing the fault on the neutral conductors of the HVdc system. This action is possible since there is a lower voltage on the neutral conductors and there is an alternative current path for the system. Like HVac breakers, modern HVdc breakers also take several milliseconds (8 ms

to 10 ms for mechanical breakers rated at 70 kV to 80 kV [18] and a minimum of 30 ms for 250 kV at 8 kA or 500 kV at 4 kA [1]) to open.

The primary isolation technique for the main conductors and the secondary technique for the neutral conductors is to isolate the faults on an HVdc system. This is achieved by taking some control action in the HVdc converter to isolate the conductors. For example, Line Commutated Converter (LCC) HVdc converters can use the force retard function of the converter, where the voltage is temporarily reversed, to reduce fault current to zero within a very short window of time to interrupt the fault [8]. However, this fast response time of the converter may leave insufficient data to accurately calculate the fault location on the transmission line. The occurrence of this problem would depend on the fault location technique used.

1.2.3 Line Fault Location Techniques Based on Impedance Measurements and Traveling Wave Detection

Most online HVac fault location systems are based on either impedance calculations or traveling wave detection techniques. Both techniques use the measurements collected from the HVac system's protection systems to determine the transmission line fault location. Fault location systems, for online HVac systems based on fault impedance calculations, are in greater prevalence among HVac fault location systems [19], [20]. Meanwhile, most online HVdc systems are primarily based on traveling wave detection techniques. This is due to the fact that this technique has increased accuracy and speed in determining the fault location. On the other hand, the HVac systems use fault location systems based on impedance calculations since the fault current rise is smaller for a HVac system. These impedance calculations are primarily

conducted in the phasor domain which uses the sequence components of the system to calculate the fault location [19], [20].

HVac fault location can be done either single ended or double ended. The single ended scheme is simpler since it only requires local information to calculate the fault. However, single ended fault detection accuracy can be impacted by loading, fault resistance and zero-sequence mutual coupling. In dual ended fault location, information from both sending and receiving ends is used to locate the fault. It has the advantage of eliminating the need for estimating the fault resistance and the zero-sequence contribution in the analysis [19], [21]. However, Dual ended fault location process has the drawback of requiring communication between relays to perform its analysis. In both cases correct extraction of the phase components can influence the accuracy of the fault location system. Further, if the system has not settled sufficiently the calculated phasors will be incorrect and thereby further impede the accuracy of the system.

Traveling wave HVac fault location eliminates the need for phasors and sequence components [19], [21]. It relies purely on the detection and the accurate time stamping of the transient fault event. Traveling wave HVac fault detection can be done either single ended or double ended. A drawback of single ended traveling wave HVac fault location is the need, to correctly discriminate between the primary traveling wave and the reflected waves, for the correct calculation of the fault location. One drawback of double ended traveling wave HVac fault location is the level of communication required to collect the information, from both sides, to calculate the fault location [19], [21]. The main problem with HVac traveling wave fault location is that if the fault occurs during the zero crossing of the waveform at the fault location, it is not detectable.

HVdc fault location systems use both techniques mentioned above. These will be discussed in more detail in Chapter 2: HVdc Line Fault Location.

1.3 Motivation for this Research

While HVdc power transmission systems do efficiently transport renewable energy from remote areas to the load centers, however maintaining the integrity of the transmission lines is very critical to the operation of the power system. Permanent or sustained faults on the line can lead to loss of service and financial losses for the transmission companies [8], [20]. More importantly, the loss of service can lead to public health hazards and the loss of key services such as heating, cooling, cooking, desalinization, and other services. Therefore, it is very important to have an effective system for identifying fault locations and for facilitating rapid or expedited repairs of the transmission network and the return of the services [20], [8].

1.3.1 Unique Challenges for HVdc Fault Location

The HVdc fault location system does present its own unique challenges for the identification of fault locations. Since the HVdc power electronic converters' very fast response time tend to quickly mitigate faults, (e.g., In the range of milliseconds), therefore there is insufficient time to locate the fault [8]. Further, many of the traditional techniques used for fault location are ineffective as they require the system to have reached the faulted steady-state mode of operation before measurements can be taken and used for the calculation of the fault location.

1.3.2 Fault Location on the Dedicated Metallic Return (DMR) Conductor

Traveling wave fault location technique or solution is one of the more popular solutions to fault location on the high voltage conductors of the HVdc transmission line. However,

although traveling wave fault location works very well for high voltage pole conductors, it fails to be very effective for Dedicated Metallic Return (DMR) conductors (also referred to as the "Neutral") or for pole conductors acting as a return path where one end of these conductors is grounded. In this case the traveling wave is absorbed by the ground and becomes unmeasurable for fault location. Therefore, it has become increasingly more crucial, to develop new HVdc fault location techniques to identify fault locations on all conductors. This is necessary since existing techniques cannot detect fault locations on all HVdc transmission line conductors.

The growing use of renewable energy to combat the worsening effects of climate change has created a new urgency in the need to maintain the integrity of the HVdc transmission network. This is required to provide critical services paramount to public safety and the future of the power grid.

1.3.2.1 Online Neutral Line Fault Locator (nLFL)

As was mentioned in above, the neutral conductor is increasingly being used in HVdc systems. However, maintaining the integrity of HVdc systems which use the neutral conductors also presents its own unique challenges. Firstly, the fact that one end of the neutral conductor is grounded, and the potential of the line is very close to zero volts, will prevent the use of traveling wave fault location systems; Secondly, the fact that the fast response time of the HVdc system would prevent the HVdc system from reaching the faulted steady-state mode of operation needed for systems based on impedance (resistance) calculations to operate with sufficient accuracy. Furthermore, even though it is possible to operate an HVdc system with a faulted neutral conductor or without a neutral conductor, the potential environmental impact due to the damage that can be caused on other systems such as underground piping infrastructures would make these options untenable.

This thesis looks at the design and the development of an online Neutral Line Fault Locator (nLFL) system that can be integrated into both new and existing HVdc systems. The nLFL system designed in this thesis operates on a passive fault location system that utilizes the pre-existing voltage and current measurements of the HVdc transmission system to detect and locate faults on the HVdc transmission line. Furthermore, the nLFL system designed in this thesis utilizes Global Positioning System (GPS) timestamping of the voltage and the current measurements, from both stations to calculate the location of faults on the HVdc transmission line.

During a fault, the nLFL captures the HVdc conductor measurements of the voltages and currents, at the time of the fault, as well as the measurements before and after the fault for analysis of the fault location. The nLFL uses regression of the measured values to extrapolate the future faulted steady-state values of the HVdc system, as if the control action of the HVdc system never took place, to mitigate the fault. The nLFL uses the extrapolated future values and the faulted steady-state measurements, to calculate a ratio of the line resistance as a ratio that is proportional to the ratio of the faulted line length to the total transmission line length. This ratio can be multiplied by the line length to find the actual distance along the line to the fault location.

The nLFL was developed and was tested in the EMT simulator PSCAD™/EMTDC™ to verify the functionality of the nLFL in an HVdc scheme. A hardware platform of the nLFL system was developed for hardware in the loop testing with the real-time EMT simulator Real-Time Digital Simulator (RTDS™) system. The real-time EMT simulator modeled the HVdc system and the nLFL platform was integrated into the simulator and was able to detect and identify the fault location. The system was installed for the field testing and for

commercialization in the ATCO Electric's East Alberta Transmission Link (EATL) in Alberta Canada.

1.4 Objective and Layout of the Thesis

Objective:

The objective of this thesis is the design and development of an online line to ground fault locator system for Dedicated Metallic Return (DMR) or pole conductors acting as return conductors.

This thesis will address the return conductor fault location issue regarding, the low voltage on the return conductor which makes it a challenge to locate faults on the return conductor. Furthermore, this thesis will address the issue of the limited time for data collection before the protection system opens the return conductor. This limits the collection of the amount of data needed for an accurate fault location.

The principal objective of this thesis is the designing of a fault location hardware and an algorithm to overcome the aforementioned limitations.

Layout of the thesis:

This thesis investigated techniques for HVdc line fault location on neutral or return conductors. The remainder of this thesis is set out as follows below:

- A review of HVdc system configurations and their protection systems;
- An investigation of line fault location techniques for HVdc neutral and return conductors;
- The principles of the proposed nLFL system developed in thesis;
- The design and construction of the physical nLFL system;

- Simulation and analysis of the nLFL system's capacity;
- Hardware in the loop testing and analysis of the nLFL system's capacity;
- Field integration, deployment, testing and analysis of the nLFL system's capacity.

Chapter 2: HVdc Line Fault Location

This chapter provides a general overview of HVdc systems, configurations, topologies and the existing fault detection schemes utilized in present day HVdc systems.

2.1 HVdc Transmission Systems

Conventional HVdc transmission systems consist of two main parts. These are the converter stations and the transmission network. The transmission network usually consists of a transmission line that ties the converter stations together. The converter stations are the interface between the ac side network and the dc side network. A converter station can either operate as a “rectifier” which takes power from the sending end ac network and feeds it into the dc transmission line, or as an “inverter” which transfers power from the dc transmission line into the receiving end ac network. The converter stations contain all the control, the protection and the measurement systems needed for the HVdc system to operate.

The two main types of HVdc converters are Line Commutated Converter (LCC), (also referred to as a Current Source Converter (CSC)) and Voltage Sourced Converter (VSC)

2.1.1 Line Commutated Converters (LCC) HVdc Converters

Modern LCC HVdc converters utilize thyristor base power electronics in the construction of the converters. These converters generally utilize a 12-pulse converter configuration to reduce harmonics generated by the converters. LCC HVdc converters require an ac voltage source to operate. LCC HVdc converters are generally used for bulk power transfer applications. This is due to the higher current carrying capacity of the power electronic devices.

The thyristors used in the LCC can only be turned on with a firing pulse when the thyristor has been forward biased, but the thyristor will turn off when the thyristor becomes reverse biased by the ac network [22]. LCC requires a strong ac voltage, i.e., the short circuit level of the ac side must be high for proper operation of the LCC.

2.1.2 Voltage Source Converters (VSC) HVdc Converters

VSC HVdc converters generally use the Insulated Gate Bipolar Transistor (IGBT) as the switching element in the converters [22]. VSC converters typically use one of these three topologies: two level converter, three level converter and Modular Multilevel Converter (MMC). Each arm of a VSC HVdc converter consist of one or several half-bridge or full bridge blocks [23]. The MMC converter [24] [25] [26] has become the topology of choice in VSCs as it inherently produces a near-sinusoidal output waveform and eliminates the need for filtering. It is also "modular" in that the basic switching module can be used to build a VSC of any voltage rating merely by stacking the necessary number of modules into the converter arm. Henceforth in this thesis, it will be implicit that when we refer to a "VSC" it will be of the MMC type, although there is nothing specific in the research to the MMC, and the results are equally valid for any other VSC topology. The structure of the converter depends on the rating of the converter. VSC HVdc converters do not require an ac voltage for operation because the power electronic devices can be independently turned on and off, by controlling the gate signal to the device [22]. This allows VSC to be more robust in the face of weak ac networks. The VSC HVdc topology is a much younger technology in comparison to the LCC HVdc topology [23]. However, their use has grown in popularity owing to the interconnection of renewable energy generation and the load center. This is specifically the case in new offshore wind development [27].

2.1.3 HVdc Applications

Generally, HVdc transmission is most often used for bulk power transmission especially, where there are great distances between the power generating station and the load center. In addition, HVdc transmission can also be used to couple two systems together. For instance, if two ac systems were operating at different frequencies, an HVdc system placed between the two grids would allow for power transfer between the two systems even though they were operating at different frequencies. Also, an HVdc system can be used to help control the stability of the power flow in the ac system.

2.2 HVdc Configurations

HVdc systems can take on several configurations. The main HVdc configurations include [8], [28]:

1. Back-to-Back HVdc scheme
2. Monopolar HVdc scheme
3. Homopolar HVdc scheme
4. Bipolar HVdc scheme
5. Bipolar Multiterminal HVdc scheme

2.2.1 Back-to-Back HVdc Scheme

In the Back-to-Back HVdc scheme both the rectifier and the inverter are in the same station as seen in Figure 2-1. Back-to-Back HVdc scheme arrangements are typically used for connecting two large asynchronous ac networks (such as the North American East and West Interconnections) together, in which an ac connection would not be possible. The Back-to-Back HVdc scheme is also needed for connecting ac networks of different frequencies, such

as the Sakuma Back-to-Back HVdc scheme which connects the 50 Hz and 60 Hz sides of the Japanese network [29]. In such an instance, the transmission network between the two converters would usually consist of a short bus work to join the two converters together [8] [28]. With an LCC topology, the current (indicated by red arrows) would be monodirectional, and the voltages would change polarity depending on whether the converters were operating in rectifier or inverter mode.

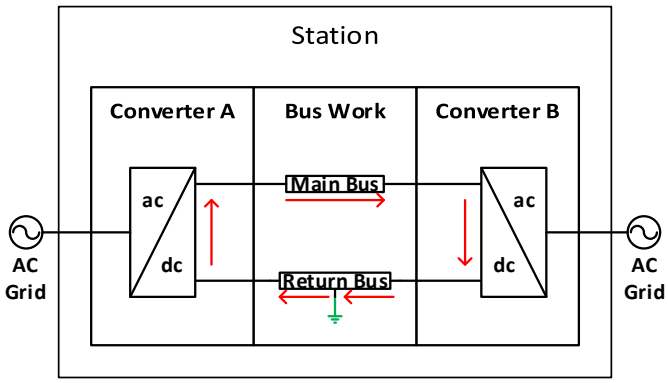

Figure 2-1: A Back-to-Back HVdc scheme with the current path indicated with red arrows.

2.2.2 Monopolar HVdc Scheme

In a Monopolar HVdc scheme, power is transferred either by a positive or negative pole and the return path can be either through the ground/earth return as seen in Figure 2-2 or a Dedicated Metallic Return (DMR) conductor as seen in Figure 2-3 [8], [28]. As before, the current direction is unidirectional for LCC converter topology, but bidirectional for VSC.

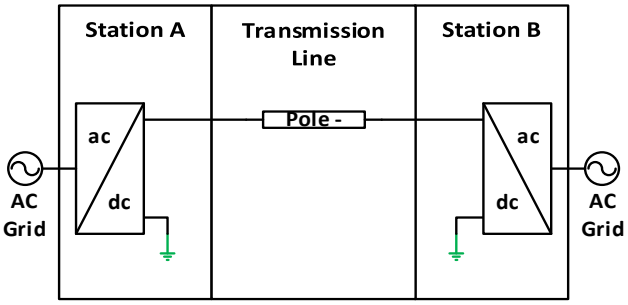

Figure 2-2: A Monopolar HVdc scheme with the stations grounded.

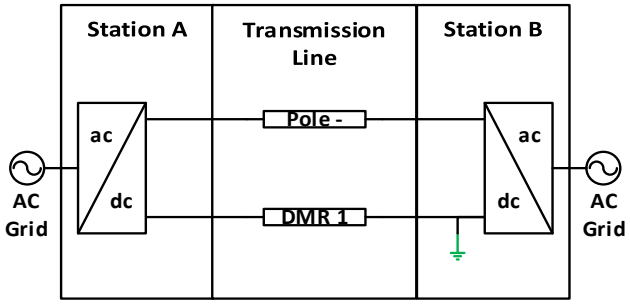

Figure 2-3: A Monopolar HVdc scheme with a DMR and a station ground.

2.2.3 Homopolar HVdc Scheme

A Homopolar HVdc scheme consists of two or more poles of the same polarity. Most often Homopolar HVdc schemes utilize negative poles. In such instances the return path can either be through the ground/earth return as seen in Figure 2-4 or the DMR conductor as seen in Figure 2-5 [8].

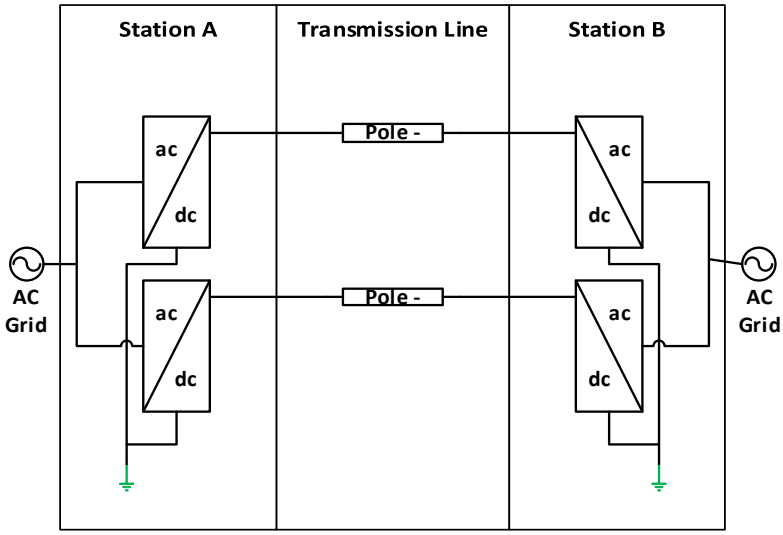

Figure 2-4: A Homopolar HVdc scheme with the stations grounded.

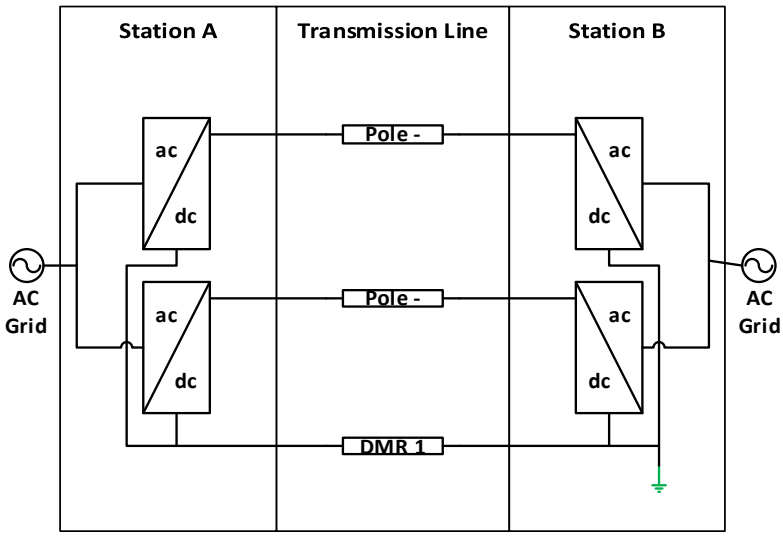

Figure 2-5: A Homopolar HVdc scheme with a DMR and a station ground.

2.2.4 Bipolar HVdc Scheme

In the Bipolar HVdc scheme, the system utilizes both a positive polarity and a negative polarity pole. Normally, the pole currents are made to be equal to minimize the current through the neutral dc or ground path as seen in Figure 2-6. However, this is not perfect, since a small, mismatch current still flows into the station or the electrode ground. Therefore, the modern trend is to have a Dedicated Metallic Return (DMR) conductor to prevent the circulating earth current from causing problems such as corrosion of underground metallic structures, ac transformers and underground water, as described in section 1.2.1. A Bipolar HVdc scheme with a DMR can be seen in Figure 2-7 [8], [28]. It should also be noted that when a DMR is used in an HVdc scheme, only one station is grounded, whereas in a non DMR HVdc scheme all stations are grounded. Grounding at one end provides an anchor to ground potential, and yet only prevents any circulating ground current as the circuit cannot be completed.

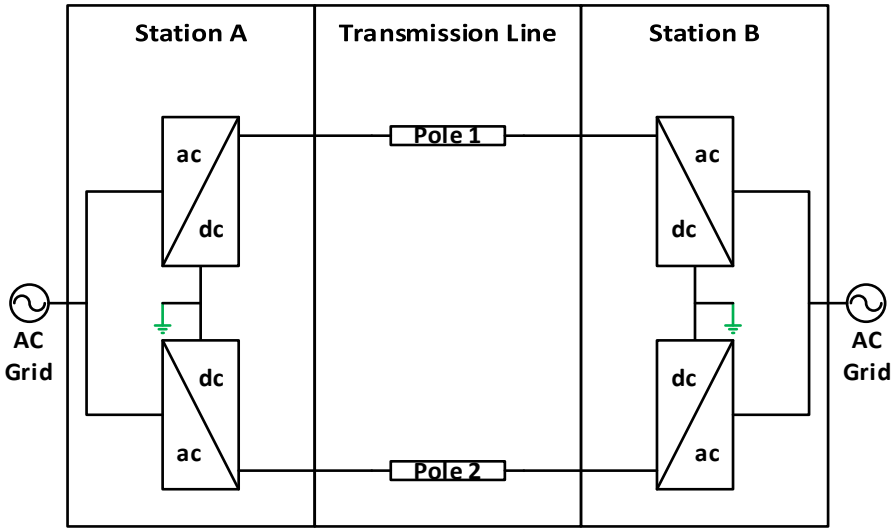

Figure 2-6: A Bipolar HVdc scheme with the stations grounded.

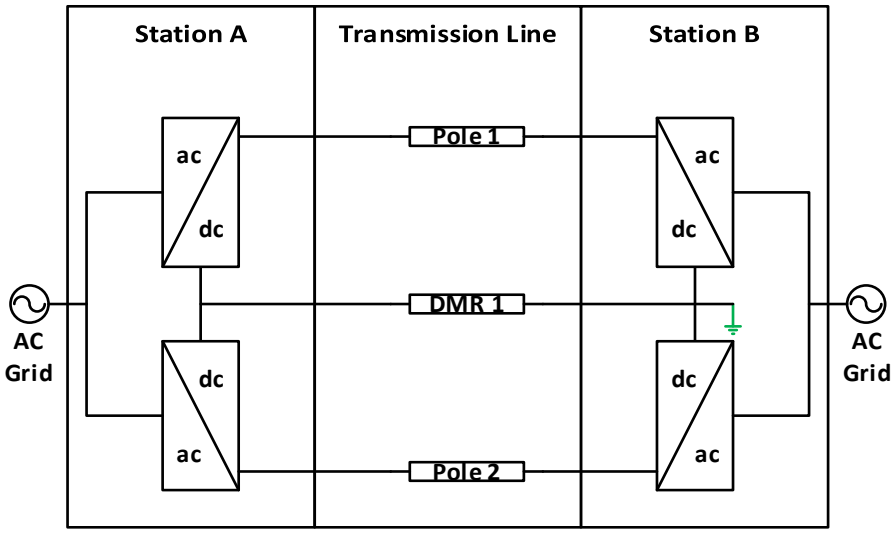

Figure 2-7: A Bipolar HVdc scheme with a DMR and a station ground.

2.2.5 Bipolar Multiterminal HVdc Scheme

The Bipolar Multiterminal HVdc scheme consists of several converters sharing the same dc transmission network. The converters in this system can act both as inverters and rectifiers depending on the requirements of the network [8]. There are two main configurations that can be used to derive larger Bipolar Multiterminal HVdc schemes. These are the series Bipolar Multiterminal scheme and parallel Bipolar Multiterminal scheme [30]. The parallel

Bipolar Multiterminal scheme can utilize a DMR in a parallel connected Bipolar Multiterminal HVdc scheme.

A parallel connected Bipolar Multiterminal HVdc scheme with the stations grounded can be seen in Figure 2-8. Similar to the Bipolar HVdc scheme, a parallel connected Bipolar Multiterminal HVdc scheme can have a small amount of current absorbed by the station ground or electrode ground. Therefore, in some parallel connected Bipolar Multiterminal HVdc schemes, a dedicated metallic return is used to prevent the circulating earth current from causing issues with other systems. A parallel connected Bipolar Multiterminal HVdc scheme with a DMR can be seen in Figure 2-9.

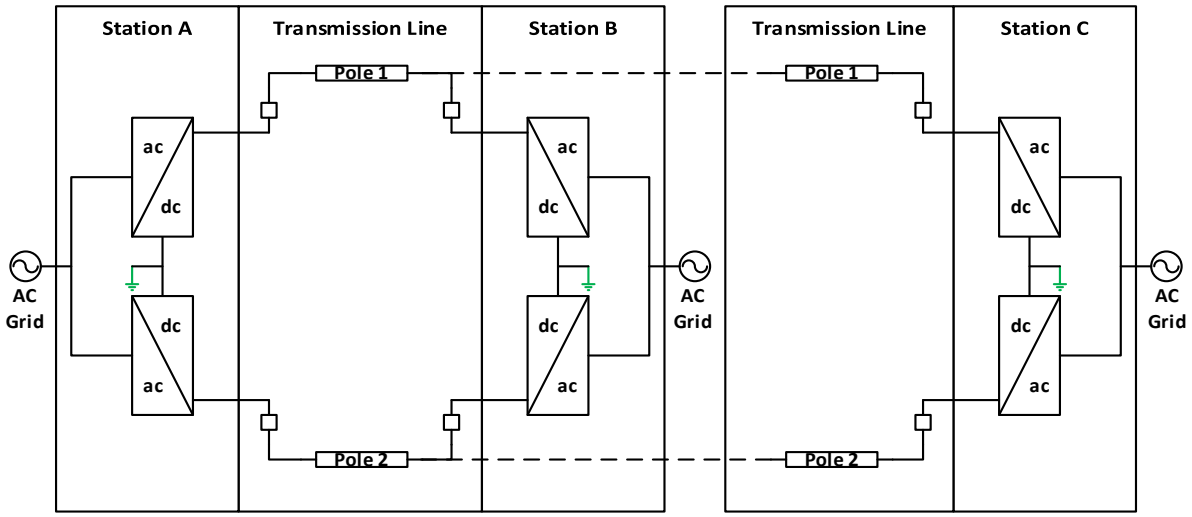

Figure 2-8: A parallel connected Bipolar Multiterminal HVdc scheme with the stations grounded.

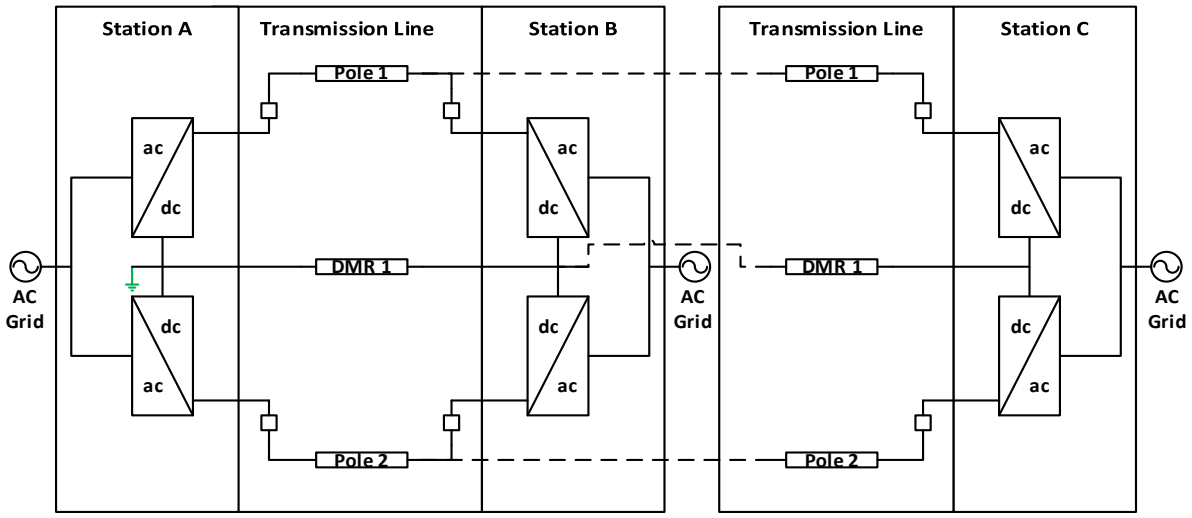

Figure 2-9: A parallel connected Bipolar Multiterminal HVdc scheme with a DMR and a station ground.

Similar to a Bipolar HVdc scheme, a parallel connected Bipolar Multiterminal HVdc scheme can also be operated in the metallic return mode. In the metallic return mode, one of the two poles is operated as normal to transfer power, while the return path would become the ground or the second pole or the DMR. Furthermore, a parallel connected Bipolar Multiterminal HVdc scheme operating in a metallic return mode with a DMR conductor, may operate with the return path being the second pole conductor or the DMR conductor or a parallel combination of the second pole and the DMR conductors.

2.3 HVdc Faults

HVdc line faults can be caused by several types of events. (e.g., A lightning strike on the transmission line or pollution) The fault could damage the transmission line conductor or insulators. This would require repairs to the line to prevent further events. Another possible event is a flashover between the conductors or the tower. A flashover could cause a fault on the HVdc system. The flashover event must be located for repair, or the insulator must be examined for cleaning, since a dirty insulator could have been the cause of the flashover event.

Furthermore, natural events such as windstorms, tornadoes, hurricanes, forest fires or collapsing trees could lead to a transmission line break or a tower collapse. Any of the above events could result in a fault on the HVdc system. Therefore, it is crucial to know the location of the event, in order to expediently facilitate the dispatch of line maintenance crews to repair the transmission line.

2.4 HVdc Line Fault Detection

Fault detection is critical to maintaining the integrity of the HVdc system. Failure to detect and mitigate faults could lead to significant damage to the HVdc converters and thereby prolong the outages. The net result is a prolonged loss of service to the customer and financial losses or penalties for the service provider. Thus, most HVdc system employ at least two levels of protection. These are primary and secondary protection [8], [31], [32]. Some protective actions can be taken within three milliseconds of the detection [8].

2.4.1 HVdc Primary Protection

Primary protection system schemes usually employ a technique that uses measurements from one end of the line to detect the fault. This is the single ended detection system. This provides for fast detection and mitigation of faults [32], [33]. Furthermore, the single ended detection system does not require any telecommunication links with other station(s). Thus, even if the telecommunication link is down, it is still possible to detect faults.

Common detection schemes for HVdc protection include overvoltage, under voltage, overcurrent, and undercurrent protection. These systems can have single level or dual level detection. The HVdc system's single level protection scheme responds to the event to clear the fault after a short, designated period of time. The delay is to allow the system to confirm the

event and to prevent false tripping of the system. The dual level protection scheme is like the single level protection scheme, except that the former has a first and second level of protection and in addition its first level protection scheme has a longer delay time than the second level [8]. Therefore, if the detection process reaches the second level of the protection scheme, it is assumed that it has already surpassed the first level and protective action would occur sooner than if only the first level of protection had occurred. The over and under level protection schemes, can determine whether the voltage or the current deviate from the set voltage or current by a specified margin in the system. If a deviation is detected, the protective actions of the system would take steps to protect the system.

Evolving fault detection technology include derivative based [10], [33] and wavelet fault detection [34]. Both methods involve the detection of the traveling waves caused by the fault on the transmission line. The derivative approach calculates the rate of change (i.e., the mathematical "derivative") of voltage or current waveforms to determine the arrival of the wave front [10], [33], [21]. The wavelet approach uses mathematical manipulation of the voltage or current measurements to extract the traveling waveform from the measurement. However, derivative based detection can also magnify noise in the measurement, and this could lead to false positives in the detection. Wavelet fault detection requires many samples for the analysis and for the detection of a fault. These factors could lead to delays in fault detection which intern could lead to damage of the converter if the delay is significant [10], [33], [21].

2.4.2 HVdc Secondary Protection

Secondary protection system schemes, usually employ dual ended detection, for detection and mitigation of faults. The most commonly employed secondary fault detection technique is the differential current fault detection [8], [35]. Differential current fault detection

is generally used as a secondary fault detection technique. Differential current fault detection works by comparing the difference in the current measurements from each station on each conductor. If the difference in the current measurements from the two ends is greater than the specified limit, then the protection systems would operate to mitigate the fault. However, since telecommunication is required for the successful detection of a fault, if the telecommunication link is lost then the system will fail in the detection of a fault.

2.5 HVdc Line Fault Location

Fault detection as presented in the previous section, is the process of determining that a fault has occurred somewhere on the transmission line. While fault location is the process of determining the location along the transmission line where the fault has occurred. There are two main types of line fault location technologies. These are based on traveling wave detection and impedance measurements [36], [21]. Line fault location technology based on traveling wave detection, utilizes the differences in arrival times of traveling waves at the station in the voltage or current to identify the line fault location [36], [21], [37]. Line fault location technology, based on impedance measurements, look at the change in impedance between the faulted and non-faulted transmission line [36], [21]. Line fault location systems based on traveling wave are predominantly used in HVdc fault location systems. Fault location systems based on traveling wave systems have a higher accuracy than fault location systems based on impedance measurements [37]. A major reason for the lower sensitivity of a fault location method based on impedance is the relatively small impedance (which is a resistance) of the dc transmission line compared to the much larger impedance (chiefly the reactance) of an ac transmission line of comparable length.

Other fault location technologies that utilize artificial neural networks or fuzzy logic controllers are primarily based on the previously mentioned two technologies, but they are presently utilizing pattern recognition of measurements to improve the accuracy of their systems [36], [13].

Other developing fault location technologies use characteristic-harmonic measurements or oscillatory frequency. The characteristic-harmonic measurement fault location method uses the 12^{th} harmonic voltage and current since it is the larger of the harmonic components. The characteristic-harmonic measurement fault location method takes advantage of the measurements, in either the parallel conductors in the DMR or the electrode line, to derive equations that eliminate the ground resistance from the calculation of the fault location [38]. The oscillatory frequency fault location method uses the station's voltage and the frequency dependent model of the transmission line to extract the oscillation frequency of the station's voltage after a fault. Since, the oscillation frequency extracted in this method, is proportional to the fault distance, this method can be used to determine the fault location [39]. However, in both cases the system must be in the faulted steady state condition for proper fault location, depending on the length of the transmission line and the protections system of the HVdc system the attainment of the faulted steady state condition needed for the analysis may not be possible.

2.5.1 Line Fault Location System Characteristics

The two main types of line fault location technologies, previously mentioned have four main characteristics. These characteristics are either online, offline, active and/or passive.

- An online line fault location system is characterised as a line fault location system that determines the line fault location immediately when the fault occurs [40], [41], [42].
- An offline line fault location system is characterised as a line fault location system that determines the fault location when the power system is powered down, following a fault on the transmission line. An external voltage source of sufficient energy must be available to perform this test [40], [41], [42].
- An active line fault location system typically injects a known voltage or current signal into the transmission system to determine the fault location. For example, the fault location system could inject an ac voltage into the transmission line and determine the fault impedance by observing the resulting voltage and current [43], [38].
- A passive line fault location system is characterised as a fault location system that does not inject energy into the transmission system to determine the fault location, but instead uses the existing energy in the power system to determine the line fault location [44], [38].

The characterization and classification of line fault location technologies are shown in Table 2-1.

Table 2-1: Line fault location characterisation.

Offline		Online	
Passive	**Active**	**Passive**	**Active**
	Travelling Wave: Single Ended		
		Travelling Wave: Double Ended	
	Impedance: Single Ended		
		Impedance: Double Ended	

2.5.2 Line Fault Location Based on Traveling Wave Detection

Fault location based on traveling wave detection, can either be done using a single ended method or a dual ended method. The single ended traveling wave fault location method can be characterised as being an online passive system or an online active system or an offline active system. While the double ended traveling wave fault location method is characterised as being an online passive system. The traveling wave characteristics can be visualized in Figure 2-10 [40].

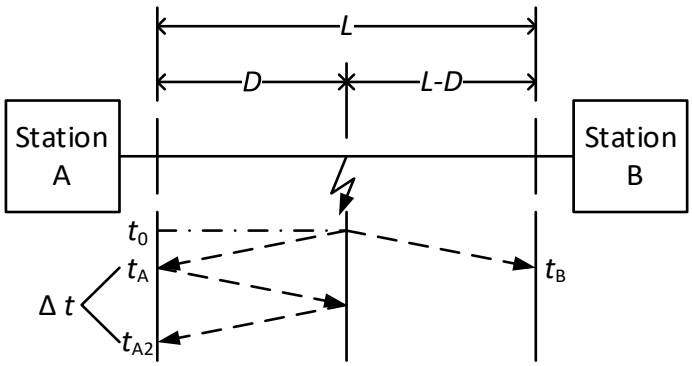

Figure 2-10: Physical representation of the traveling waves in an HVdc system.

2.5.2.1 Single Ended Line Fault Location Based on Traveling Wave Detection

In the single ended line fault location method, based on traveling wave detection, each station detects the arrival of the initial wave front as well as the secondary wave front that is reflected from the station to the fault and then, from the fault back to the station. The fault

location can be determined by using Equation (2.1) [34]. The Inability to properly discriminate between the wave fronts is the major drawback of this system. The wave front of the traveling wave is not always a crisp signal. It has a rise time due to the different component frequencies on the transmission line. This makes determination of the arrival time of the wave front difficult, particularly in the presence of noise. This situation reduces the accuracy of the detection and further increases the total time delay, which in turn introduces errors into the fault location calculated. For overhead lines, the propagation velocity is typically close to the speed of light (see Equation (2.2)). The propagation velocity can be estimated either experimentally when the line is constructed, or analytically if the frequency dependent parameters of the transmission line are known [45], [32].

$$D = \frac{\Delta t}{2} v \qquad (2.1)$$

$$v \cong c \qquad (2.2)$$

where:

D = Distance from the station to the fault location for the conductor under evaluation

Δt = Time delay between the arrival times of two consecutive wave fronts at a station

v = Propagation velocity for the conductor under evaluation

c = Speed of light

2.5.2.1.1 Online Passive Single Ended Line Fault Location Based on Traveling Wave Detection

In an online passive single ended traveling wave line fault location system, the line fault location system uses the existing measurements of the HVdc system to calculate the line fault location. In some cases, a surge capacitor is installed at the HVdc station at the point at which the transmission line exits the HVdc station. The surge capacitor is used to detect the

arrival of the wave front at the HVdc station. Under normal operating conditions the surge capacitor is charge to the operating voltage of the HVdc system. However, during a line fault the surge capacitor is discharged. This discharge is due to the arrival of the wave front, caused by the line fault's traveling wave, reaching the HVdc station. Subsequent reflections can also be observed as partial discharges of the surge capacitor.

The online passive single ended traveling wave line fault location system, is typically used on the pole conductors since these conductors are normally energised. However, the online passive single ended traveling wave line fault location system is not typically used on DMR conductors or pole conductors which are acting as a return conductors or electrode conductors, since these conductors are typically at a low or zero voltage and are grounded on one end.

2.5.2.1.2 Online Active Single Ended Line Fault Location Based on Traveling Wave Detection

An online active single ended traveling wave line fault location system, requires the injection of energy into the HVdc system to calculate the line fault location. One type of online active single ended traveling wave line fault location system, is the pulse echo fault location system that uses time domain reflectometry. In the pulse echo line fault location system, a pulse is injected into the line and the reflection of the waveform from the remote station or from the fault location, is detected at the transmission station at the sending end [46]. The waveform propagates along the transmission line at the propagation velocity of the transmission line (This is approximately close to the speed of light). The fault location can be calculated using Equation (2.1) [47]. However, since in very long transmission lines the injected pulse will be dampened by the filtering effects of the line, a fault location may not be identifiable, especially since the pulse must travel there and back for detection.

The online active single ended traveling wave line fault location system is recommended for pole conductors, which are acting as a return conductors or electrode conductors, since these conductors are typically at a low or zero voltage and are grounded on one end. This allows the generated pulse to be easily distinguished from the other signals or noise in the system. The online active single ended traveling wave line fault location system, is not typically used on the pole conductor since these conductors are normally at higher voltage which in turn makes the equipment needed for generating the pulse much more expensive. Furthermore, it becomes increasingly more difficult to distinguish the pulse from other signals and noise in the system.

2.5.2.1.3 Offline Active Single Ended Line Fault Location Based on Traveling Wave Detection

In an offline active single ended traveling wave line fault location system, the line fault location system uses a voltage source with sufficient energy, to inject a waveform into the offline HVdc transmission line to calculate the line fault location. In an offline active single ended traveling wave line fault location system, an independent line fault location system is connected to the transmission line under test. This independent system is then responsible for injecting the pulse and detecting the fault location from the reflected wave form.

The offline active single ended traveling wave line fault location system can be used on the pole conductors, the DMR conductors and the electrode conductors since all these conductors are de-energised when the HVdc system is out of service.

2.5.2.2 Double Ended Line Fault Location Based on Traveling Wave Detection

The dual ended line fault location method is based on the traveling wave detection method. The detection of the initial wave front's arrival time at each station is the key to

determining the line fault location. After the arrival time is determined the line fault location can be determined by using Equation (2.3) [34]. Although this method is still susceptible to wave front distortion, the method is more robust since the readings are taken at both sides and it is only needed to determine and distinguish the first wave front's arrival at the station. This method is very effective in determining the fault location. Thus, this method has been implemented in commercially available products [45], [32].

$$D = \frac{L}{2} + \frac{(t_A - t_B)v}{2} \qquad (2.3)$$

where:

L = Total length for the conductor under evaluation

D = Distance from the station to the fault location for the conductor under evaluation

v = Propagation velocity for the conductor under evaluation

t_A = The time of arrival of the first wave front at a Station A

t_B = The time of arrival of the first wave front at a Station B

2.5.2.2.1 Online Passive Double Ended Line Fault Location Based on Traveling Wave Detection

In the online passive double ended traveling wave line fault location system, the line fault location system uses the existing measurements of the HVdc system to calculate the line fault location. In the double ended method, there are some cases in which a surge capacitor is installed at the HVdc station, just as the transmission line exits the HVdc station, where it is used to detect the arrival of the wave front at the HVdc station. Under normal operating conditions the surge capacitor is charge to the operating voltage of the HVdc system. However, during a line fault the surge capacitor is discharged. This is due to the arrival of the wave front caused by the line fault reaching the HVdc station.

The online passive double ended traveling wave line fault location system is typically used on the pole conductors. These conductors are normally energised. However, the online passive double ended traveling wave line fault location system is not typically used on DMR conductors or pole conductors, which are acting as return conductors or electrode conductors since these conductors are typically at a low or zero voltage and are grounded on one end. Furthermore, the fact that one end of the return conductor is grounded is sufficient to prevent the successful detection of the traveling wave.

2.5.3 Line Fault Location Based on Impedance Measurements

Fault location based on impedance measurements can either be achieved by using a single ended method or a dual ended method. The single ended impedance measurement line fault location method can be characterised as being an online passive system or an online active system or an offline active system. However, the dual ended impedance measurement line fault location method is often characterised as being an online passive system. The impedance measurements can be visualized in Figure 2-11 [40].

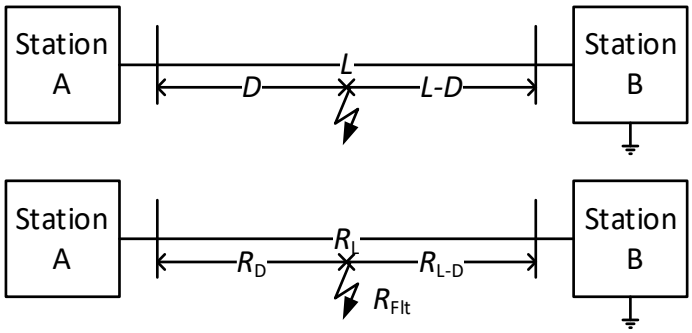

Figure 2-11: Physical representation of the impedance measurements of the HVdc system.

2.5.3.1 Single Ended Line Fault Location Based on Impedance Measurements

In the single ended line fault location method based on impedance measurements, each station independently measures the impedance of the line before and after the fault relative to

its station's location. The fault location can be calculated using Equation (2.4). The calculation is based on the measured voltages and currents present on the line or injected into the line. The fault location is determined by the change in the line impedance. One major challenge of this method is that the fault impedance is unknown. This fact causes the impedance calculation to be less accurate and this results in less accurate fault locations. Another challenge is seen in line fault location for very long transmission lines. Here the system may not have stabilised sufficiently for the impedance to be accurately calculated from the measured values. This results in a reduction of the fault location accuracy.

$$D = \frac{R_{\mathrm{D}} - R_{\mathrm{Flt}}}{R_{\mathrm{L}}} L \qquad (2.4)$$

where:

L = Total length for the conductor under evaluation

D = Distance from the station to the fault location for the conductor under evaluation

R_{D} = Resistance from the station to the fault location for the conductor under evaluation

R_{L} = Total resistance for the conductor under evaluation

R_{Flt} = Resistance of the fault on the conductor under evaluation (Unknown)

2.5.3.1.1 Online Passive Single Ended Line Fault Location Based on Impedance Measurements

In an online passive single ended line fault location system based on impedance measurements, the line fault location system uses the existing measurements of the HVdc system to calculate the line fault location. This method does not require dedicated measurement equipment for its implementation.

The online passive single ended line fault location system based on impedance measurements, is not typically used on the pole conductors, since the pole controls could

operate too fast to accurately determine the line fault location. Similarly, the online passive single ended line fault location system based on impedance measurements, is not typically used on DMR conductors or pole conductors, which are acting as a return conductors or electrode conductors, since these conductors have typically little or no measurable values in balanced operating mode.

2.5.3.1.2 Online Active Single Ended Line Fault Location Based on Impedance Measurements

In an online active single ended line fault location system based on impedance measurements, ac signals are injected into the active transmission line. Additional line filters at the stations, filter out these ac signals from the station and thereby prevent the injection of these unwanted frequencies into the HVdc converters. These injected ac signals are measured by the line fault location system's measurement system. This fault location utilizes a procedure similar to the one used by the single ended line fault location system, based on impedance measurement, found in HVac systems to calculate the fault location. However, this method also suffers from similar issues as the HVac fault location. The determination of the line parameters for the fault location and correct determination of the zero-sequence for the fault location are difficult since the fault impedance is unknown. Furthermore, the expense of implementing this solution is problematic owing to the expensive inline filtering required to remove the injected ac signals. In addition, there is the expense of the equipment needed to generate the ac signal. In addition, the expense of the system would increase as the line length increases to satisfy the level of energy needed to generate an ac signal that has sufficient magnitude to traverse the total line length.

An online passive single ended line fault location system based on impedance measurements, is not typically used on pole conductors since the pole controls could operate

too fast, to accurately determine the line fault location and filtering would be cost prohibitive. However, the online passive single ended line fault location system based on impedance measurements can be used on DMR conductors or pole conductors which are acting as return conductors or electrode conductors. These conductors operate at a much lower voltage than the pole conductors. This makes the implementation less cost prohibitive.

2.5.3.1.3 Offline Active Single Ended Line Fault Location Based on Impedance Measurement

In an offline active single ended line fault location system based on impedance measurements, ac signals are injected into the offline transmission line. These injected ac signals are measured by the line fault location system's measurement system. The system utilizes a similar procedure to the single ended HVac line fault location system based on impedance measurements, to calculate the fault location. However, this method suffers from the same issues as similar HVac fault location systems, in that line parameters may not be precisely known. Also, since the actual fault impedance is unknown, the zero-sequence component cannot be accurately determined. In contrast, the online active single ended line fault location system based on impedance measurements, does not require any additional inline filters to prevent the injection of the ac signal into the HVdc converters since the HVdc converters would be offline and out of service. However, the expense of the equipment needed to generate the ac signal is still a factor, since an increase in the line length will increase the cost of the equipment needed to generate an ac signal, with sufficient magnitude, to traverse the total line length.

The offline active single ended line fault location system, based on impedance measurements, can be used on pole conductors, DMR conductors or pole conductors which are

acting as a return conductors or electrode conductors as all the conductors are de-energised since the HVdc system is out of service.

2.5.3.2 Double Ended Line Fault Location Based on Impedance Measurement

In the double ended line fault location method based on impedance measurements, the measurements from both stations are used to calculate the impedance of the line from both before and after the fault. The fault location can be calculated using Equation (2.5).

$$D = \frac{R_{\mathrm{D}}}{R_{\mathrm{L}}} L \qquad (2.5)$$

where:

L = Total length for the conductor under evaluation

D = Distance from the station to the fault location for the conductor under evaluation

R_{D} = Resistance from the station to the fault location for the conductor under evaluation

R_{L} = Total resistance for the conductor under evaluation

The calculation is based on the measured voltages and currents present on the line. The fault location is determined by the change in the line impedance which is proportional to the change in the length of the line. One benefit this method has over the single ended line fault location method, based on impedance measurements, is that the fault impedance is not required in the impedance calculation. This eliminates the unknown factor and improves the accuracy of the line fault location system. However, the double ended line fault location method, based on impedance measurements method, still has the same challenge as the single ended line fault location method base on impedance measurement method. The challenge relates to the settling time. The settling time of the very long transmission lines, becomes an issue where the system

may not have stabilised sufficiently for the impedances to be accurately calculated from the measured values. This can result in a reduction of the fault location accuracy.

2.5.3.2.1 Online Passive Double Ended Line Fault Location Based on Impedance Measurement

The online passive double ended impedance measurement line fault location system, will use the existing measurements of the HVdc stations to calculate the line fault location. This type of line fault location system has been proposed mainly for neutral or return conductors [48] of the HVdc system. The implementation of this method is cost effective since it only uses the existing measurements present in the HVdc system.

The online passive double ended line fault location system based on impedance measurements, can be used for pole conductors, DMR conductors or pole conductors which are acting as a return conductors or electrode conductors. This is possible provided that the controls and/or the protection system give sufficient time for the system to settle to the new faulted steady-state mode of operation before clearing of the fault occurred. Furthermore, the shorter the transmission line the better this system would work. This is due to the fact that it would take less time for the HVdc system to settle with a shorter transmission line than with a longer transmission line.

The online passive double ended line fault location, based on traveling waves has proven to be a highly accurate method for fault location on pole conductors with the rapid control response of the pole conductor. For this reason, it would be practical to disqualify the use of the online passive double ended line fault location system based on impedance measurements, for line fault location on the pole conductors, owing to the rapid response of the HVdc system. However, the online passive double ended line fault location system based

on impedance measurement, could prove to be a practical low-cost solution for the neutral or return conductors since it is a low-cost system that can be implemented on new or existing HVdc systems. However, the challenges related to the settling time of the HVdc system owing to the long line lengths must be addressed.

Therefore, this thesis proposes a solution that is applicable to the online passive double ended impedance measurement line fault location method. This thesis proposes a forecasting method to determine the faulted steady-state impedance of the transmission line. This proposed method will calculate the faulted steady-state impedance of the line. This calculation will be based on the transient fault data captured by the fault location system prior to the clearing of the fault by the protection system of the HVdc system. The forecasting of the faulted steady-state impedance is based on the statistical principal of regression, which is used to curve fit the measured values to forecast the faulted steady-state impedance of the HVdc system's transmission line.

2.6 Chapter Summary

This chapter described the HVdc system and the presently used protection methods of the HVdc system. The main characteristics and configurations of HVdc systems were also described. Furthermore, fault detections schemes currently implemented in HVdc control systems were reviewed. The detections schemes reviewed included both primary and secondary detection schemes. Then finally offline, online, active, and passive characteristics of a line fault locations system were reviewed. The online passive fault location characteristics discussed in this chapter are the main characteristics of the online Neutral Line Fault Locator (nLFL) proposed for fault location on neutral or dedicated metallic return conductors.

Chapter 3: A New Algorithm for an Online Neutral Line Fault Locator (nLFL)

This chapter proposes a highly effective new online algorithm for locating faults on the DMR or return conductor, referred to as a "Online Neutral Line Fault Locator (nLFL)". The chapter also examines the need and reason for developing the proposed nLFL. The performance of the nLFL is analyzed in the subsequent chapters.

3.1 Online Neutral Line Fault Locator Implementation Challenges

As was discussed in the previous chapter, line fault location is crucial to the successful operation and maintenance of the HVdc system. Most existing systems require additional hardware and highly sensitive equipment for online line fault location. For example, most commercial online waveform capture systems, install additional high frequency surge capacitors to capture traveling wave fronts' arrival at the stations. The arrival of the wave fronts is then timestamped using high accuracy GPS clocks. In a neutral or a DMR line configuration, one end of the transmission line is grounded at one of the converter stations. The installation of the surge capacitor at the converter station requires that one end of the surge capacitor to be grounded and the other end to be connected to the transmission line. Thus, a surge capacitor connected at the grounded station would be grounded on both ends of the surge capacitor, thereby preventing any waveform capture.

Direct wave front capture from the HVdc control measurements is possible since it would require no additional equipment. The HVdc control system samples and timestamps each of its measurements. The accuracy required for HVdc system control recorders are in the

range of milliseconds to hundreds of microseconds. Therefore, based on the Equation (2.3) a fault recorder with a timer accurate to one millisecond, would have a fault location accuracy of ±150.0 km and a fault recorder with a timer accurate to one hundred microseconds, would have a fault location accuracy of ±15.0 km.

Fault location systems that use impedance calculations can use the existing HVdc measurements and timestamps to calculate the fault location in the faulted steady-state condition of the HVdc system. The timestamping of the event is only used for ensuring that the measurements used are from the same time. However, obtaining measurements from the faulted steady-state condition can become increasingly difficult as the length of transmission lines or cables are increased. Such increases in line length result in a longer transient settling time for the system, which further delays the faulted steady-state measurements needed for calculation. In addition, the fact that the HVdc protection's systems can react to clear the fault from the system, prior to the system reaching the new faulted steady-state condition, is also problematic. If the HVdc system does not reach its faulted steady-state condition, prior to the activation of the HVdc protection system, the accuracy of the fault location system will be reduced.

The development of a system to interpolate the faulted steady-state condition of the system without protective control action, will enhance the capability and accuracy of this fault location scheme. Thus, the remainder of this chapter looks at the online Neutral Line Fault Locator (nLFL) design and developed based on this proposed technique.

3.2 Online Neutral Line Fault Locator Operational Configurations for the HVdc Systems

Transmission lines need to be energised either by the HVdc converters or by an external excitation system before an online fault location system can determine the line fault location. The proposed nLFL is designed to use the existing HVdc measurements to determine the line fault location. In the discussion to follow, the converters are assumed to be LCC, although the methodology can be adapted for VSC as well.

The online fault locater in a Bipolar HVdc scheme with a DMR, requires an operating mode that energises the DMR with sufficient energy to monitor and measure the voltage and the current on the DMR conductors. There is little to no current flowing through the DMR in the bipolar operating mode of a Bipolar HVdc scheme as seen in Figure 3-1. Therefore, fault detection using the proposed algorithm does not work in this scenario.

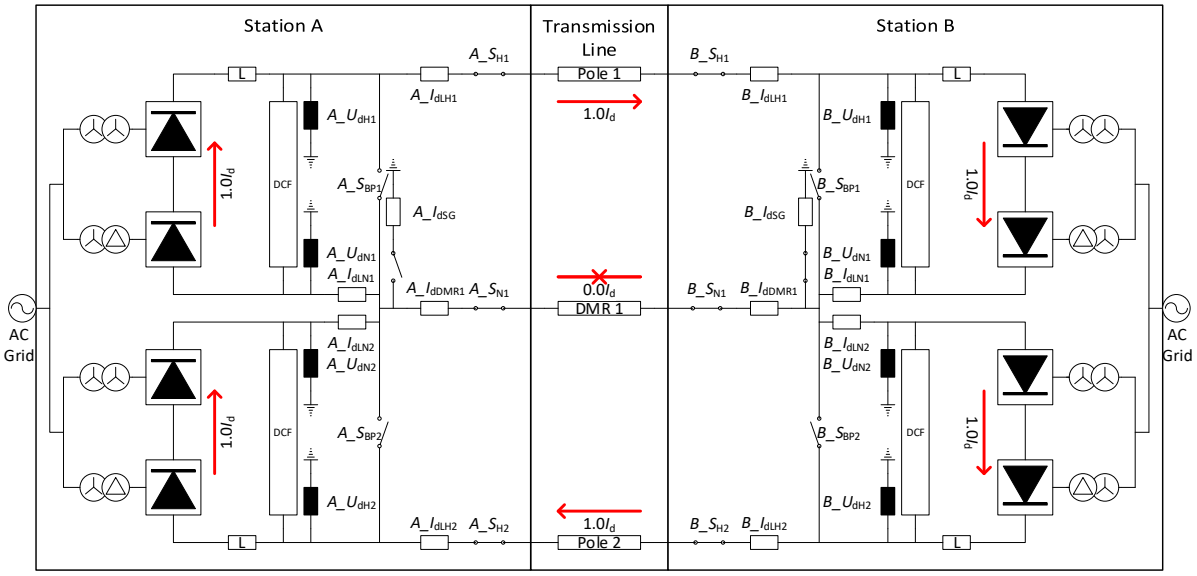

Figure 3-1: Current flow in a Bipolar LCC-HVdc scheme with a DMR, operating in a bipolar mode of operation.

The first operating mode in which a Bipolar HVdc scheme can be used to determine a line fault location, is when the Bipolar HVdc scheme is running in a metallic return mode of operation. Figure 3-2 shows the energised path of the Bipolar HVdc scheme operating in a monopolar metallic return mode of operation [22].

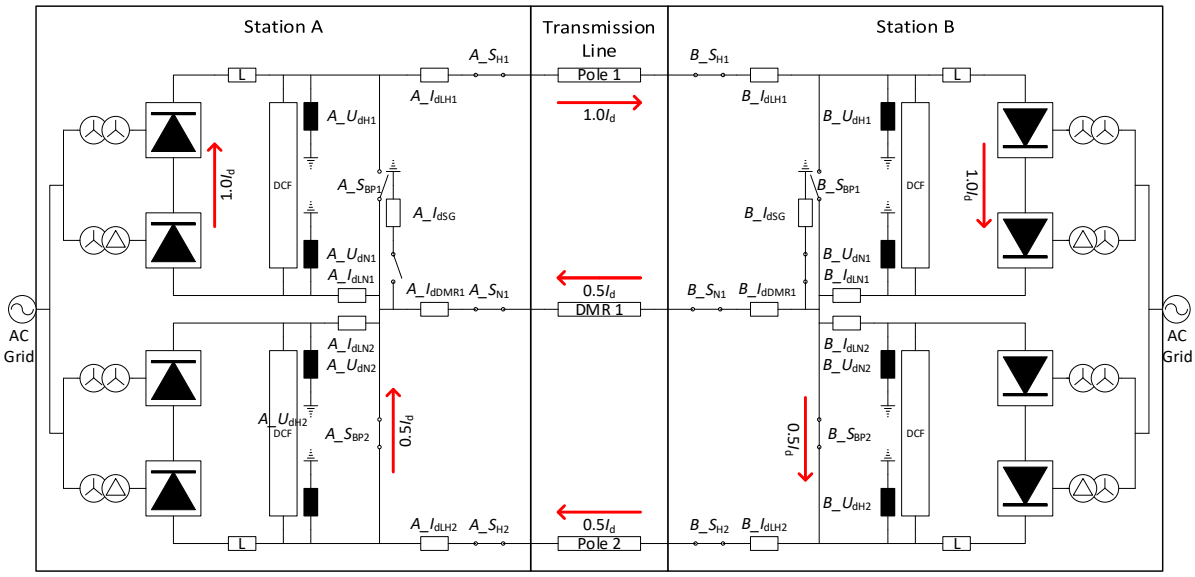

Figure 3-2: Current flow in a Bipolar LCC-HVdc scheme with a DMR, operating in a metallic return mode of operation.

The second operating mode in which a Bipolar HVdc scheme can be used, to determine a fault location, is when the HVdc scheme is running in an unbalanced mode of operation. Figure 3-3 shows the energised path of the Bipolar HVdc scheme operating in an unbalanced mode of operation.

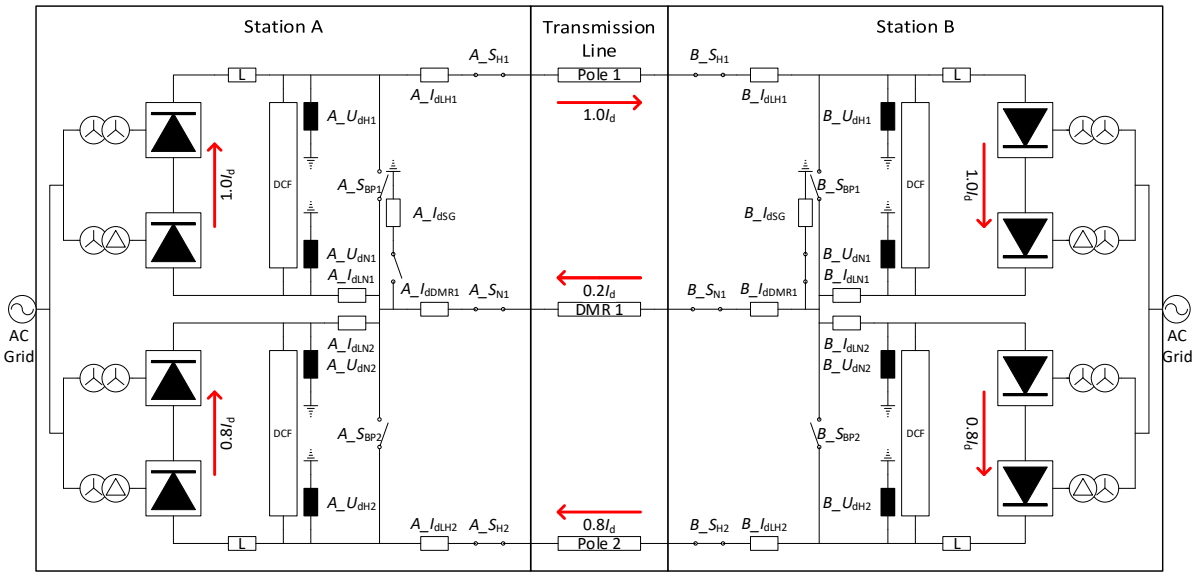

Figure 3-3: Current flow in a Bipolar LCC-HVdc scheme with a DMR, operating in an unbalanced mode of operation.

A parallel connected Bipolar Multiterminal HVdc scheme with a DMR, can carry out online fault location only in operating modes that energise the DMR with sufficient energy to monitor and measure the voltage and the current on the DMR conductors. In the bipolar operating modes of a parallel connected Bipolar Multiterminal HVdc scheme, little to no current is flowing in the DMR as seen in Figure 3-4. The first operating mode in which a parallel connected Bipolar Multiterminal HVdc scheme can be used to determine a line fault location, is when the parallel connected Bipolar Multiterminal HVdc scheme is running in a metallic return mode of operation. Figure 3-5 shows the energised path of the parallel connected Bipolar Multiterminal HVdc scheme operating in a metallic return mode of operation.

The second operating mode in which a parallel connected Bipolar Multiterminal HVdc scheme can operate, to determine a fault location is when the HVdc system is running in an unbalanced mode of operation. Figure 3-6 shows the energised path of the parallel connected Bipolar Multiterminal HVdc scheme operating in an unbalanced mode of operation.

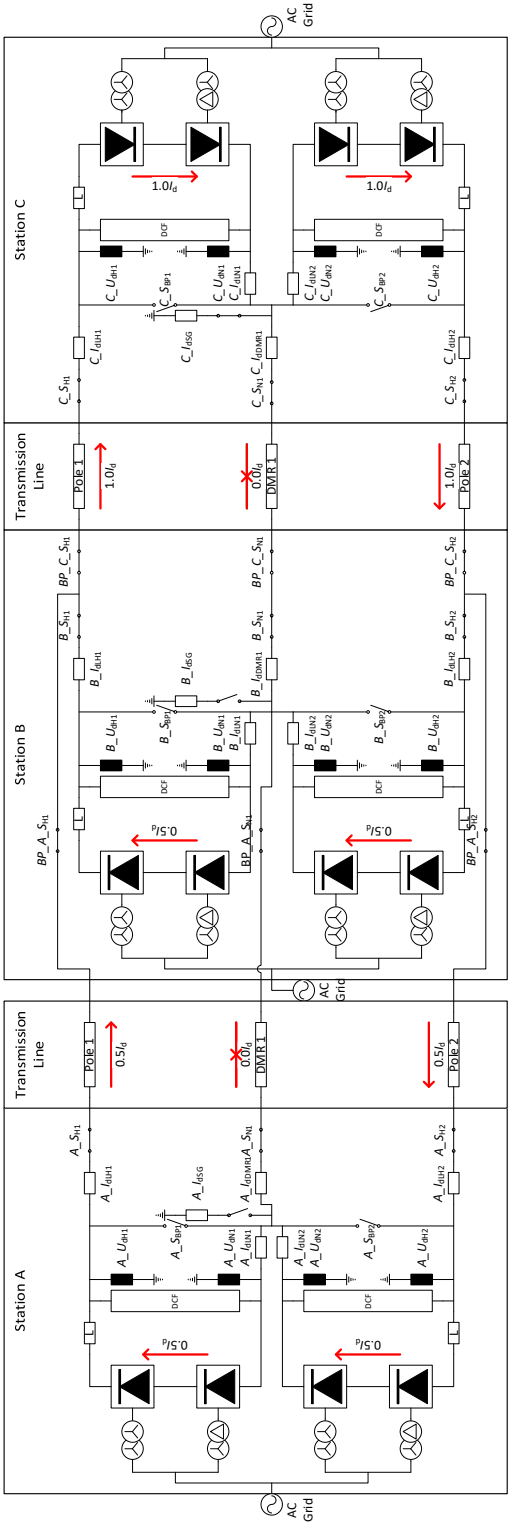

Figure 3-4: Current flow in a parallel connected Bipolar Multiterminal LCC-HVdc scheme with a DMR, operating in a bipolar mode of operation.

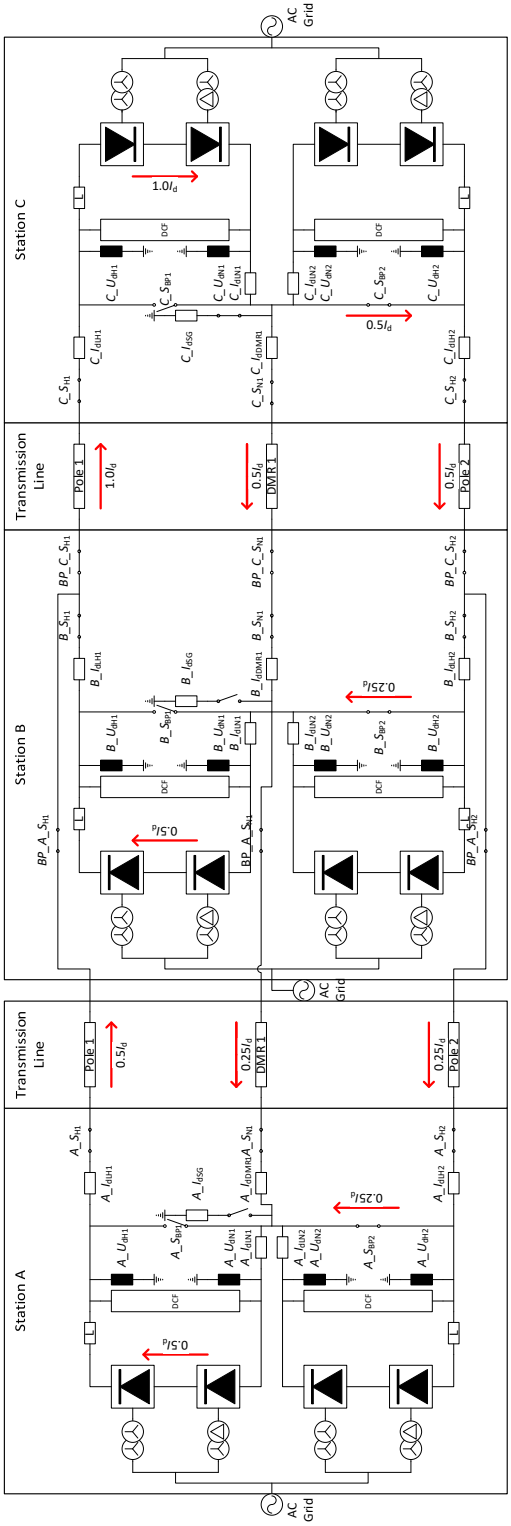

Figure 3-5: Current flow in a parallel connected Bipolar Multiterminal LCC-HVdc scheme with a DMR, operating in a metallic return mode of operation.

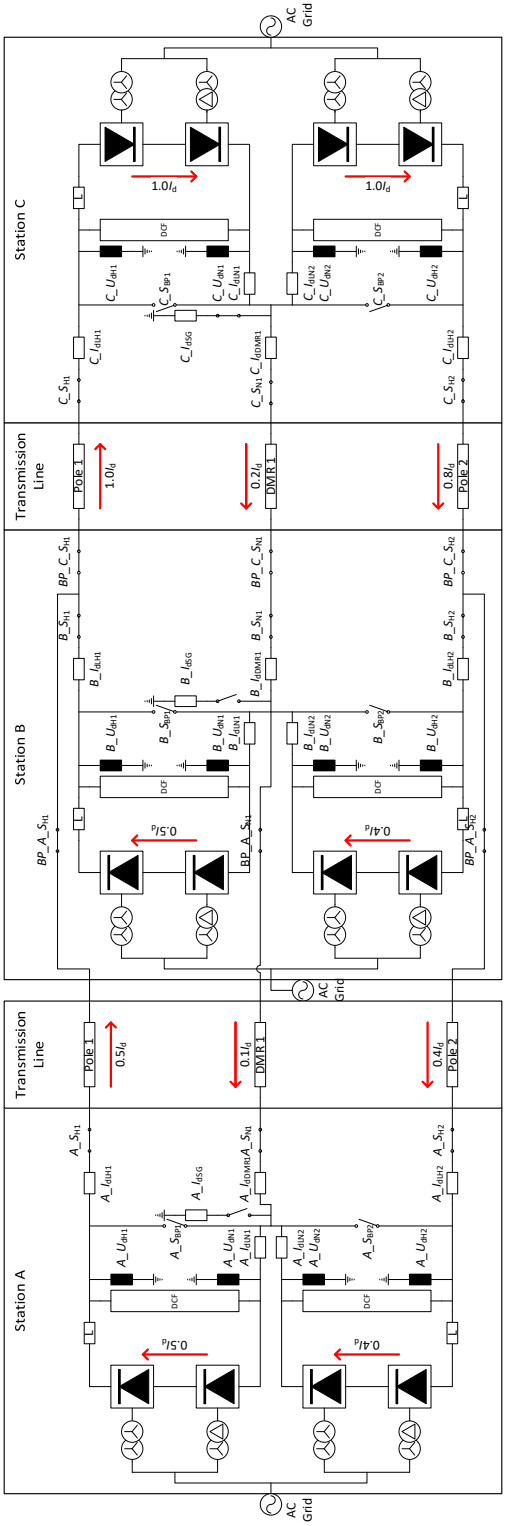

Figure 3-6: Current flow in a parallel connected Bipolar Multiterminal LCC-HVdc scheme with a DMR, operating in an unbalanced mode of operation.

Online fault location can be performed on both the Monopolar and the Homopolar HVdc scheme with a DMR. This does not require any alterations in the operating modes of the Monopolar or the Homopolar HVdc scheme. Since the DMR is energised during monopolar or homopolar operations of a Monopolar or a Homopolar HVdc scheme, the fault location can be determined during the normal operation of a Monopolar or a Homopolar HVdc scheme. Figure 3-7 shows the energised path of a Monopolar HVdc scheme, during the monopolar operation of the system, which could be used to determine a line fault location. Figure 3-8 shows the energised path of a Homopolar HVdc scheme, during homopolar operation of the system, which could be used to determine a line fault location.

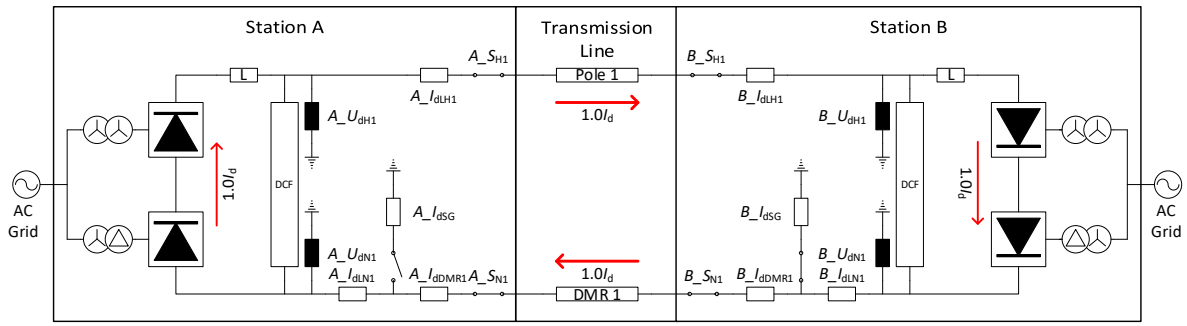

Figure 3-7: Current flow in a Monopolar HVdc scheme with a DMR, operating in a monopolar mode of operation.

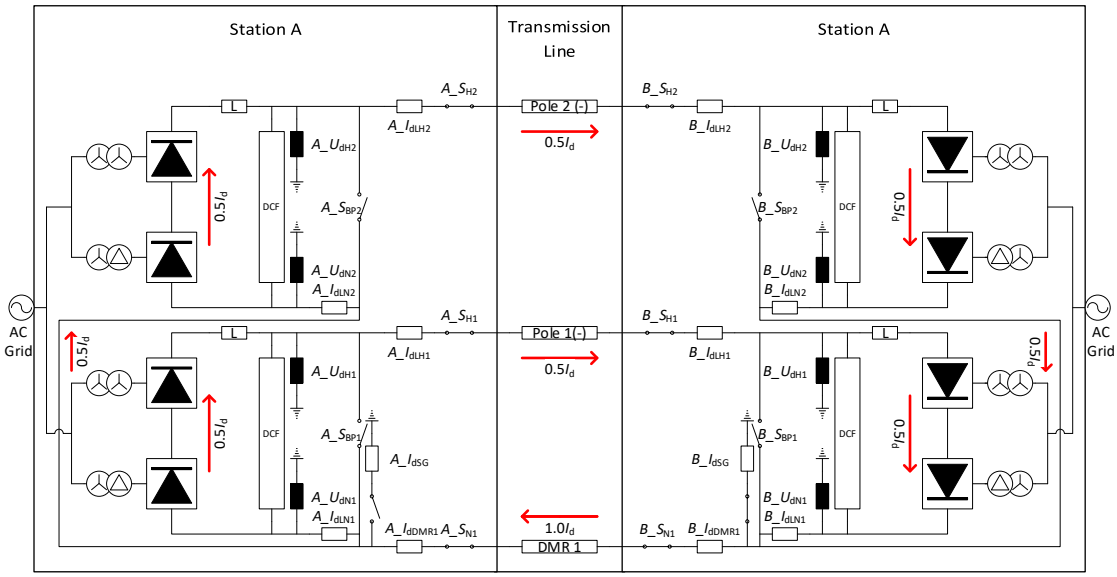

Figure 3-8: Current flow in a Homopolar HVdc scheme with a DMR, operating in a homopolar mode of operation.

The proposed nLFL system can be used in all the schemes and configurations discussed in this section. The nLFL system is a point-to-point fault location system. Thus, the faults on the neutral conductors can be determined on each of the individual conductors between any two station(s) or substation(s) provided that all the voltage and the current measurements at the station(s) or substation(s) are available to calculate the fault location. The required voltage and current measurements are discussed in subsequent sections.

3.3 Online Neutral Line Fault Locator Proposed Test System

Although the proposed method will be initially tested using offline and real-time simulations, there is no substitute for field testing. For this purpose, the author has installed an nLFL system on the Eastern Alberta Transmission Link (EATL) HVdc system running from Brooks, Alberta, Canada (Newell Converter Station) to Gibbons, Alberta, Canada (Heathfield Converter Station). The EATL HVdc system owned and operated by ATCO Electric is a suitable test system for the nLFL prototype tests. (ATCO Electric is the end customer for the

author's proposed device, and the EATL HVdc system is the actual line on which the nLFL system has been installed). The EATL HVdc system is currently configured as a 500 kV Monopolar HVdc system capable of transmitting 1000 MW. The conductor for a second HVdc pole has been installed for future expansion. This conductor is currently used as a return path in parallel with the DMR.

The HVdc transmission corridor consists of a 485.0 km long overhead transmission line configured with two pole conductors and one DMR conductor as seen in Figure 3-9 below. The HVdc system is a Monopolar HVdc scheme in which only one pole conductor can be used as the primary path while the DMR or the secondary pole conductor can be used independently or in parallel as the return path.

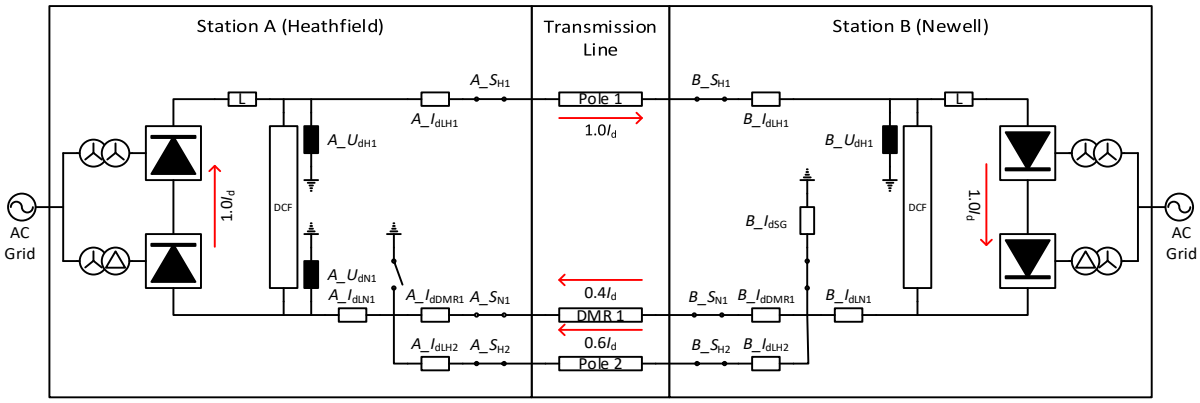

Figure 3-9: EATL HVdc system configuration.

The benefit of this system is that in case of a fault on one of the parallel return paths (i.e., the DMR 1 or the Pole 2 conductor), the affected conductor can be disconnected and the Monopolar HVdc scheme can continue its operation. This allows for real world faults to be applied to the system during commercial operation for testing and verification of the nLFL system.

3.3.1 Online Neutral Line Fault Locator Hardware Integration in EATL

In general, the nLFL system would be integrated directly into the measurement system when the HVdc system is being constructed. Thereby tying the nLFL system directly into the voltage and current measurements coming from the voltage transducers and current transducers. The tying of the nLFL directly into the measurement system would give the nLFL system the most optimal accuracy and performance to capture and timestamp the events without additional delays or distortions.

However, since the EATL HVdc system is already constructed and is already in service, it is not possible to integrate the nLFL system directly into the measurement system of the EATL HVdc system. The nLFL system will read measurements from the Transient Data Measurement (TDM) bus via the Analog Interface Module 2 (AIM2). The AIM2 reads the TDM bus data and outputs the analog voltage readings from the TDM bus to the nLFL to read. This process does potentially introduce latency and possible measurement errors into the system, but as the nLFL relies on the characteristic response of the voltages and currents and not the exact arrival times of the signals, the errors introduced by this stage can be mitigated by the nature of the algorithm.

The EATL HVdc system provides the nLFL system with the following measurements listed below in Table 3-1 for each station and illustrated in Figure 3-10.

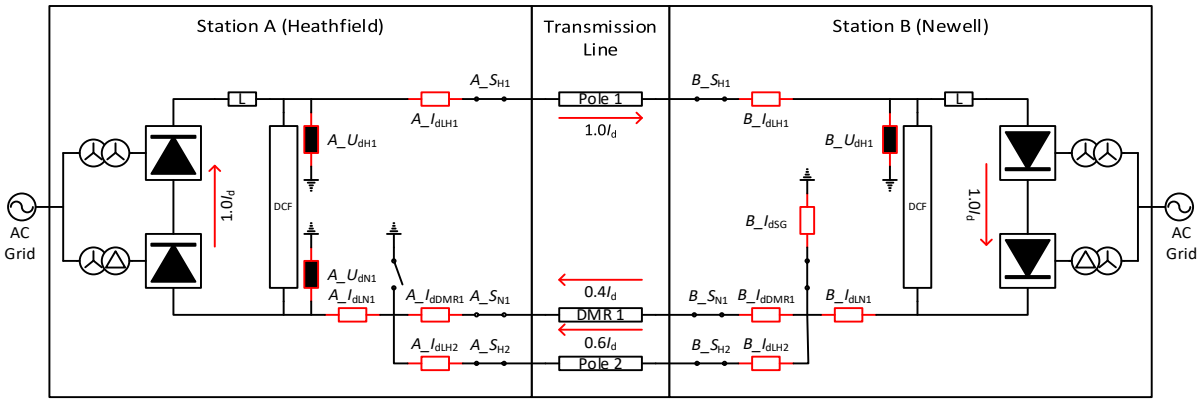

Figure 3-10: EATL measurement locations.

Table 3-1: EATL measurements available for capture by the nLFL.

Measurements	Heathfield Station (Station A)	Newell Station (Station B)
Pole 1 voltage	A_U_{dH1}	B_U_{dH1}
Neutral 1 voltage	A_U_{dN1}	No transducer installed in EATL (Not recorded by the nLFL's DMU)
Pole 2 voltage	No transducer installed in EATL (Not recorded by the nLFL's DMU)	No transducer installed in EATL (Not recorded by the nLFL's DMU)
Pole 1 current	A_I_{dLH1}	B_I_{dLH1}
Neutral 1 current	A_I_{dLN1}	B_I_{dLN1} (Not recorded by the nLFL's DMU)
DMR 1 current	A_I_{dDMR1}	B_I_{dDMR1}
Pole 2 current	A_I_{dLH2}	B_I_{dLH2}
Ground current	No transducer installed in EATL (Not recorded by the nLFL's DMU)	B_I_{dSG}
Ground current high resolution	No transducer installed in EATL (Not recorded by the nLFL's DMU)	B_I_{dSGHR}

The measurements provided at each station are recorded by the nLFL stations located at each converter station (Station A and Station B). Each nLFL station records the available measurements at the station at a rate of 100,000 samples per second and timestamps each sample using a GPS timestamp accurate to 100 ns, to inshore that measurements taken from both stations can be correlated during event processing. The nLFL stations will interchange measurement data only after a fault event has been detected.

It should be noted that the nLFL records the voltages and currents on the Pole 1 conductor. However, these measurements are not used in the calculation of either the DMR 1 conductor fault location or the Pole 2 conductor fault location. Figure 3-11 and Figure 3-12 depict the voltage and current transients on the Pole 1 conductor. From these images a small transient event is observed on the Pole 1 conductor's voltages and currents, but they are of insufficient magnitude to calculate a reasonable fault location.

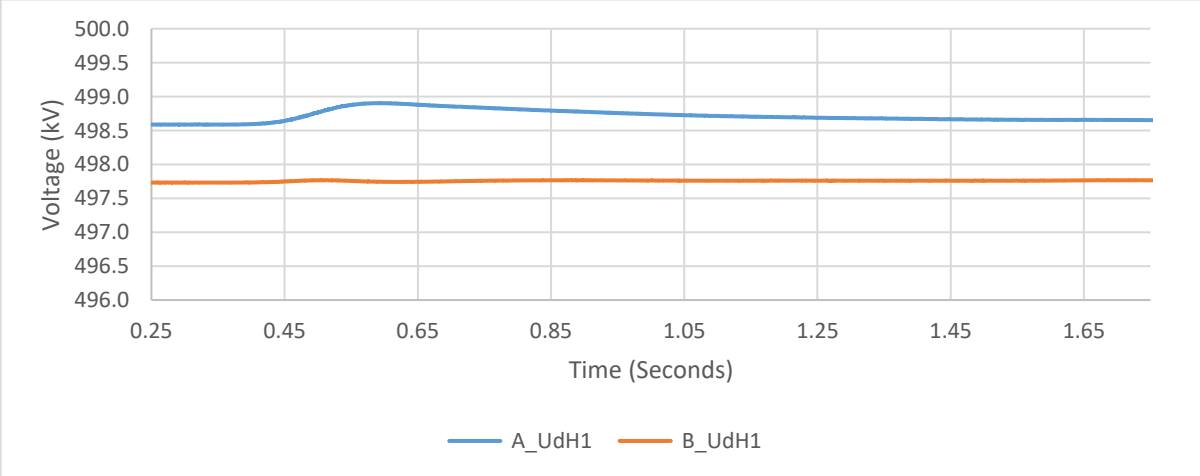

Figure 3-11: HVdc converter stations Pole 1 voltage during a DMR 1 fault.

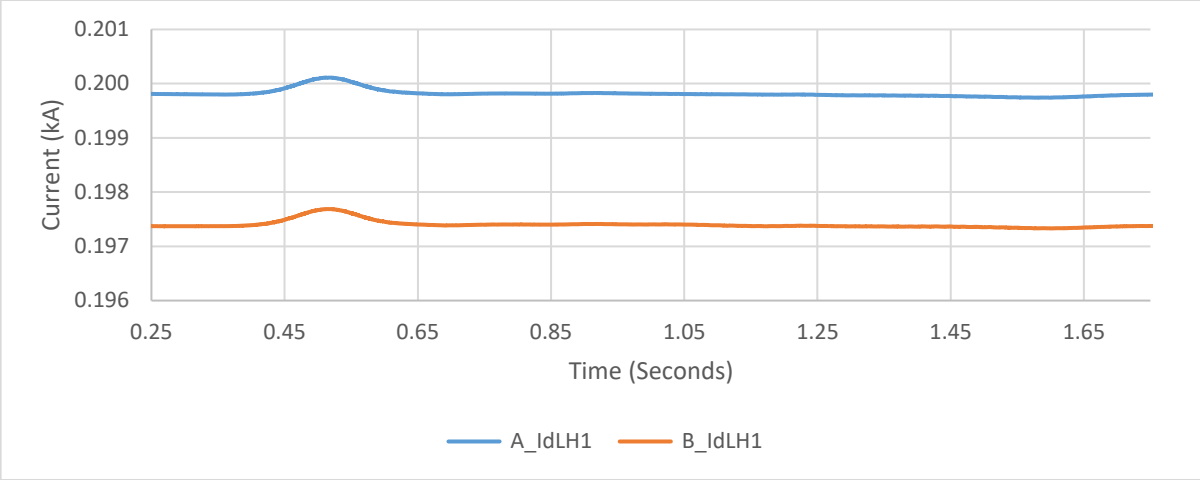

Figure 3-12: HVdc converter stations Pole 1 current during a DMR 1 fault.

3.3.2 Online Neutral Line Fault Locator Fault Location Sources of Error

Although the proposed nLFL system can detect and calculate the fault location, there are practical limitations to the accuracy of the nLFL system. The main sources of error for the nLFL system lies in the measurement devices and the fact that environmental conditions can impact the characteristics of the transmission line.

Similarly, the measurement devices used to measure the voltage and the current of the HVdc system also introduce errors in the nLFL systems' calculation. This is due to the accuracy and the precision of the measurements taken by the voltage and current transducers.

3.4 Online Neutral Line Fault Locator Algorithm Design

The proposed online Neutral Line Fault Locator (nLFL) is a new online fault location system designed for determining faults on neutral or return conductors (e.g., DMR 1 or Pole 2) in a HVdc system. Finding the fault location for faults on neutral or return conductors are problematic since the normal operating voltage is very close to zero, and changes very marginally with a fault. If the fault were not rapidly cleared, it could still be located with a long measurement duration, but alas, the protective action of the HVdc system operates too rapidly

to capture sufficient measurements to accurately determine the fault location. The thesis proposes a novel nLFL system that overcomes these two major issues and allows accurate fault location on neutral or return conductors, with sufficient accuracy to be used for expedited restoration and repair of faulted conductors.

The nLFL system consists of two main components. The first component of the nLFL system is the software that processes and analyzes the measured data, to determine the fault location. This will be discussed in the following sections. The second component is the hardware used to capture the real time current measurements and voltage measurements for analysis. This will be discussed in Chapter 4: Online Neutral Line Fault Locator (nLFL) Hardware Architecture.

The nLFL system implements an online double ended passive fault location algorithm, that utilizes the impedance of the transmission line derived from the measured values of the HVdc system, to calculate the fault location on the neutral conductors. The nLFL's fault location algorithm uses an equivalent model of the HVdc system, to simplify the HVdc transmission line to a resistive electric circuit, such that the resistances of the line can be calculated before and after the fault has occurred. The nLFL system uses the derived equations from the impedance of the line and the measured values from the DMU to calculate the fault location. Since the HVdc system must reach steady-state after the fault to obtain an accurate fault location, the nLFL system must project the HVdc system into its future faulted steady-state condition after the fault in the absence of any of the HVdc system's protective actions. The nLFL algorithm uses regression to forecast the future values of the HVdc system in steady-state after the fault to calculate the fault location in the faulted steady-state condition.

3.4.1 Online Neutral Line Fault Locator Fault Detection Algorithm

The fault must first be detected before a fault can be located. To detect the fault the nLFL system implements a rate of change detection algorithm. The rate of change detection algorithm processes the signals after the signals are filtered to remove any noise, that could lead to false event detections and after the dc component of the signal is also filtered, to ensure that only transient fault events are being detected on the system. The nLFL system uses a low-pass filter to remove the high frequency noise due to converter switching, harmonics and aliasing due to sampling from the HVdc system and the nLFL system's ADCs. The nLFL system also uses a dc rejection filter to remove the dc component of the signal.

Except for the rapid rate change caused by a major transient fault event, the filtered signal from the filter stage does not incorporate any other transient event or noise from other factors. The resulting filtered signals are then processed by the rate of change detector. If the rate of change exceeds the specified rate of change threshold the algorithm triggers the DMU, to capture the pre and post event samples and timestamps of the signals based on the specified configurations of the DMU. The DMU is also triggered to record the trigger time of the event. This process is visualized in Figure 3-13. Once this process is completed the data is sent to the computer for the processing of the fault location by the nLFL algorithm.

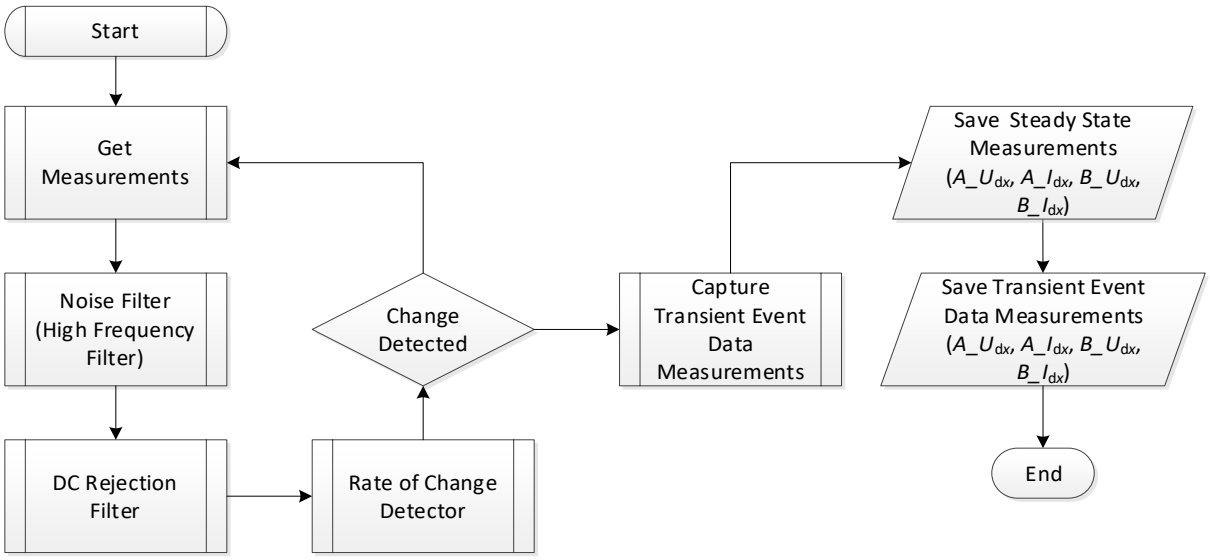

Figure 3-13: Fault detection algorithm flow chart.

Triggering of the nLFL system was done by detecting transient fault events from the voltage at the ungrounded HVdc station and transient fault events from the ground current at the grounded HVdc station. Fault detection at the ungrounded HVdc station was done by using the voltage(s) of the conductor(s) at the ungrounded HVdc station. This detection scheme was found to be a reliable fault detection mechanism for the return conductor at the ungrounded HVdc station since the voltage of the return conductor at the ungrounded HVdc station is proportional to the voltage drop(s) across the return conductor. Thus, a change in the impedance(s) of the return conductor(s) during a fault produces a significant transient fault event on the voltage measurements at the ungrounded HVdc station for fault detection.

However, it should be noted that for faults closer to the grounded HVdc station, the change in the return conductor(s') impedance is less, as more of the return conductor remains connected to the ungrounded HVdc station. Thus, the voltage transient, due to the fault occurring closer to the grounded HVdc station results, in a much smaller voltage transient at

the ungrounded HVdc station. This makes it difficult to detect faults close to the grounded HVdc station from the ungrounded HVdc station.

Fault detection using the ground current measurement, can detect faults across the entire length of the return conductor, which includes faults close to the grounded HVdc station. Faults can be detected across the entire length of the return conductor since the combined impedance of the fault and the return conductor is usually greater than the HVdc station's ground impedance. This results in a large ground current transient, in the event of a fault on the return conductor.

Thus, to ensure that both sides trigger during a fault, the nLFL system's DMU sends a remote trigger signal to the opposite HVdc station's DMU when it triggers to force the other HVdc station's DMU to trigger and collect the data needed for the fault location process. As the nLFL system uses the characteristic response of the system (and not the inception of the fault) to calculate the fault location no accuracy is lost when the nLFL system uses remote triggering to aid in the fault detection process.

3.4.2 Online Neutral Line Fault Locator Faulted Conductor Selection Algorithm

Once the fault is detected, the faulted conductor must be identified. Since the collapsing voltage field, induces a transient on the parallel conductors in the transmission line, the detection of a transient event on a conductor is not necessarily the most reliable means of accurately identifying the faulted conductor. There is literature that discusses the classification of the transient fault event to identify which of the conductors are faulted, but there are few available references of this classification system being implemented in practice.

The most common way to identify a faulted conductor is to identify a difference in the currents between the two ends of each of the conductor. Under normal conditions the sending end and the receiving ends of each of the conductor are approximately the same. However, after a fault the current in the faulted conductor will be different at the sending and the receiving ends of the conductor, while the current in the unfaulted conductor will remain similar at the sending and the receiving ends. The nLFL system uses the differential current classification method to identify which of the conductors in the transmission line is faulted. With the faulted conductor identified, the fault location can now be identified.

3.4.3 Online Neutral Line Fault Locator HVdc System Model for Algorithm

As discussed in previous sections, the nLFL is only capable of detecting fault locations when the HVdc system is operating in a mode that energises the DMR or neutral conductor sufficiently to obtain accurate measurements. In this thesis, the EATL HVdc system is used as a real-world example for analysis as well as field testing. As the EATL HVdc system is a Bipolar HVdc scheme currently configured to operate as a Monopolar HVdc scheme with a paralleled DMR 1 and Pole 2 return path, the equations for this system will be developed in this section. The equations developed for the DMR 1, and Pole 2 conductor are very similar and could be generalized for any pole or configuration.

Thus, to complete the double ended impedance analysis for the nLFL algorithm, the HVdc system seen in Figure 3-14 is represented by the simple equivalent electric circuit model seen in Figure 3-15. The HVdc converters at either end is represented by fixed voltage sources for the purposes of steady-state analysis of the system. The standard π-model of a transmission line can represent the three conductor bundles of the transmission line, for each of the three conductors in the transmission line. However, since the HVdc system is running at steady-state

dc, the ripples in the current and the voltage can be ignored, because the inductive and the capacitive components will tend to zero and infinity since the frequency of the system is zero. Thus, the π-model of each conductor becomes purely resistive as modeled in Figure 3-15. The grounding point of the converter station can be modeled as a fixed resistive element to ground to represent the impedance of the station grounding. The ground resistance is fixed and should vary very little over time with the appropriate design of the ground electrode and selection of an appropriate ground electrode location.

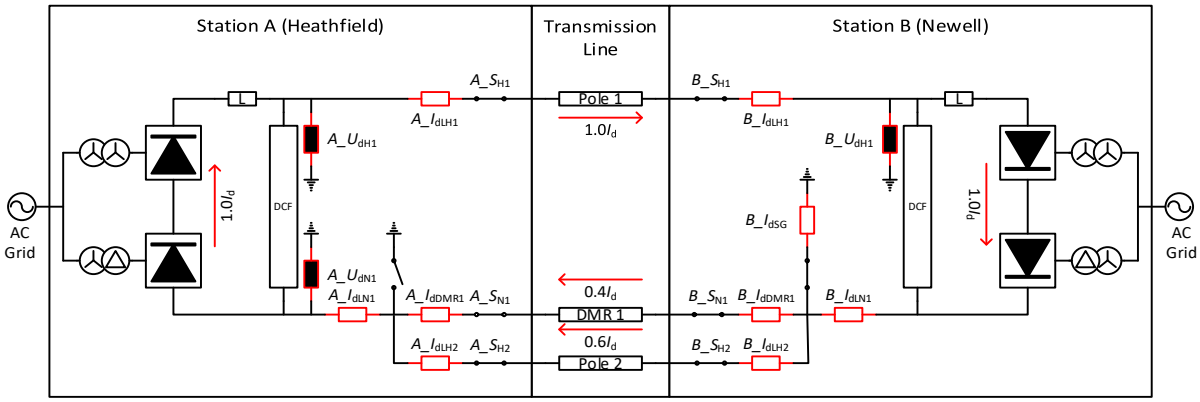

Figure 3-14: EATL HVdc system with its available measurement points.

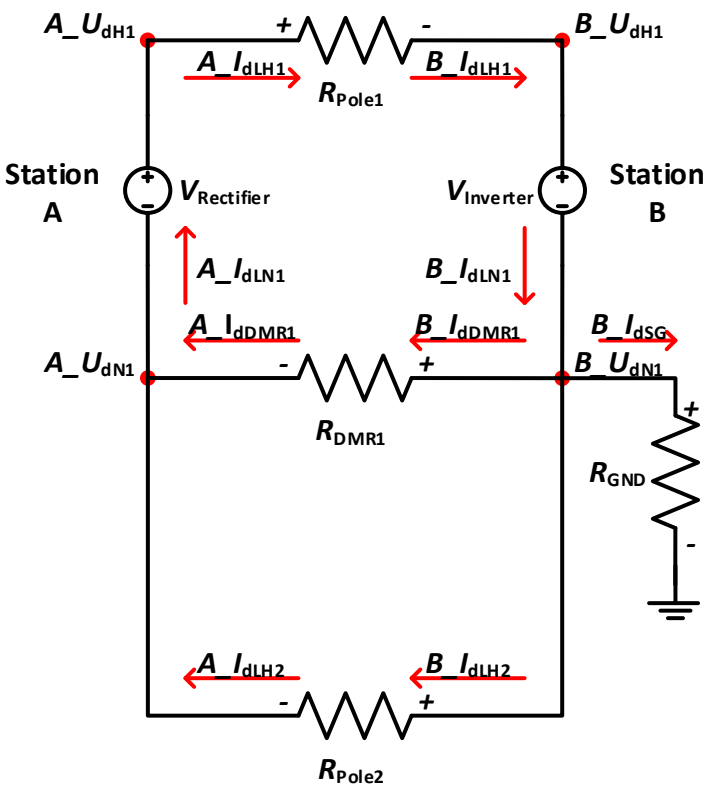

Figure 3-15: Equivalent circuit of the EATL HVdc system with its available measurement points.

From the equivalent circuit shown in Figure 3-15, one can derive equations to determine the resistance of each of the 3 conductors. The resistance of the Pole 1 conductor can be seen in Equation (3.1). The resistance of the Pole 2 conductor is approximately equal to the Pole 1 conductor since the Pole 1 conductor and the Pole 2 conductor use the same conductor type, the same configuration and are located at the same height above ground and the same distance from the DMR 1 conductor but are on opposite sides of the DMR 1 conductor. Given these facts, the impedance of the Pole 1 conductor and the Pole 2 conductor impedances will be approximately the same, as seen in Equation (3.2). Based on the impedance calculated for the Pole 2 conductor, the DMR 1 conductor resistance can be calculated as shown in Equation (3.3) and the derivation can be found in Appendix A: Monopolar Fault Location Calculation.

$$R_{\text{Pole1}} = \frac{(A\_U_{\text{dH1}} - B\_U_{\text{dH1}})}{A\_I_{\text{dLH1}}} \quad (3.1)$$

$$R_{\text{Pole2}} \cong R_{\text{Pole1}} \quad (3.2)$$

$$R_{\text{DMR1}} = \frac{R_{\text{Pole2}} \times \left(A\_U_{\text{dN1}} - (B\_I_{\text{dSG}} \times R_{\text{GND}})\right)}{(R_{\text{Pole2}} \times A\_I_{\text{dLN1}}) - \left(A\_U_{\text{dN1}} - (B\_I_{\text{dSG}} \times R_{\text{GND}})\right)} \quad (3.3)$$

where:

R_{Pole1} = Total resistance for conductor Pole 1

R_{Pole2} = Total resistance for conductor Pole 2

R_{DMR1} = Total resistance for conductor DMR 1

R_{GND} = Resistance of the ground electrode

A_U_{dH1}= Station A voltage for conductor Pole 1

A_U_{dN1}= Station A voltage for conductor Neutral 1

A_I_{dLH1}= Station A current for conductor Pole 1

A_I_{dLN1}= Station A current for conductor Neutral 1

B_U_{dH1}= Station B voltage for conductor Pole 1

In general, the resistance of any unfaulted conductor can be calculated as follows in Equation (3.4).

$$R_x = \frac{(A\_U_{\text{d}x} - B\_U_{\text{d}x})}{A\_I_{\text{d}x}} \quad (3.4)$$

where:

R_x = Total resistance for conductor x

$A\_U_{\text{d}x}$ = Station A voltage for conductor x

$B\_U_{\text{d}x}$ = Station B voltage for conductor x

$A\_I_{\text{d}x}$ = Station A current for conductor x

The subscript "*x*" identifies the faulted conductor (DMR 1 or Pole 2).

During a fault on any of the three conductors, the faulted conductor can be modeled as two resistors with a fault resistor connected at the intersection of the two resistors going to ground. An example of the faulted equivalent circuit can be seen in Figure 3-16.

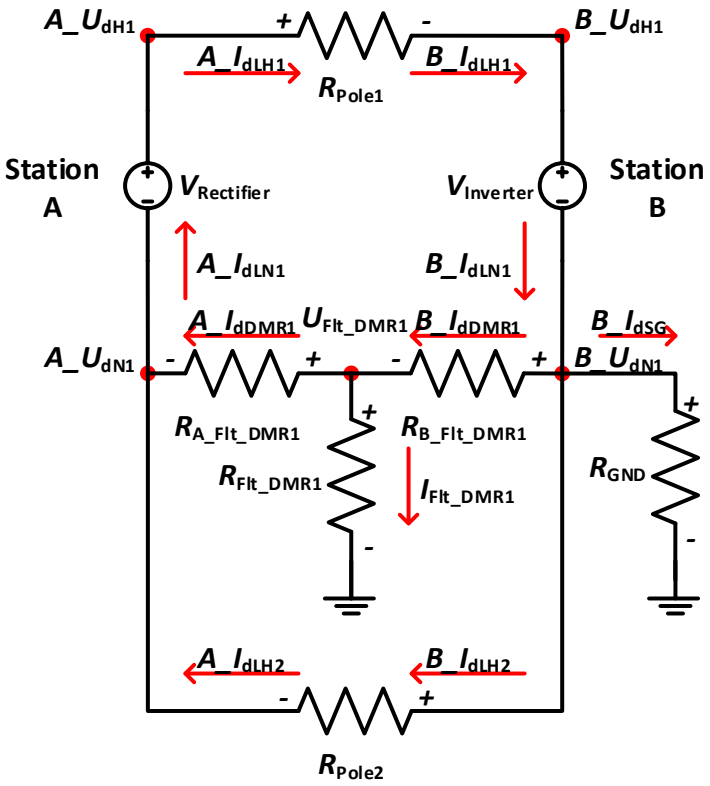

Figure 3-16: Equivalent circuit of the EATL HVdc system faulted on DMR 1.

Since it is given that the system can be modeled in its faulted state, an equation can be derived for each conductor representing the fault location along the line as a percentage of the line from either station to the fault location. In Figure 3-16, the fault location from Station A and Station B respectively along DMR 1, can be found by using Equation (3.5) and (3.6) respectively. The derivation of the equations can be found in Appendix A: Monopolar Fault Location Calculation.

$$X_{\text{A\_Flt\_DMR1}} = \frac{A\_U_{\text{dN1}} - B\_U_{\text{dN1}} + (B\_I_{\text{dDMR1}} \times R_{\text{DMR1}})}{R_{\text{DMR1}} \times (-A\_I_{\text{dDMR1}} + B\_I_{\text{dDMR1}})} \quad (3.5)$$

$$X_{\text{B\_Flt\_DMR1}} = \frac{B\_U_{\text{dN1}} - A\_U_{\text{dN1}} - (A\_I_{\text{dDMR1}} \times R_{\text{DMR1}})}{R_{\text{DMR1}} \times (-A\_I_{\text{dDMR1}} + B\_I_{\text{dDMR1}})} \quad (3.6)$$

where:

$X_{\text{A\_Flt\_DMR1}}$ = Percentage of total line length from Station A to the fault location for conductor DMR 1

$X_{\text{B\_Flt\_DMR1}}$ = Percentage of total line length from Station B to the fault location for conductor DMR 1

R_{DMR1} = Total resistance for conductor DMR 1

A_U_{dN1} = Station A voltage for conductor Neutral 1

B_U_{dN1} = Station B voltage for conductor Neutral 1

A_I_{dDMR1} = Station A current for conductor DMR 1

$B\_ I_{\text{dDMR1}}$ = Station B current for conductor DMR 1

Figure 3-17 shows that the fault location from Station A and Station B respectively along Pole 2, can be found by using Equation (3.7) and (3.8) respectively. The derivation of the equations can be found in Appendix A: Monopolar Fault Location Calculation.

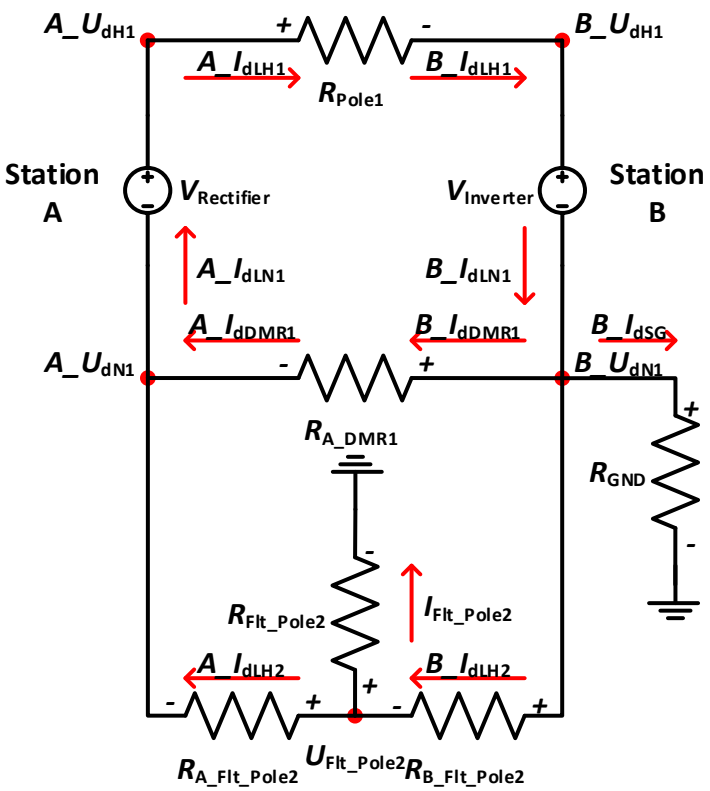

Figure 3-17: Equivalent circuit of the EATL HVdc system faulted on Pole 2.

$$X_{\text{A\_Flt\_Pole2}} = \frac{A\_U_{\text{dN1}} - B\_U_{\text{dN1}} + (B\_I_{\text{dLH2}} \times R_{\text{Pole2}})}{R_{\text{Pole2}} \times (-A\_I_{\text{dLH2}} + B\_I_{\text{dLH2}})} \quad (3.7)$$

$$X_{\text{B\_Flt\_Pole2}} = \frac{B\_U_{\text{dN1}} - A\_U_{\text{dN1}} - (A\_I_{\text{dLH2}} \times R_{\text{Pole2}})}{R_{\text{Pole2}} \times (-A\_I_{\text{dLH2}} + B\_I_{\text{dLH2}})} \quad (3.8)$$

where:

$X_{\text{A\_Flt\_Pole2}}$ = Percentage of total line length from Station A to the fault location for conductor Pole 2

$X_{\text{B\_Flt\_Pole2}}$ = Percentage of total line length from Station B to the fault location for conductor Pole 2

R_{Pole2} = Total resistance for conductor Pole 2

A_U_{dN1} = Station A voltage for conductor Neutral 1

B_U_{dN1} = Station B voltage for conductor Neutral 1

$A\_ I_{\text{dLH2}}$ = Station A current for conductor Pole 2

$B\_ I_{\text{dLH2}}$ = Station B current for conductor Pole 2

It can be seen that the Fault Distance Equation from Station A for the DMR 1 (Equation (3.5)) is very similar to the Fault Distance Equation from Station A for the Pole 2 (Equation (3.7)), thus the Fault Distance Equation from Station A can be generalized to Equation (3.9). Similarly, the Fault Distance Equation from Station B for the DMR 1 (Equation (3.6)) is very similar to the Fault Distance Equation from Station B for the Pole 2 (Equation (3.8)), therefore the Fault Distance Equation from Station B can be generalized to Equation (3.10).

$$X_{\mathrm{A\_Flt}\_x} = \frac{A\_U_{\mathrm{d}x} - B\_U_{\mathrm{d}x} + (B\_I_{\mathrm{d}x} \times R_x)}{R_x \times (-A\_I_{\mathrm{d}x} + B\_I_{\mathrm{d}x})} \qquad (3.9)$$

$$X_{\mathrm{B\_Flt}\_x} = \frac{B\_U_{\mathrm{d}x} - A\_U_{\mathrm{d}x} - (A\_I_{\mathrm{d}x} \times R_x)}{R_x \times (-A\_I_{\mathrm{d}x} + B\_I_{\mathrm{d}x})} \qquad (3.10)$$

where:

$X_{\mathrm{A\_Flt}\_x}$ = Percentage of total line length from Station A to the fault location for conductor x

$X_{\mathrm{B\_Flt}\_x}$ = Percentage of total line length from Station B to the fault location for conductor x

R_x = Total resistance for conductor x

$A\_U_{\mathrm{d}x}$ = Station A voltage for conductor x

$B\_U_{\mathrm{d}x}$ = Station B voltage for conductor x

$A\_I_{\mathrm{d}x}$ = Station A current for conductor x

$B\_I_{\mathrm{d}x}$ = Station B current for conductor x

The subscript "*x*" identifies the faulted conductor (DMR 1 or Pole 2).

It should be noted that the two Fault Distance Equations $X_{\mathrm{A\_Flt}\_x}$ and $X_{\mathrm{B\_Flt}\_x}$ are symmetric percentages. This means that $X_{\mathrm{A\_Flt}\_x}$ is equal to *100.0%* - $X_{\mathrm{B\_Flt}\_x}$ and vice versa where $X_{\mathrm{B\_Flt}\_x}$ is equal to *100.0%* - $X_{\mathrm{A\_Flt}\_x}$.

When the fault distance to the fault from the station is given the actual fault location can be calculated using Equation (3.11) and (3.12).

$$D_{\text{A\_Flt\_}x} = X_{\text{A\_Flt\_}x} \times L_x \quad (3.11)$$

$$D_{\text{B\_Flt\_}x} = X_{\text{B\_Flt\_}x} \times L_x \quad (3.12)$$

where:

$D_{\text{A\_Flt\_}x}$ = Distance from Station A to the fault location for conductor x

$D_{\text{B\_Flt\_}x}$ = Distance from Station B to the fault location for conductor x

$X_{\text{A\_Flt\_}x}$ = Percentage of total line length from Station A to the fault location for conductor x

$X_{\text{B\_Flt\_}x}$ = Percentage of total line length from Station B to the fault location for conductor x

L_x = Total length for conductor x

The subscript "*x*" identifies the faulted conductor (DMR 1 or Pole 2).

Furthermore, as the B_U_{dN1} was not provided for the EATL HVdc system, B_U_{dN1} can be determined by the measured ground resistance and the measured current through the ground B_I_{dSG} as seen in Equation (3.13)

$$B\_U_{\text{dN1}} = R_{\text{GND}} \times B\_I_{\text{dSG}} \quad (3.13)$$

where:

R_{GND} = Resistance of the ground electrode for Station B

B_U_{dN1} = Station B voltage for conductor Neutral 1

B_I_{dGS} = Station B current for ground electrode

3.4.4 Online Neutral Line Fault Locator Fault Distance Algorithm

For this analysis, the horizontal axis origin is Station A. Thus, a fault at Station A (i.e., the ungrounded station) will be at the beginning of the transmission line at a fault distance of 0.0%, while a fault at Station B (i.e., the grounded station) will be at the end of the transmission line at a fault distance of 100.0%. Thus, all calculated fault locations will be specified as a fault distance from Station A.

As discussed in the previous section, the Fault Distance Equations are derived assuming that the HVdc system is operating in a faulted steady-state condition. However, operating the HVdc system in the faulted steady-state condition after a fault could cause damage to the HVdc converters. To prevent such damage, the HVdc system's control and protection scheme reacts to clear the fault. The HVdc system's control and protection scheme can detect and respond to a fault event, in milliseconds, and take quick steps to clear the event by control action or by opening a breaker to isolate the faulted conductor. The clearing of the fault can be completed in less than one second if a breaker is opened on the return conductor(s). In general, the HVdc system's control and protection scheme will operate during the transient period, prior to the HVdc system reaching the faulted steady-state conditions.

Therefore, in the real world, HVdc protection must act rapidly to clear the fault and protect the HVdc system from damage. Hence it must operate in the transient period prior to the system reaching the faulted steady-state condition. Therefore, the voltage and the current measurements are only available in the initial transient period, referred to as the "Transient event data," must be used. The transient event data includes the measurements of:

- A_U_{dN1} = Station A voltage for conductor Neutral 1
- A_I_{dLH2} = Station A current for conductor Pole 2
- A_I_{dDMR1} = Station A current for conductor DMR 1
- B_I_{dLH2} = Station B current for conductor Pole 2
- B_I_{dDMR1} = Station B current for conductor DMR 1
- B_I_{dSG} = Station B current for ground electrode

Figure 3-18 shows the Station A DMR 1 current and Figure 3-19 the neutral voltage with protection and without protection. It should be noted that the DMR 1 is grounded only at

one end, so the pre-fault voltage on the DMR 1 is (-12) kV in this case, due to the line voltage drop. Three periods are identified:

- The pre-fault (steady state) period;
- The transient period;
- The post-transient period (faulted steady state). If the protection does not operate, the current would go to its steady-state faulted value.

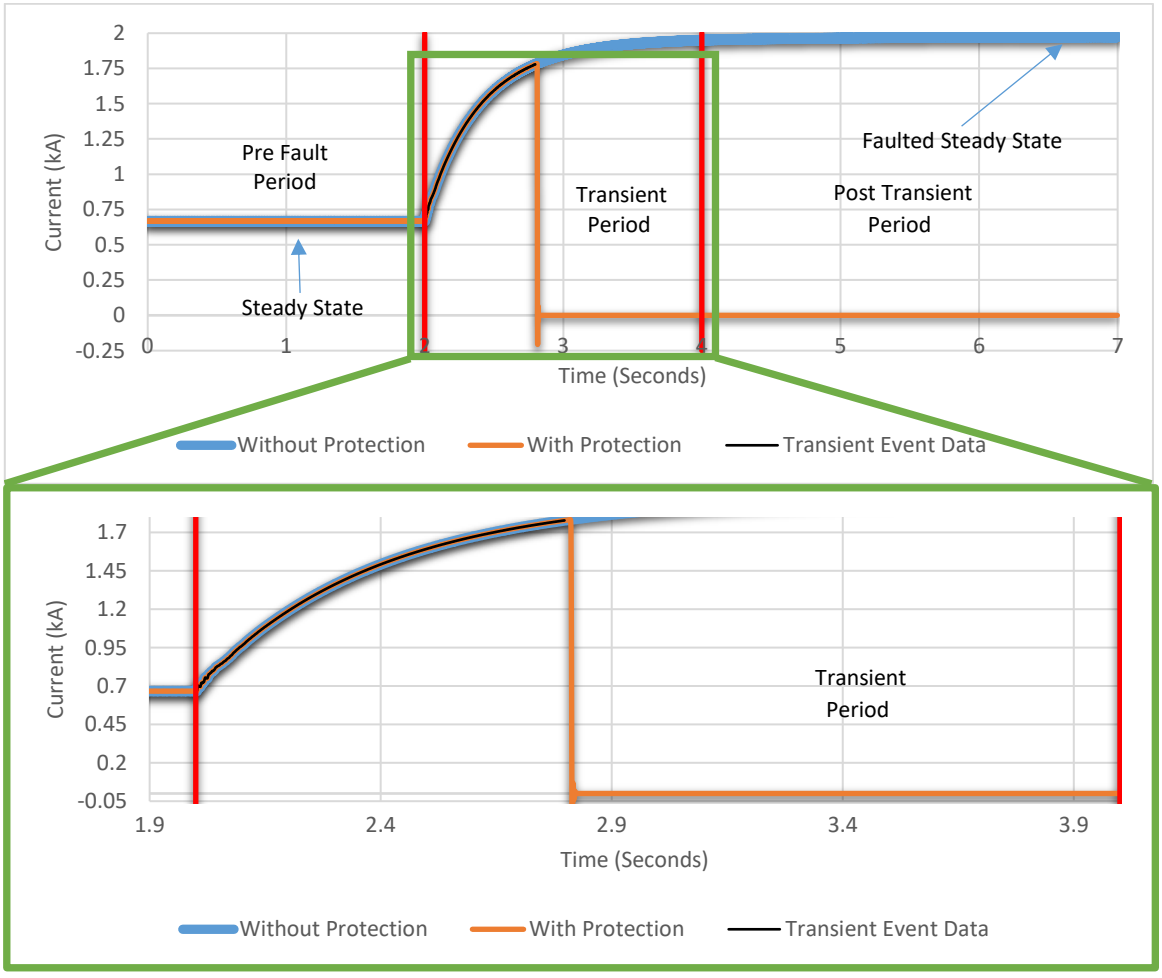

Figure 3-18: Station A DMR 1 current (A_I_{dDMR1}) with and without protection and showing transient event data.

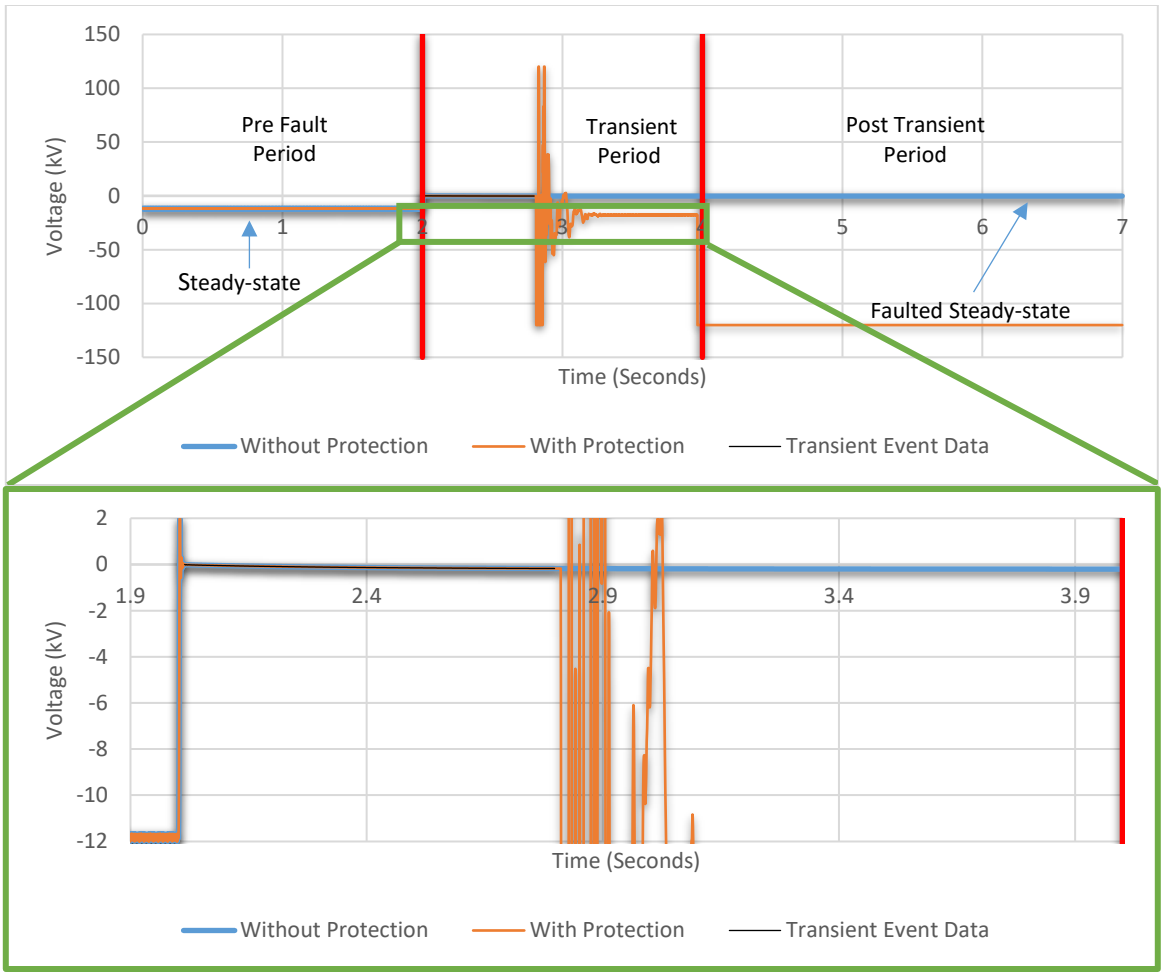

Figure 3-19: Station A neutral voltage (A_U_{dN1}) with and without protection showing transient event data.

Since the Fault Distance Equation requires the steady-state voltages and currents after the fault, the transient data must be used to estimate these values, i.e., the voltages and the currents that would have resulted if the system had been allowed to reach its faulted steady-state. To do this, regression analysis is used as discussed next.

3.4.4.1 Online Neutral Line Fault Locator Fault Distance Regression Algorithm

Regression is a statistical method used to characterise the relationship between a related set of data points. In an HVdc system the current and the voltage measurements taken during a transient fault event have a strong characteristic relationship. This relationship can be

correlated by using regression to determine a characteristic response equation for the current and the voltage measurements.

Detailed simulations have shown that the DMR 1 and the Pole 2 conductor currents and voltages have (e.g., Figure 3-20 and Figure 3-21) a predominantly decaying exponential response with time. Therefore, the current and the voltage measurements taken at the ungrounded station can be fitted to an exponential proportional rate growth or decrease function as shown in Equation (3.14) and illustrated in Figure 3-20 and Figure 3-21.

As the current and the voltage waveforms are assumed to have the form of an exponential proportional rate growth or decrease function as shown in Equation (3.14). It is then assumed that the remainder of the waveform which would have resulted at time (*t*) greater than the transient (i.e., without protection action), would also be predictable by the exponential proportional rate growth or decrease function. If Equation (3.14) is used, then steady-state current or voltage $y(\infty) = \lim_{t\to\infty} y(t) = \left(Y_0 - \frac{V_0}{K}\right)$.

$$y(t) = Y_0 - \frac{V_0}{K} \times (1 - e^{-Kt}) \qquad (3.14)$$

where:

y = Curve fit value

t = Time in seconds

Y_0 = Fitting parameter 1

V_0 = Fitting parameter 2

K = Fitting parameter 3

To demonstrate the computation process, the DMR 1 current and the neutral voltage from the transient event data are examined. The regression based response of the DMR 1 current and the neutral voltage using only the transient event data collected for the DMR 1

current and the neutral voltage waveform without protection can be seen in Figure 3-20 and Figure 3-21. Figure 3-20 and Figure 3-21 shows that the regression based curve fitting process, can accurately determine the DMR 1 current and the neutral voltage in the faulted steady-state condition using only the transient event data collected during the transient period.

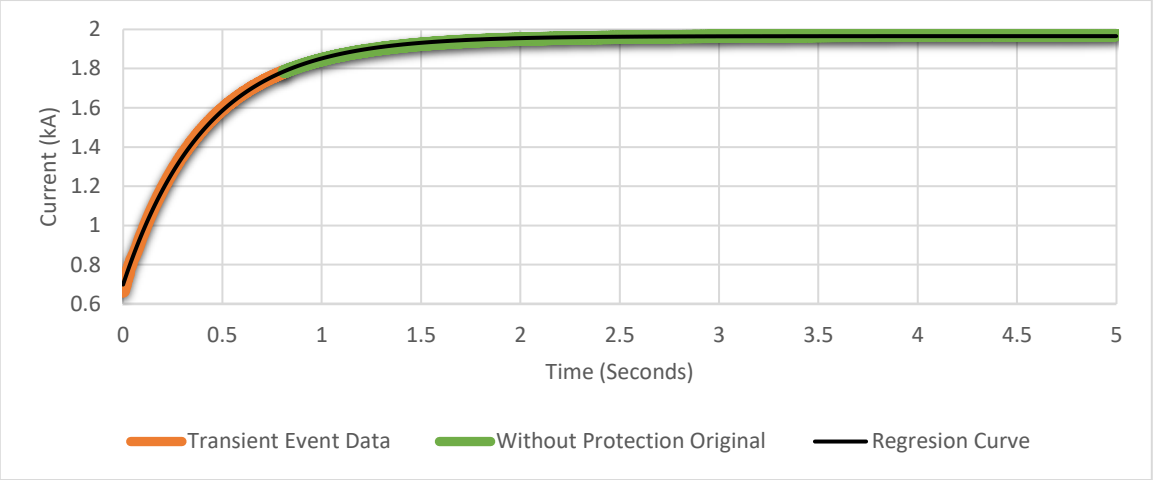

Figure 3-20: Regression based projection of the Station A DMR 1 current (A_I_{dDMR1}) without protection developed from transient event data.

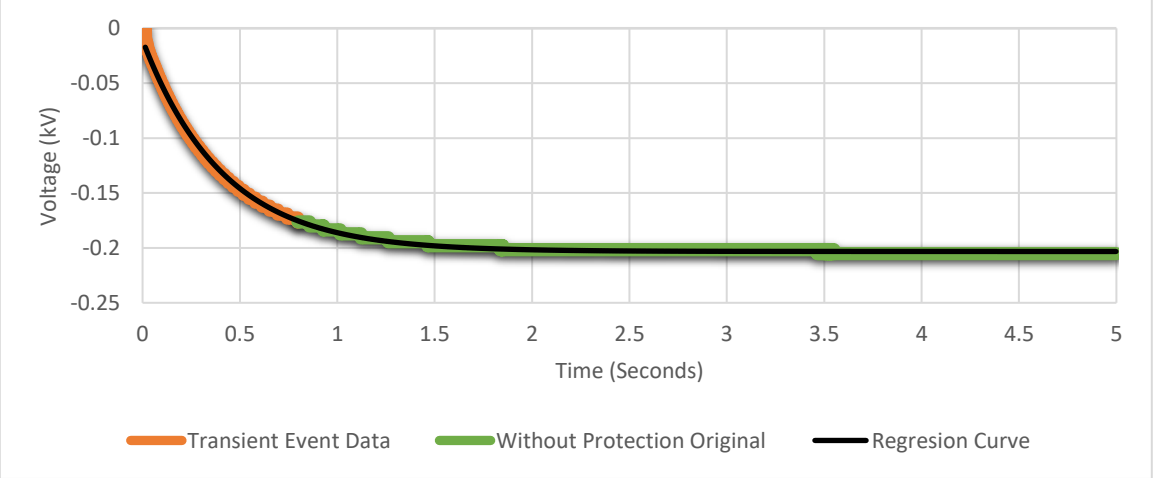

Figure 3-21: Regression based projection of the Station A neutral voltage (A_U_{dDMR1}) without protection developed from transient event data.

However, to evaluate the Fault Distance Equation (3.9) or (3.10) ($X_{A\_Flt\_x}$ or $X_{B\_Flt\_x}$), the estimated values of the equation's variables (A_U_{dx}, A_I_{dx}, B_I_{dx}, and B_U_{dx}[2]) are needed. Therefore, it is possible for small errors in each of these estimates to be compounded. To avoid the compounding errors in the calculation, regression analysis can be used to fit the time evolution of the Fault Distance Equation ($X_{A\_Flt\_x}$ or $X_{B\_Flt\_x}$) itself, where each (time) point of $X_{A\_Flt\_x}$ or $X_{B\_Flt\_x}$ is obtained from either Equation (3.9) or (3.10) with A_U_{dx}, A_I_{dx}, B_I_{dx}, and B_U_{dx}[2] being the instantaneous values during the transient as shown in Figure 3-22 and Figure 3-23. This method can reduce the compounding of errors caused by the derivation of each of the voltages and the currents in the faulted steady-state condition, before calculating the Fault Distance Equation. The asymmetrical sigmoidal function shown in Equation (3.15) is used to model the time varying response of the Fault Distance Equation ($X_{A\_Flt\_x}$ or $X_{B\_Flt\_x}$). For the asymmetrical sigmoidal function shown in Equation (3.15), the steady-state fault distance is $y(\infty) = \lim_{t\to\infty} y(t) = d$.

$$y(t) = d + \frac{a - d}{\left[1 + \left(\frac{t}{c}\right)^{b}\right]^{m}} \qquad (3.15)$$

where:

- y = Curve fit value
- t = Time in seconds
- a = Fitting parameter 1
- b = Fitting parameter 2
- c = Fitting parameter 3
- d = Fitting parameter 4
- m = Fitting parameter 5

[2] If B_U_{dx} is not measured, then B_U_{dx} can be calculated as $B\_U_{dx} = R_{GND} \times B\_I_{dSG}$ is used.

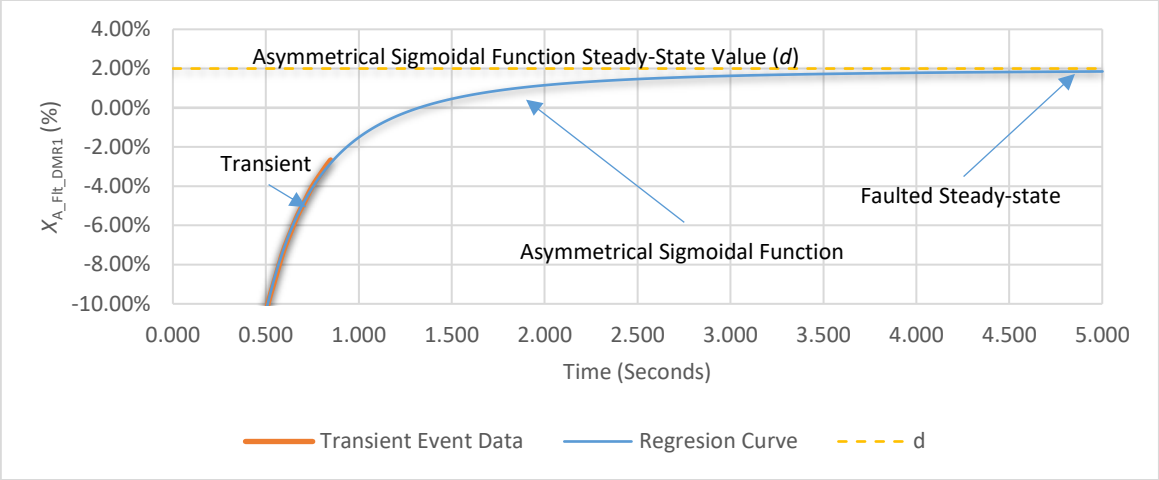

Figure 3-22: Recorded (transient) and fitted fault position error, for a DMR 1 conductor fault located at 2.0% of the transmission line length from Station A that is operating at 100 MW.

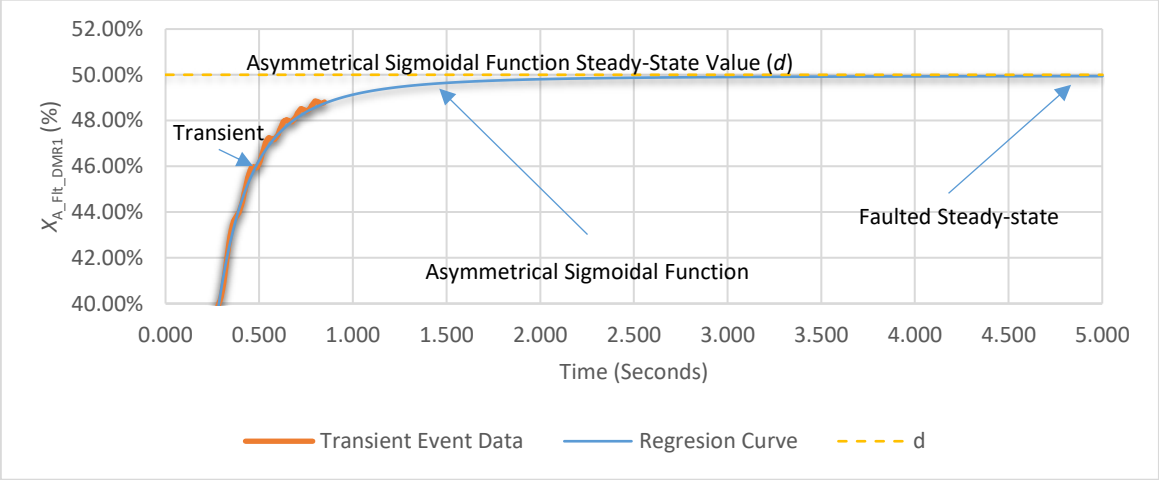

Figure 3-23: Recorded (transient) and fitted fault position error, for a DMR 1 conductor fault located at 50.0% of the transmission line length from Station A that is operating at 100 MW.

The time varying response of the Fault Distance Equations must follow the time varying response of the Fault Distance Equations' variables. The dominant variables of the Fault Distance Equations are A_I_{dx} and B_I_{dx}. In the post transient period B_I_{dx} dominates the Fault Distance Equation and B_I_{dx} has an asymmetrical sigmoidal response to a fault. Therefore, the time varying response of the Fault Distance Equations is an asymmetrical sigmoidal function as illustrated in Figure 3-22 and Figure 3-23. The fitting parameter for an

asymmetrical sigmoidal function for faults on the DMR 1 and the error in the calculated fault location are listed in Table 3-2.

Table 3-2 Time varying Fault Distance Equation asymmetric sigmoidal variables.

Fault Distance (%)	a	b	c	d	m	Error (%)
0%	-10.7194	16.0092	1.2772	-0.0007	0.1568	0.067%
2%	-10.5981	15.8532	1.2629	0.0195	0.1575	0.053%
25%	-9.7213	15.6399	1.2354	0.2485	0.1746	0.153%
50%	-8.6483	15.1168	1.1565	0.4995	0.1948	0.047%
75%	-51740.2619	0.2486	4706.9670	0.7496	80.6409	0.041%
90%	0.3335	77.6773	5.0658	0.9036	0.0932	0.367%
95%	0.6071	74.8515	5.0406	0.9459	0.1008	0.413%
98%	0.9559	71.0915	4.5086	0.9764	2.1969	0.363%
100%	0.99991	40.31028	0.59043	1.00003	1.67155	0.003%

The resistance of the conductor required for the Fault Distance Equation can be calculated from the pre fault measurements. The active calculation of the conductor resistance from the pre fault period is done to mitigate changes in the conductor resistance. Factors such as aging and changes in the environmental condition (i.e., temperature) can affect the conductor resistance [49], [50].

In summary, since the HVdc system's control and protection scheme will activate to protect the HVdc system from damage, only the transient fault data collected during the transient period is available to calculate the fault location. Since the transient fault data is the only data available to calculate the fault location, the Fault Distance Equation must be

evaluated with the transient fault data and then curve fitted to a known characteristic time response using the regression-based curve fitting process. The equation derived from the characteristic time response of the Fault Distance Equation can be used to calculate, the fault distance for a time $t \rightarrow \infty$ in the post transient period. The analytical process of the nLFL is illustrated in Figure 3-24.

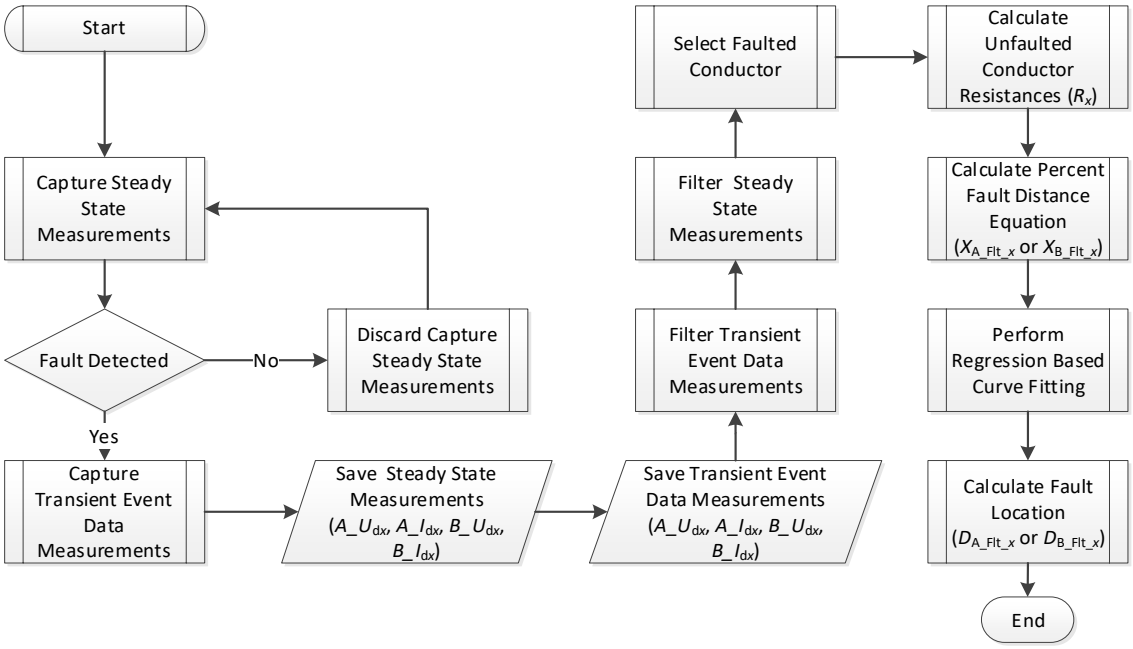

Figure 3-24: Online Neutral Line Fault Locator (nLFL) Algorithm.

3.4.4.2 Online Neutral Line Fault Locator Selection of the Sampling Time and the Accuracy

The current and the voltage measurements taken closer to the grounded station require less time to settle to their faulted steady-state values, than the current and the voltage measurements taken at the ungrounded station (e.g., settling time for the case of Station B DMR 1 current (B_I_{dDMR1}) in Figure 3-25 is smaller than that of Station A DMR 1 current (A_I_{dDMR1}) in Figure 3-25). This shortened settling time at the grounded station, is a result of

the parallel grounding paths between the station's ground and the faulted conductor that is grounded.

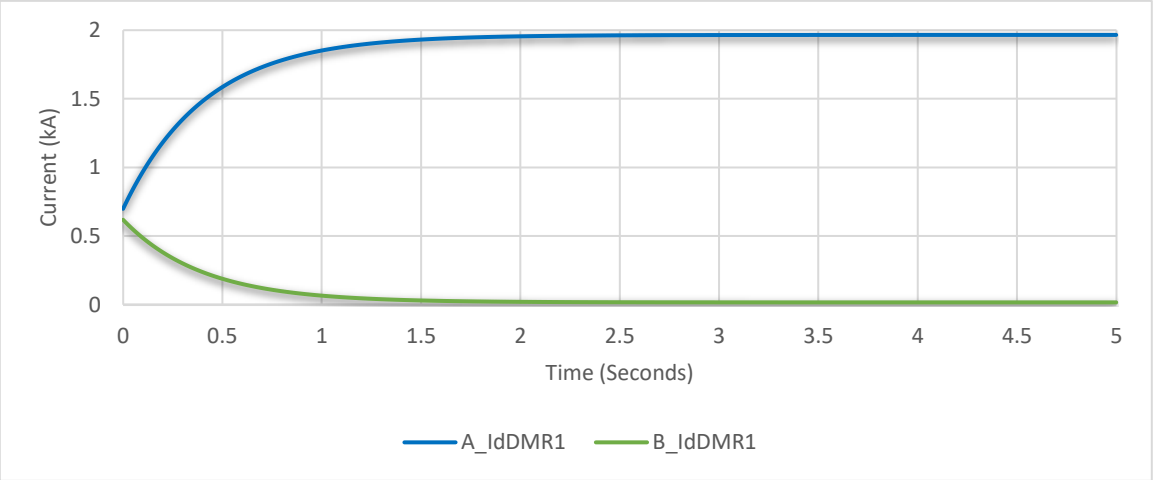

Figure 3-25: DMR 1 current settling time comparison for Station A (A_I_{dDMR1}) and Station B (B_I_{dDMR1}) for a fault at Station A.

Similarly, the fault location also determines the inductance and capacitance of the remaining transmission line sections and causes the stretching or the compression of the transient period. Figure 3-22 and Figure 3-23 show the transient response of $X_{A\_Flt\_DMR1}$ for faults at 2% and 50% of the line lengths. From these plots, it takes $X_{A\_Flt\_DMR1}$ more time to settle to its faulted steady-state value for faults near the ungrounded station (i.e., Station A located at 0% of the line length), than faults near the grounded station (i.e., Station B located at 100% of the line length).

Observations show that collecting insufficient data from the transient period could severely reduce the accuracy of the nLFL as the time varying response of the Fault Distance Equation may not be determinable from too small a transient event data period.

Given the observations discussed above, an acceptable transient event data period must be determined for suitable operation of the nLFL. Figure 3-26 shows the impact of increasing

the transient event period on the estimation of the steady-state Fault Distance Equation value ($X_{A\_Flt\_x}$ or $X_{B\_Flt\_x}$). The transient event data used for this analysis is captured at a rate of 100,000 samples per second (1 sample every 10 μs). The accuracy of the determined steady-state value of $X_{A\_Flt\_x}$ or $X_{B\_Flt\_x}$ is improved if the initial transient period in which samples are taken is increased. Hence, it is necessary to obtain a sample set over a sufficiently large transient interval. If this interval is too small, the errors can be large. If an accuracy of less than 1% is desired, Figure 3-26 shows that using a period of at least 650 ms is necessary. In this implementation 900 ms was used, as it resulted in an average error of approximately 0.5%. A typical present day existing commercial neutral or DMR fault locator would be a single ended offline active system using traveling waves (also referred to as "Time domain reflectometry" or "Pulse echo" fault location) and would have an accuracy less than 1% or 2% [51], [52], [53]. Thus, the proposed nLFL can meet the currently available specifications for commercial neutral or DMR fault locators. It should be noted that these commercial fault locators are restricted to faults located at a maximum distance of 200.0 km to 300.0 km [51], while the nLFL will be shown to be suitable for fault locations up to 1000.0 km.

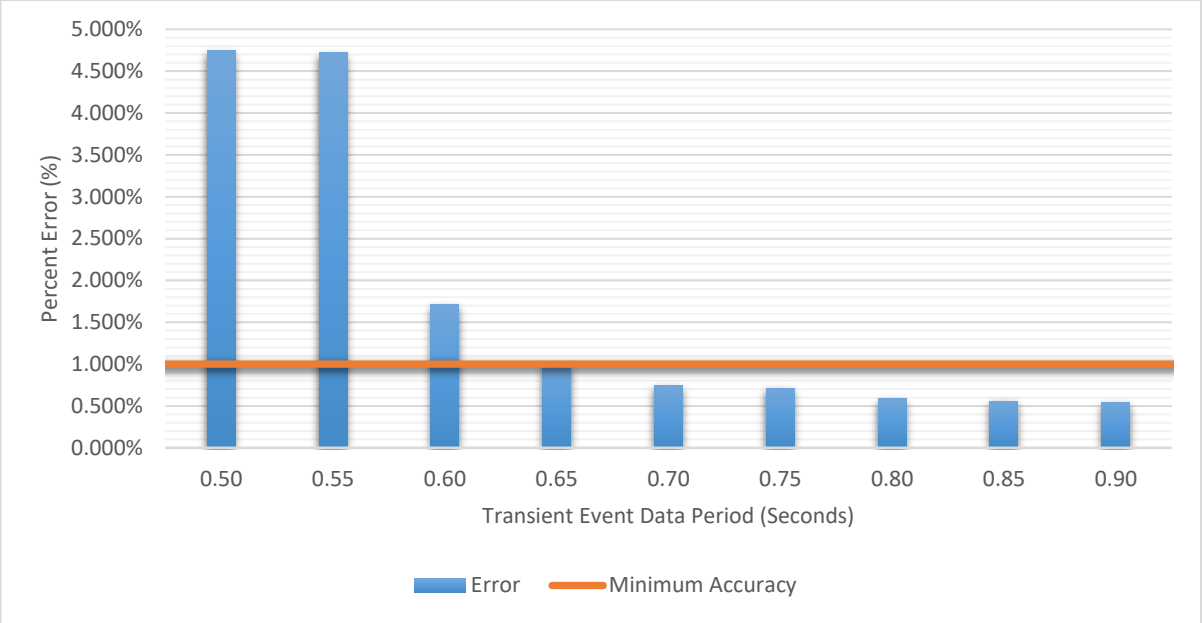

Figure 3-26: Average fitting error (considering several fault locations) as a function of transient event recording interval length.

3.4.4.3 Other Contributors to the Accuracy of the Online Neutral Line Fault Locator

Another, vital component to the accuracy of the nLFL, is the level of noise in the voltages and the currents collected in the transient event data period. If the noise in the transient fault data is too large, then it will mask the characteristic response of the system, thereby preventing the modeling of the time response of the Fault Distance Equation and invalidating the fault location calculation. Therefore, the signal to noise ratio must be as minimal as possible to allow for correct interpretation of the Fault Distance Equations' time response. The filtering of the transient fault data is required to reduce the signal to noise ratio for calculation. However, the filtering must not add any additional distortions, such as stretching or compression or shifting to the transient fault data. These types of distortions could change the characteristic response of the Fault Distance Equation.

The accuracy and resolution of the measurement equipment used in the HVdc system to capture the voltage and the current measurements is another key aspect to the accuracy of

the nLFL system. The accuracy of the nLFL system is only as good as the measurement data it uses to calculate the fault location. Therefore, if the voltage and the current measurement equipment has poor accuracy, then the accuracy of the nLFL's fault location system will also be poor. This will lead to incorrect fault locations. Therefore, selection of voltage and current measurement equipment with high accuracy and resolution will enhance the performance of the nLFL system.

Overall, given a sufficient transient fault data period with minimal noise and sufficient resolution of the measured values, the regression of the Fault Distance Equation can be used to determine the faulted steady-state condition of the HVdc system. This allows the nLFL system to calculate a fault location with an acceptable accuracy. The studies conducted will be discussed in Chapter 5: Online Neutral Line Fault Locator (nLFL) Testing and Performance Analysis.

3.4.4.4 The Impact of the Fault Resistance (R_{Flt}) on the Online Neutral Line Fault Locator

As discussed in Section 3.4.4, the nLFL uses regression on the transient measurements of the fault distances ($X_{A\_Flt\_x}$ or $X_{B\_Flt\_x}$), to determine the steady state fault location of the HVdc system. Regression analysis is necessary to estimate the steady state values, since the HVdc system's protective action clears the fault before the actual steady state is reached. This section investigates the sensitivity of $X_{A\_Flt\_x}$ and $X_{B\_Flt\_x}$ to changes in the fault resistance (R_{Flt}) ranging from 0.1 Ω to 10 Ω.

It has been stated that the double ended fault location method implemented by the nLFL is not affected by changes in the R_{Flt}. This statement was made since $X_{A\_Flt\_x}$ and $X_{B\_Flt\_x}$ does

not reference the fault resistance. Thus, mathematically the specific value of R_{Flt} does not impact the calculation of the fault distance.

However, as it will be shown in this section, R_{Flt} does impact the settling time of $X_{A\_Flt\_DMR1}$ to converge to its steady state value. A change in the fault resistance changes the voltage drop across the faulted section of the conductor. Thus, an increase (decrease) in R_{Flt} will result in a decrease (increase) in the voltage across the faulted section of the conductor. This results in a decrease (increase) in the transient period. Figure 3-27 depicts the simulation results showing the different convergence rates for $X_{A\_Flt\_DMR1}$ for R_{Flt} ranging from 0.1 Ω to 10 Ω. It is clear that the larger the resistance, the faster the convergence. The fault is applied at $t_0 = 0$ at the 2% location (i.e., very close to the ungrounded station, which results in the longest settling time as discussed in Section 3.4.4.2)

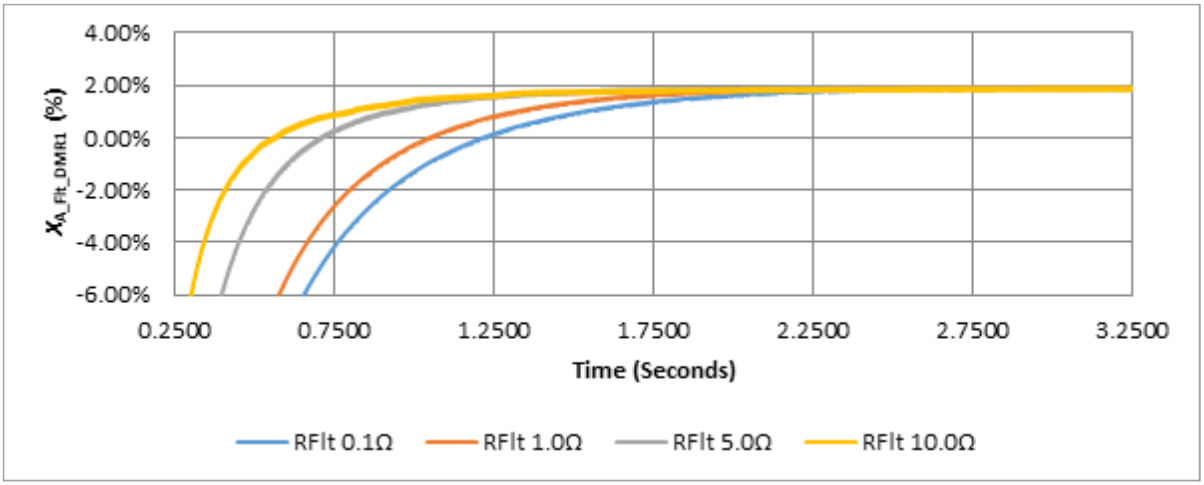

Figure 3-27: The response of the fault distance to a DMR 1 conductor fault located at 2% of the total line length from Station A for fault resistances varied between 0.1 Ω to 10 Ω, when the HVdc system is operating at 1000 MW.

As discussed in Section 3.4.4.2 there is only a short time window available for the regression based curve fitting process owing to the fact that the protection system will respond to disconnect the neutral conductor and thereby prohibiting further measurements. This time

will depend on the HVdc system's configuration and the breaker properties. From the above discussion, it is clear that a smaller R_{Flt} increases the transient period for the HVdc system to reach the faulted steady state. In Chapter 5: Online Neutral Line Fault Locator (nLFL) Testing and Performance Analysis, it will be shown, that for R_{Flt} = 0.1 Ω, a window of 900 ms would maintain a target accuracy of under 1.0%. Based on the discussion in this section, the 900 ms window would be sufficient for the nLFL system to calculate an accurate fault location for a variety of R_{Flt} values. Table 3-3 shows the calculated fault location for $X_{A\_Flt\_DMR1}$ for R_{Flt} ranging from 0.1 Ω to 10 Ω. The result confirms that $X_{A\_Flt\_DMR1}$ converges to the expected fault location in all cases of R_{Flt} with an acceptable error when a measurement window of 900 ms is used.

Table 3-3: Computed fault distance to a fault located at 2% of the total line length for fault resistances varied between 0.1 Ω to 10 Ω.

Fault Resistance (R_{Flt})	**$X_{A\_Flt\_DMR1}$ at time $t \rightarrow \infty$**
0.1	2.015%
1.0	2.002%
5.0	1.951%
10.0	1.946%

3.5 Online Neutral Line Fault Locator Sensitivity for the Fault Distance Equations

3.5.1 Sensitivity of the Fault Distance Equations to the Pre-Fault Conductor Resistance (R_x)

The fault distance ($X_{A\_Flt\_x}$ or $X_{B\_Flt\_x}$) derived from Equation (3.9) and (3.10) are sensitive to changes in the pre-fault conductor resistance (R_x) as they are a ratio between the pre-fault and the post-fault resistance of the transmission line. Thus, an error in R_x will cause

an error in the calculated fault distance. The sensitivity of $X_{A\_Flt\_x}$ and $X_{B\_Flt\_x}$ to a percentage change of -5.0% to 5.0% in R_x is listed in Table 3-4 and illustrated in Figure 3-28 for a fault at Station A.

Table 3-4: Sensitivity of the fault distance ($X_{A\_Flt\_x}$ and $X_{B\_Flt\_x}$) to changes in the pre-fault conductor resistance (R_x) for a fault at Station A.

R_x	$X_{A\_Flt\_x}$ Error (%)	$X_{B\_Flt\_x}$ Error (%)
Original	0.0000%	0.0000%
5.0%	0.0577%	-0.0577%
4.5%	0.0522%	-0.0522%
4.0%	0.0466%	-0.0466%
3.5%	0.0410%	-0.0410%
3.0%	0.0353%	-0.0353%
2.5%	0.0295%	-0.0295%
2.0%	0.0238%	-0.0238%
1.5%	0.0179%	-0.0179%
1.0%	0.0120%	-0.0120%
0.5%	0.0060%	-0.0060%
0.0%	0.0000%	0.0000%
-0.5%	-0.0061%	0.0061%
-1.0%	-0.0122%	0.0122%
-1.5%	-0.0184%	0.0184%
-2.0%	-0.0247%	0.0247%
-2.5%	-0.0311%	0.0311%
-3.0%	-0.0375%	0.0375%
-3.5%	-0.0439%	0.0439%
-4.0%	-0.0505%	0.0505%
-4.5%	-0.0571%	0.0571%
-5.0%	-0.0638%	0.0638%

Legend	
Map	Error Description
	Max Positive Error
	Zero Error
	Max Negative Error

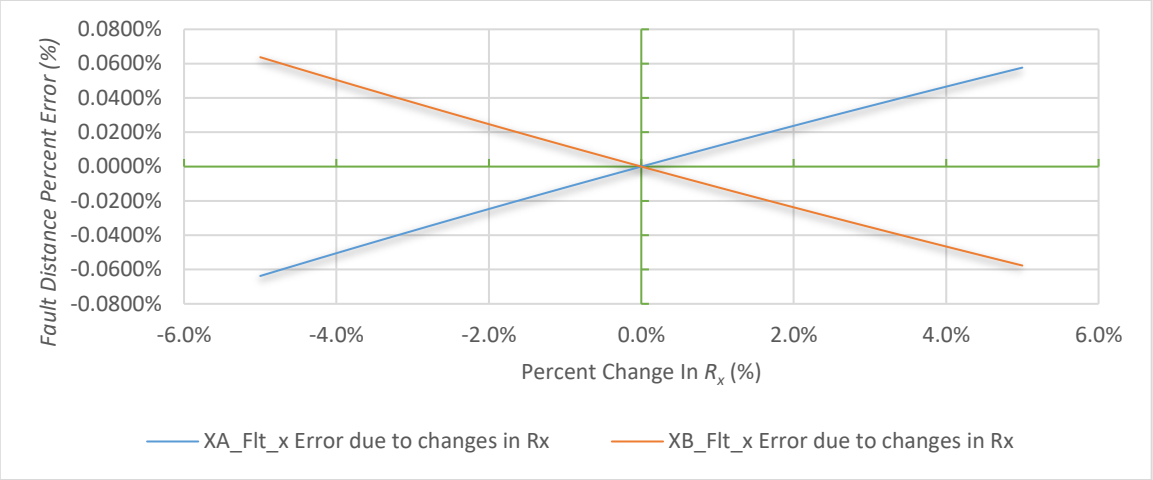

Figure 3-28: Sensitivity of the fault distance ($X_{A\_Flt\_x}$ and $X_{B\_Flt\_x}$) to changes in the pre-fault conductor resistance (R_x) for a fault at Station A.

R_x changes with the environmental conditions and the loading conditions of the transmission line. More specifically, the environmental temperature and the temperature rise owing to the loading of the transmission line can change R_x. The linear temperature approximation for resistivity in Equation (3.16) can be used to calculate the resistance of the transmission line owing to temperature changes on the transmission line conductors [54]. This makes the use of a fixed R_x value impractical. Thus, if an online calculation of R_x can be conducted on a continuous basis, its most recent value prior to the fault event would be available for the precise environmental and loading conditions. This will yield a more accurate calculation of the fault location.

$$\rho(T) = \rho_0\big(1 + \alpha(T - T_0)\big) \qquad (3.16)$$

where:

ρ = Conductor resistivity as a function of temperature

ρ_0 = Conductor resistivity at ambient temperature T_0

T = Current temperature

T_0 = Ambient temperature

α = Temperature coefficient of resistivity

As the fault distance ($X_{A\_Flt\_x}$ or $X_{B\_Flt\_x}$) are symmetric with respect to the fault location (i.e., $X_{A\_Flt\_x}$ + $X_{B\_Flt\_x}$ = 100%), the error due to an error in R_x is also symmetric. Hence the traces of $X_{A\_Flt\_x}$ and $X_{B\_Flt\_x}$ in Figure 3-28 have the same magnitude, but opposite signs for any percent change in R_x.

3.5.1.1 Rationalization for the Sensitivity Results of $X_{A\_Flt\_x}$ and $X_{B\_Flt\_x}$ with Respect to R_x

The simulated observations of the previous sub-section can be rationalized by mathematically calculating the sensitivity of the fault distance ($X_{A\_Flt\_x}$ or $X_{B\_Flt\_x}$) to the pre-fault conductor resistance (R_x). To do this, we calculate the partial derivative of $X_{A\_Flt\_x}$ and $X_{B\_Flt\_x}$ with respect to R_x in Equations (3.17) and (3.18) respectively. As $\frac{\partial X_{A\_Flt\_x}}{\partial R_x}$ and $\frac{\partial X_{B\_Flt\_x}}{\partial R_x}$ are both sensitive to the inverse square of R_x, which means that as the transmission line becomes longer $X_{A\_Flt\_x}$ and $X_{B\_Flt\_x}$ are less sensitive to changes in R_x.

$$\frac{\partial X_{\text{A\_Flt\_}x}}{\partial R_x} = \frac{-A\_U_{\text{d}x} + B\_U_{\text{d}x}}{{R_x}^2 \times (-A\_I_{\text{d}x} + B\_I_{\text{d}x})} \tag{3.17}$$

$$\frac{\partial X_{\text{B\_Flt\_}x}}{\partial R_x} = \frac{-B\_U_{\text{d}x} + A\_U_{\text{d}x}}{{R_x}^2 \times (-A\_I_{\text{d}x} + B\_I_{\text{d}x})} \tag{3.18}$$

where:

$X_{\text{A\_Flt\_}x}$ = Percentage of total line length from Station A to the fault location for conductor x

$X_{\text{B\_Flt\_}x}$ = Percentage of total line length from Station B to the fault location for conductor x

R_x = Total resistance for conductor x

$A\_U_{\text{d}x}$ = Station A voltage for conductor x

$B\_U_{\text{d}x}$ = Station B voltage for conductor x

$A\_I_{\text{d}x}$ = Station A current for conductor x

$B\_I_{\text{d}x}$ = Station B current for conductor x

The subscript "*x*" identifies the faulted conductor (DMR 1 or Pole 2).

3.5.2 Sensitivity of the Fault Distance Equations to the Electrode Ground Resistance (R_{GND})

The fault distance ($X_{\text{A\_Flt\_}x}$ or $X_{\text{B\_Flt\_}x}$) derived from Equation (3.9) and (3.10) where $B\_U_{\text{d}x}$ is substituted for Equation (3.13) are not very sensitive to changes in the electrode ground resistance (R_{GND}) as the electrode ground resistance is designed to be very small, to facilitate the correct operation of the control and protection systems. This results in a very small voltage at the grounded station, and therefore R_{GND} should have a very small impact on the calculation of the Fault Distance Equations. Thus, an error in R_{GND} is not expected to cause a very large error in the calculated fault distance. The sensitivity of $X_{\text{A\_Flt\_}x}$ and $X_{\text{B\_Flt\_}x}$ to a percentage change of -5.0% to 5.0% in R_{GND} is listed in Table 3-5 and illustrated in Figure 3-29, and the maximum error is a mere 0.01%.

Table 3-5: Sensitivity of the fault distance ($X_{A\_Flt\_x}$ and $X_{B\_Flt\_x}$) to changes in the ground electrode resistance (R_{GND}) for a fault at Station A.

R_{GND}	$X_{A\_Flt\_x}$ Error (%)	$X_{B\_Flt\_x}$ Error (%)
Original	0.0000%	0.0000%
5.0%	-0.0057%	0.0057%
4.5%	-0.0051%	0.0051%
4.0%	-0.0046%	0.0046%
3.5%	-0.0040%	0.0040%
3.0%	-0.0034%	0.0034%
2.5%	-0.0028%	0.0028%
2.0%	-0.0023%	0.0023%
1.5%	-0.0017%	0.0017%
1.0%	-0.0011%	0.0011%
0.5%	-0.0006%	0.0006%
0.0%	0.0000%	0.0000%
-0.5%	0.0006%	-0.0006%
-1.0%	0.0011%	-0.0011%
-1.5%	0.0017%	-0.0017%
-2.0%	0.0023%	-0.0023%
-2.5%	0.0028%	-0.0028%
-3.0%	0.0034%	-0.0034%
-3.5%	0.0040%	-0.0040%
-4.0%	0.0046%	-0.0046%
-4.5%	0.0051%	-0.0051%
-5.0%	0.0057%	-0.0057%

Legend	
Map	Error Description
	Max Positive Error
	Zero Error
	Max Negative Error

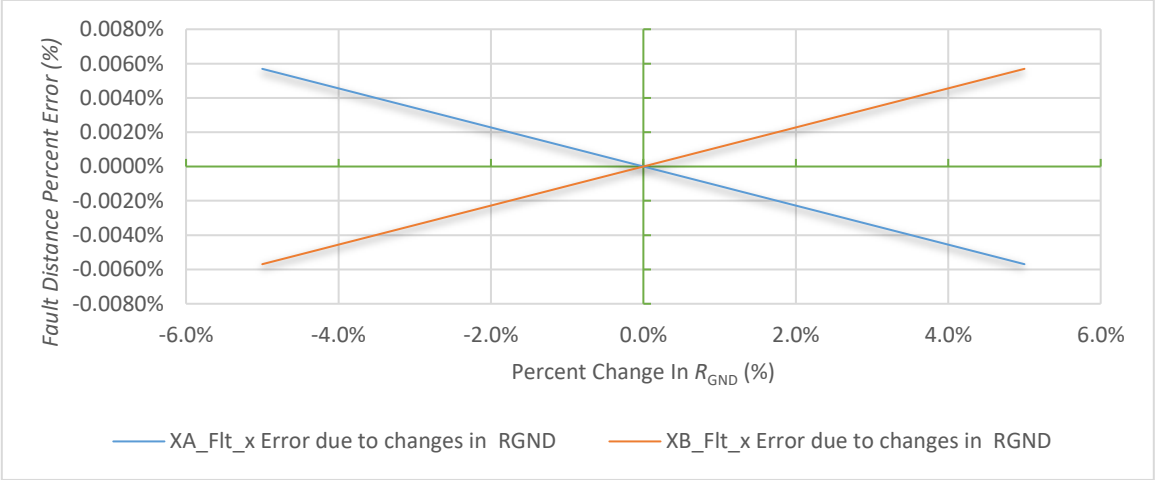

Figure 3-29: Sensitivity of the fault distance ($X_{A\_Flt\_x}$ and $X_{B\_Flt\_x}$) to changes in the ground electrode resistance (R_{GND}) for a fault at Station A.

Corrosion of the electrode can result in changes in the R_{GND} [16], [55]. Electrode corrosion is primarily due to the use of the electrode as part of the current path. However, as the DMR is present in these systems the earth return path should rarely be used and therefore, the corrosion of the electrode should be much slower over time. Furthermore, as R_{GND} has little impact on the calculation of $X_{A\_Flt\_x}$ or $X_{B\_Flt\_x}$, the changes due to corrosion have a marginal impact on the calculated fault distance.

Similar to the discussion of sensitivity of $X_{A\_Flt\_x}$ and $X_{B\_Flt\_x}$ to R_x as discussed in Section 3.5.1 above, $X_{A\_Flt\_x}$ and $X_{B\_Flt\_x}$ are also symmetric with respect to the fault location (i.e., $X_{A\_Flt\_x} + X_{B\_Flt\_x} = 100\%$), the error due to an error in R_{GND} is also symmetric. Hence the traces of $X_{A\_Flt\_x}$ and $X_{B\_Flt\_x}$ in Figure 3-29 have the same magnitude, but opposite signs for any percent change in R_{GND}.

3.5.2.1 Rationalization for the Sensitivity Results of $X_{A\_Flt\_x}$ and $X_{B\_Flt\_x}$ with Respect to R_{GND}

The simulated observations of the previous sub-section regarding the sensitivity to location prediction due to the electrode ground resistance (R_{GND}) can be rationalized by mathematically calculating the partial derivatives $\frac{\partial X_{A\_Flt\_x}}{\partial R_{GND}}$ and $\frac{\partial X_{B\_Flt\_x}}{\partial R_{GND}}$. Note that $\frac{\partial X_{A\_Flt\_x}}{\partial R_{GND}}$ and $\frac{\partial X_{B\_Flt\_x}}{\partial R_{GND}}$ are both sensitive to the inverse of R_x, which means that as the transmission line becomes longer $X_{A\_Flt\_x}$ and $X_{B\_Flt\_x}$ are less sensitive to changes in R_{GND}. Furthermore, $\frac{\partial X_{A\_Flt\_x}}{\partial R_{GND}}$ and $\frac{\partial X_{B\_Flt\_x}}{\partial R_{GND}}$ are both sensitive to changes in Station B ground current (B_I_{dSG}). Therefore, any error in the B_I_{dSG} will translate to an error in R_{GND} and cause an error in the calculation of $X_{A\_Flt\_x}$ or $X_{B\_Flt\_x}$.

$$\frac{\partial X_{\text{A\_Flt\_}x}}{\partial R_{\text{GND}}} = -\frac{B\_I_{\text{dSG}}}{R_x \times (-A\_I_{\text{d}x} + B\_I_{\text{d}x})} \quad (3.19)$$

$$\frac{\partial X_{\text{B\_Flt\_}x}}{\partial R_{\text{GND}}} = -\frac{B\_I_{dSG}}{R_x \times (-A\_I_{\text{d}x} + B\_I_{\text{d}x})} \quad (3.20)$$

where:

$X_{\text{A\_Flt\_}x}$ = Percentage of total line length from Station A to the fault location for conductor x

$X_{\text{B\_Flt\_}x}$ = Percentage of total line length from Station B to the fault location for conductor x

R_x = Total resistance for conductor x

R_{GND} = Resistance of the ground electrode for Station B

$A\_I_{\text{d}x}$ = Station A current for conductor x

$B\_I_{\text{d}x}$ = Station B current for conductor x

B_I_{dSG} = Station B current for ground electrode

The subscript "*x*" identifies the faulted conductor (DMR 1 or Pole 2).

3.5.3 Individual Sensitivity of the Fault Distance Equations to the Terminal Voltage and Line Current Measurements

The fault distance ($X_{\text{A\_Flt\_}x}$ or $X_{\text{B\_Flt\_}x}$) derived from Equation (3.9) and (3.10) are sensitive to changes in the individual voltages (i.e., $A\_U_{\text{d}x}$ and $B\_U_{\text{d}x}$) and line currents (i.e., $A\_I_{\text{d}x}$ and $B\_I_{\text{d}x}$) at Stations A and B, respectively.

The Station A conductor voltage ($A\_U_{\text{d}x}$) is floating and represents the voltage drop across the entire faulted transmission line and the fault resistance. Thus, an error in $A\_U_{\text{d}x}$ will cause an error in the calculated fault distance. The sensitivity of $X_{\text{A\_Flt\_}x}$ to a percentage change of -5.0% to 5.0% in $A\_U_{\text{d}x}$ is illustrated in Figure 3-30.

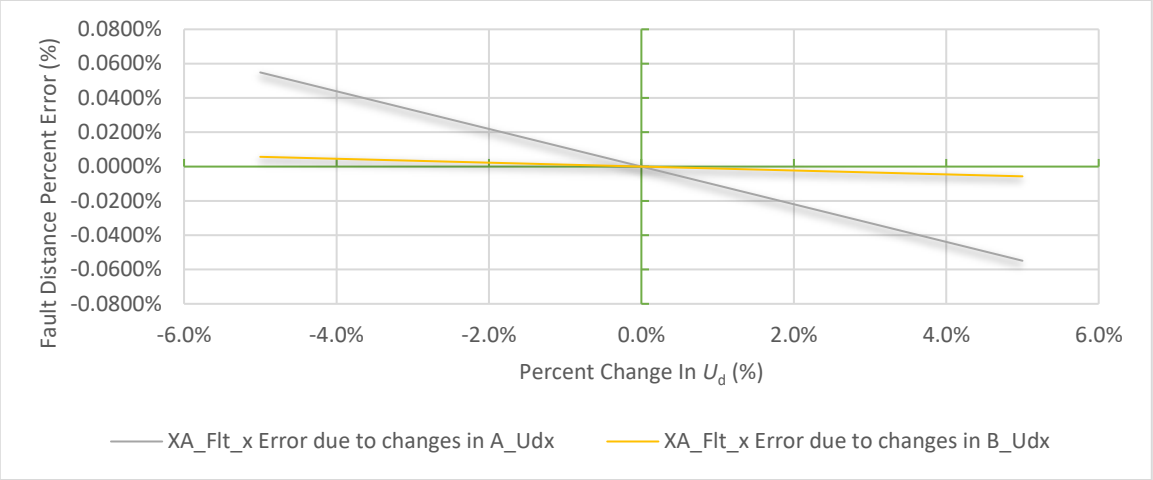

Figure 3-30: Sensitivity of the fault distance ($X_{A\_Flt\_x}$) to changes in the individual voltages (A_U_{dx} and B_U_{dx}) for a fault at Station A.

The Station B conductor voltage (B_U_{dx}) is a function of the electrode ground resistance (R_{GND}) as seen in Equation (3.13). Since R_{GND} has minimal impact on the Fault Distance Equations as explained in Section 3.5.2, B_U_{dx} also has minimal impact on the Fault Distance Equations for the same reason. Thus, an error in B_U_{dx} will not cause a large error in the calculated fault distance. The sensitivity of $X_{A\_Flt\_x}$ to a percentage change of -5.0% to 5.0% in B_U_{dx} is illustrated in Figure 3-30.

As Station A is not grounded, the Station A conductor current (A_I_{dx}) is floating, thus A_I_{dx} is not directly influencing the calculated fault distance. Thus, an error in A_I_{dx} will not cause a large error in the calculated fault distance. The sensitivity of $X_{A\_Flt\_x}$ to a percentage change of -5.0% to 5.0% in A_I_{dx} is illustrated in Figure 3-31.

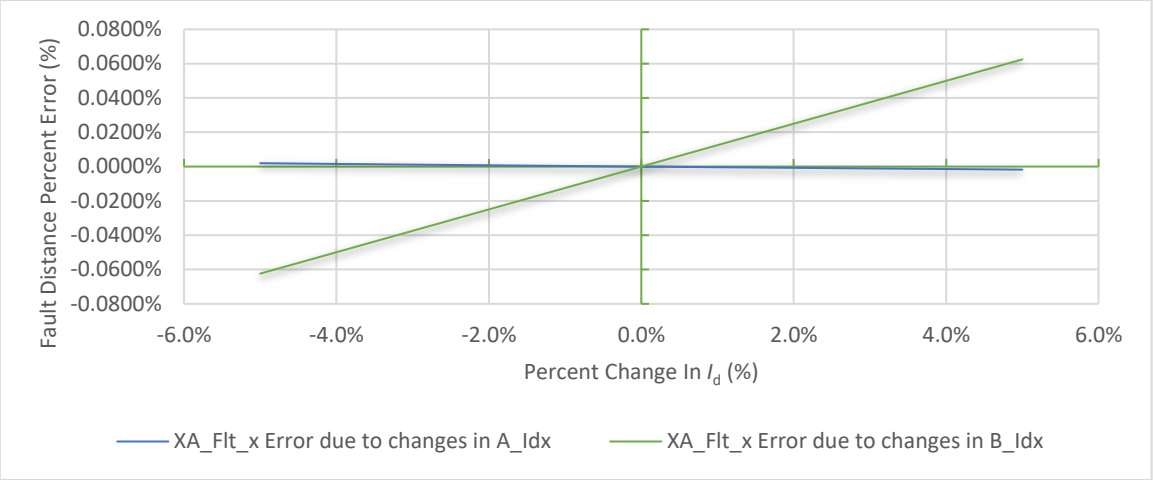

Figure 3-31: Sensitivity of the fault distance ($X_{A\_Flt\_x}$) to changes in the individual currents (A_I_{dx} and B_I_{dx}) for a fault at Station A.

An error in the Station B conductor current (B_I_{dx}) will distort the relationship between B_I_{dx} and the fault current, and the station ground current (B_I_{dGS}). This will result in an error in the calculated fault distance. The sensitivity of $X_{A\_Flt\_x}$ to a percentage change of -5.0% to 5.0% in B_I_{dx} is illustrated in Figure 3-31.

As the measurement accuracy and resolution for the voltage and the current are primarily driven by the accuracy of the transducers, it is important to minimize this error by selecting accurate and high-resolution transducers with low noise [56], [57], [58]. It can also be seen that these errors in calculating each of the individual voltages and currents in the faulted steady state could increase the error of $X_{A\_Flt\_x}$ or $X_{B\_Flt\_x}$. In the nLFL algorithm developed in Section 3.4.4, these sources of error are considered in developing a curve fitting algorithm for determining $X_{A\_Flt\_x}$ and $X_{B\_Flt\_x}$.

Similar to the discussion of sensitivity of $X_{A\_Flt\_x}$ and $X_{B\_Flt\_x}$ to R_x as discussed in Section 3.5.1 above, $X_{A\_Flt\_x}$ and $X_{B\_Flt\_x}$ are also symmetric with respect to the fault location (i.e., $X_{A\_Flt\_x} + X_{B\_Flt\_x} = 100\%$), the errors due to errors in A_U_{dx}, B_U_{dx}, A_I_{dx} and B_I_{dx} are

also symmetric. Hence $X_{A\_Flt\_x}$ and $X_{B\_Flt\_x}$ has the same magnitude, but opposite signs for any percentage change in A_U_{dx}, B_U_{dx}, A_I_{dx} and B_I_{dx}.

3.5.3.1 Rationalization for the Sensitivity Results of $X_{A\_Flt\_x}$ and $X_{B\_Flt\_x}$ with Respect to the Terminal Voltage and Line Current Measurements

The simulated observations of the previous sub-section can be rationalized by mathematically calculating the sensitivity of the fault distance ($X_{A\_Flt\_x}$ or $X_{B\_Flt\_x}$) to the individual voltages and currents (A_U_{dx}, B_U_{dx}, A_I_{dx} and B_I_{dx}). To do this, we calculate the partial derivative of $X_{A\_Flt\_x}$ and $X_{B\_Flt\_x}$ with respect to A_U_{dx}, B_U_{dx}, A_I_{dx} and B_I_{dx} individually. Results are provided in Equations (3.21) and (3.22), respectively. As $\frac{\partial X_{A\_Flt\_x}}{\partial A\_U_{dx}}$, $\frac{\partial X_{B\_Flt\_x}}{\partial A\_U_{dx}}$, $\frac{\partial X_{A\_Flt\_x}}{\partial B\_U_{dx}}$, $\frac{\partial X_{B\_Flt\_x}}{\partial B\_U_{dx}}$, $\frac{\partial X_{A\_Flt\_x}}{\partial A\_I_{dx}}$, $\frac{\partial X_{B\_Flt\_x}}{\partial A\_I_{dx}}$, $\frac{\partial X_{A\_Flt\_x}}{\partial B\_I_{dx}}$ and $\frac{\partial X_{B\_Flt\_x}}{\partial B\_I_{dx}}$ are all sensitive to the inverse of R_x, which means that as the transmission line becomes longer $X_{A\_Flt\_x}$ and $X_{B\_Flt\_x}$ are less sensitive to changes in A_U_{dx}, B_U_{dx}, A_I_{dx} and B_I_{dx}.

$$\nabla X_{\mathrm{A\_Flt\_}x} = \begin{bmatrix} \frac{\partial X_{\mathrm{A\_Flt\_}x}}{\partial A\_U_{\mathrm{d}x}} \\ \frac{\partial X_{\mathrm{A\_Flt\_}x}}{\partial B\_U_{\mathrm{d}x}} \\ \frac{\partial X_{\mathrm{A\_Flt\_}x}}{\partial A\_I_{\mathrm{d}x}} \\ \frac{\partial X_{\mathrm{A\_Flt\_}x}}{\partial B\_I_{\mathrm{d}x}} \end{bmatrix} = \begin{bmatrix} \frac{1}{R_x \times (-A\_I_{\mathrm{d}x} + B\_I_{\mathrm{d}x})} \\ -\frac{1}{R_x \times (-A\_I_{\mathrm{d}x} + B\_I_{\mathrm{d}x})} \\ \frac{A\_U_{\mathrm{d}x} - B\_U_{\mathrm{d}x} + (B\_I_{\mathrm{d}x} \times R_x)}{R_x \times (-A\_I_{\mathrm{d}x} + B\_I_{\mathrm{d}x})^2} \\ \frac{-(A\_I_{\mathrm{d}x} \times R_x) - A\_U_{\mathrm{d}x} + B\_U_{\mathrm{d}x}}{R_x \times (-A\_I_{\mathrm{d}x} + B\_I_{\mathrm{d}x})^2} \end{bmatrix} \quad (3.21)$$

$$\nabla X_{\mathrm{B\_Flt\_}x} = \begin{bmatrix} \frac{\partial X_{\mathrm{B\_Flt\_}x}}{\partial A\_U_{\mathrm{d}x}} \\ \frac{\partial X_{\mathrm{B\_Flt\_}x}}{\partial B\_U_{\mathrm{d}x}} \\ \frac{\partial X_{\mathrm{B\_Flt\_}x}}{\partial A\_I_{\mathrm{d}x}} \\ \frac{\partial X_{\mathrm{B\_Flt\_}x}}{\partial B\_I_{\mathrm{d}x}} \end{bmatrix} = \begin{bmatrix} -\frac{1}{R_x \times (-A\_I_{\mathrm{d}x} + B\_I_{\mathrm{d}x})} \\ \frac{1}{R_x \times (-A\_I_{\mathrm{d}x} + B\_I_{\mathrm{d}x})} \\ \frac{-(B\_I_{\mathrm{d}x} \times R_x) + B\_U_{\mathrm{d}x} - A\_U_{\mathrm{d}x}}{R_x \times (-A\_I_{\mathrm{d}x} + B\_I_{\mathrm{d}x})^2} \\ -\frac{B\_U_{\mathrm{d}x} - A\_U_{\mathrm{d}x} - (A\_I_{\mathrm{d}x} \times R_x)}{R_x \times (-A\_I_{\mathrm{d}x} + B\_I_{\mathrm{d}x})^2} \end{bmatrix} \quad (3.22)$$

where:

$X_{\mathrm{A\_Flt\_}x}$ = Percentage of total line length from Station A to the fault location for conductor x

$X_{\mathrm{B\_Flt\_}x}$ = Percentage of total line length from Station B to the fault location for conductor x

R_x = Total resistance for conductor x

$A\_U_{\mathrm{d}x}$ = Station A voltage for conductor x

$B\_U_{\mathrm{d}x}$ = Station B voltage for conductor x

$A\_I_{\mathrm{d}x}$ = Station A current for conductor x

$B\_I_{\mathrm{d}x}$ = Station B current for conductor x

The subscript "*x*" identifies the faulted conductor (DMR 1 or Pole 2).

3.5.4 Cumulative Sensitivity of the Fault Distance Equations to the Terminal Voltage and Line Current Measurements

The fault distance ($X_{\mathrm{A\_Flt\_}x}$ or $X_{\mathrm{B\_Flt\_}x}$) derived from Equation (3.9) and (3.10) are sensitive to changes in the cumulative conductor voltages (i.e., $A\_U_{\mathrm{d}x}$ and $B\_U_{\mathrm{d}x}$) and line currents (i.e., $A\_I_{\mathrm{d}x}$ and $B\_I_{\mathrm{d}x}$) at Stations A and B, respectively.

The cumulative sensitivities of the fault distance ($X_{A\_Flt\_x}$ or $X_{B\_Flt\_x}$) to changes in A_U_{dx}, B_U_{dx}, A_I_{dx} and B_I_{dx} indicate that the error in $X_{A\_Flt\_x}$ and $X_{B\_Flt\_x}$ is maximized when the error difference between A_I_{dx} and B_I_{dx} is maximized. For instance, the error in $X_{A\_Flt\_x}$ or $X_{B\_Flt\_x}$ is maximized when the error in A_I_{dx} is negative and the error in B_I_{dx} is positive. The absolute error is maximized when the error in A_U_{dx}, B_U_{dx} and A_I_{dx} are negative and the error in B_I_{dx} is positive. The sensitivity of $X_{A\_Flt\_x}$ to a percentage change of -5.0% to 5.0% in A_U_{dx}, B_U_{dx}, A_I_{dx} and B_I_{dx} is listed in Table 3-6 and illustrated in Figure 3-32. The sensitivity of $X_{B\_Flt\_x}$ to a percentage change of -5.0% to 5.0% in A_U_{dx}, B_U_{dx}, A_I_{dx} and B_I_{dx} is illustrated in Figure 3-33.

The plots in Figure 3-32 and Figure 3-33 each depict a four-dimensional dataset in a three-dimensional space. The plateaued areas in Figure 3-32 and Figure 3-33 are artificial and are due to the fact that discrete steps were used for the errors in B_U_{dx} and A_I_{dx}, and Microsoft Excel was used to generate the plot which did not allow for smooth fitting. In reality, the surface ought to be smooth, and so if smaller steps had been selected, the plateauing would not be obvious.

The cumulative sensitivity of the Fault Distance Equations shows that the cumulative errors in the voltage and the current measurements could have a considerable impact on the accuracy of the fault distances. The selection of high accuracy and high-resolution transducers with low noise will minimize the measured voltage and the current errors and thus improve the accuracy of the fault distance calculations.

Similarly, plot $X_{B\_Flt\_x}$ is shown in Figure 3-33, and is essentially a flipping of the plot of $X_{A\_Flt\_x}$ along the horizontal plane, i.e., the plots of $X_{A\_Flt\_x}$ and $X_{B\_Flt\_x}$ in Figure 3-32 and

Figure 3-33 have the same magnitude, but opposite signs for any percent value change in the individual voltage and current measurements. This is due to the symmetry of $X_{A\_Flt\_x}$ and $X_{B\_Flt\_x}$ with respect to the fault location (i.e., $X_{A\_Flt\_x} + X_{B\_Flt\_x} = 100\%$), the error due to an error in the individual voltage and current measurements are also symmetrical. Hence the plots of $X_{A\_Flt\_x}$ and $X_{B\_Flt\_x}$ in Figure 3-32 and Figure 3-33 have the same magnitude, but opposite signs for percent change in the individual voltage and current measurements.

Table 3-6: Sensitivity of the fault distance ($X_{A\_Flt\_x}$) to changes in the terminal voltages and line currents for a fault at Station A.

Sum of XA_Flt_x Error (%)		A_UdN1	A_IdDMR1																							
		-5.0%	-2.5%	0.0%	2.5%	5.0%	-5.0%	-2.5%	0.0%	2.5%	5.0%	-5.0%	-2.5%	0.0%	2.5%	5.0%	-5.0%	-2.5%	0.0%	2.5%	5.0%	-5.0%	-2.5%	0.0%	2.5%	5.0%
B_IdDMR1	B_UdN1																									
-5.0%	-5.0%	0.000%	-0.001%	-0.002%	-0.003%	-0.004%	-0.029%	-0.029%	-0.029%	-0.029%	-0.030%	-0.058%	-0.057%	-0.057%	-0.056%	-0.056%	-0.087%	-0.085%	-0.084%	-0.083%	-0.082%	-0.116%	-0.113%	-0.112%	-0.110%	-0.108%
	-2.5%	-0.003%	-0.004%	-0.005%	-0.005%	-0.006%	-0.032%	-0.032%	-0.032%	-0.032%	-0.032%	-0.061%	-0.060%	-0.060%	-0.059%	-0.058%	-0.090%	-0.088%	-0.087%	-0.086%	-0.085%	-0.119%	-0.116%	-0.114%	-0.112%	-0.111%
	0.0%	-0.006%	-0.007%	-0.008%	-0.008%	-0.009%	-0.035%	-0.035%	-0.035%	-0.035%	-0.035%	-0.064%	-0.063%	-0.062%	-0.062%	-0.061%	-0.093%	-0.091%	-0.090%	-0.088%	-0.087%	-0.122%	-0.119%	-0.117%	-0.115%	-0.113%
	2.5%	-0.009%	-0.010%	-0.010%	-0.011%	-0.012%	-0.038%	-0.038%	-0.038%	-0.038%	-0.038%	-0.067%	-0.066%	-0.065%	-0.065%	-0.064%	-0.096%	-0.094%	-0.093%	-0.091%	-0.090%	-0.125%	-0.122%	-0.120%	-0.118%	-0.116%
	5.0%	-0.012%	-0.013%	-0.013%	-0.014%	-0.014%	-0.041%	-0.041%	-0.041%	-0.041%	-0.040%	-0.070%	-0.069%	-0.068%	-0.067%	-0.067%	-0.099%	-0.097%	-0.095%	-0.094%	-0.093%	-0.128%	-0.125%	-0.123%	-0.121%	-0.119%
-2.5%	-5.0%	0.033%	0.031%	0.029%	0.028%	0.026%	0.004%	0.003%	0.002%	0.001%	0.000%	-0.025%	-0.025%	-0.026%	-0.026%	-0.026%	-0.054%	-0.053%	-0.053%	-0.053%	-0.052%	-0.083%	-0.082%	-0.081%	-0.079%	-0.078%
	-2.5%	0.030%	0.028%	0.027%	0.025%	0.023%	0.001%	0.000%	-0.001%	-0.002%	-0.003%	-0.028%	-0.028%	-0.028%	-0.029%	-0.029%	-0.057%	-0.056%	-0.056%	-0.055%	-0.055%	-0.086%	-0.084%	-0.083%	-0.082%	-0.081%
	0.0%	0.027%	0.025%	0.024%	0.022%	0.021%	-0.002%	-0.003%	-0.004%	-0.005%	-0.005%	-0.031%	-0.031%	-0.031%	-0.031%	-0.031%	-0.060%	-0.059%	-0.059%	-0.058%	-0.058%	-0.089%	-0.087%	-0.086%	-0.085%	-0.084%
	2.5%	0.024%	0.022%	0.021%	0.019%	0.018%	-0.005%	-0.006%	-0.007%	-0.007%	-0.008%	-0.034%	-0.034%	-0.034%	-0.034%	-0.034%	-0.063%	-0.062%	-0.061%	-0.061%	-0.060%	-0.092%	-0.090%	-0.089%	-0.088%	-0.086%
	5.0%	0.021%	0.019%	0.018%	0.017%	0.015%	-0.008%	-0.009%	-0.009%	-0.010%	-0.011%	-0.037%	-0.037%	-0.037%	-0.037%	-0.037%	-0.066%	-0.065%	-0.064%	-0.064%	-0.063%	-0.095%	-0.093%	-0.092%	-0.090%	-0.089%
0.0%	-5.0%	0.066%	0.063%	0.061%	0.058%	0.056%	0.037%	0.035%	0.033%	0.031%	0.030%	0.008%	0.007%	0.006%	0.005%	0.004%	-0.021%	-0.021%	-0.022%	-0.022%	-0.022%	-0.050%	-0.050%	-0.049%	-0.049%	-0.049%
	-2.5%	0.063%	0.060%	0.058%	0.055%	0.053%	0.034%	0.032%	0.030%	0.029%	0.027%	0.005%	0.004%	0.003%	0.002%	0.001%	-0.024%	-0.024%	-0.025%	-0.025%	-0.025%	-0.053%	-0.052%	-0.052%	-0.052%	-0.051%
	0.0%	0.060%	0.057%	0.055%	0.053%	0.050%	0.031%	0.029%	0.027%	0.026%	0.024%	0.002%	0.001%	0.000%	-0.001%	-0.002%	-0.027%	-0.027%	-0.027%	-0.028%	-0.028%	-0.056%	-0.055%	-0.055%	-0.054%	-0.054%
	2.5%	0.057%	0.054%	0.052%	0.050%	0.048%	0.028%	0.026%	0.025%	0.023%	0.022%	-0.001%	-0.002%	-0.003%	-0.004%	-0.004%	-0.030%	-0.030%	-0.030%	-0.030%	-0.031%	-0.059%	-0.058%	-0.058%	-0.057%	-0.057%
	5.0%	0.054%	0.051%	0.049%	0.047%	0.045%	0.025%	0.023%	0.022%	0.020%	0.019%	-0.004%	-0.005%	-0.006%	-0.006%	-0.007%	-0.033%	-0.033%	-0.033%	-0.033%	-0.033%	-0.062%	-0.061%	-0.061%	-0.060%	-0.059%
2.5%	-5.0%	0.099%	0.095%	0.092%	0.089%	0.086%	0.070%	0.067%	0.064%	0.062%	0.059%	0.041%	0.039%	0.037%	0.035%	0.033%	0.012%	0.011%	0.009%	0.008%	0.007%	-0.017%	-0.017%	-0.018%	-0.018%	-0.019%
	-2.5%	0.096%	0.092%	0.089%	0.086%	0.083%	0.067%	0.064%	0.062%	0.059%	0.057%	0.038%	0.036%	0.034%	0.032%	0.031%	0.009%	0.008%	0.007%	0.006%	0.005%	-0.020%	-0.020%	-0.021%	-0.021%	-0.022%
	0.0%	0.093%	0.089%	0.086%	0.083%	0.080%	0.064%	0.061%	0.059%	0.056%	0.054%	0.035%	0.033%	0.031%	0.030%	0.028%	0.006%	0.005%	0.004%	0.003%	0.002%	-0.023%	-0.023%	-0.024%	-0.024%	-0.024%
	2.5%	0.090%	0.086%	0.083%	0.080%	0.077%	0.061%	0.058%	0.056%	0.054%	0.051%	0.032%	0.030%	0.028%	0.027%	0.025%	0.003%	0.002%	0.001%	0.000%	-0.001%	-0.026%	-0.026%	-0.027%	-0.027%	-0.027%
	5.0%	0.087%	0.083%	0.080%	0.078%	0.075%	0.058%	0.055%	0.053%	0.051%	0.049%	0.029%	0.027%	0.026%	0.024%	0.023%	0.000%	-0.001%	-0.002%	-0.003%	-0.004%	-0.029%	-0.029%	-0.029%	-0.029%	-0.030%
5.0%	-5.0%	0.132%	0.127%	0.123%	0.119%	0.115%	0.103%	0.099%	0.096%	0.092%	0.089%	0.074%	0.071%	0.068%	0.066%	0.063%	0.045%	0.043%	0.041%	0.039%	0.037%	0.016%	0.015%	0.013%	0.012%	0.011%
	-2.5%	0.129%	0.124%	0.120%	0.116%	0.113%	0.100%	0.096%	0.093%	0.090%	0.087%	0.071%	0.068%	0.065%	0.063%	0.060%	0.042%	0.040%	0.038%	0.036%	0.034%	0.013%	0.012%	0.010%	0.009%	0.008%
	0.0%	0.126%	0.121%	0.117%	0.114%	0.110%	0.097%	0.093%	0.090%	0.087%	0.084%	0.068%	0.065%	0.062%	0.060%	0.058%	0.039%	0.037%	0.035%	0.033%	0.032%	0.010%	0.009%	0.008%	0.006%	0.005%
	2.5%	0.123%	0.118%	0.115%	0.111%	0.107%	0.094%	0.090%	0.087%	0.084%	0.081%	0.065%	0.062%	0.060%	0.057%	0.055%	0.036%	0.034%	0.032%	0.030%	0.029%	0.007%	0.006%	0.005%	0.004%	0.003%
	5.0%	0.120%	0.116%	0.112%	0.108%	0.105%	0.091%	0.087%	0.084%	0.081%	0.078%	0.062%	0.059%	0.057%	0.054%	0.052%	0.033%	0.031%	0.029%	0.028%	0.026%	0.004%	0.003%	0.002%	0.001%	0.000%

Legend			
Error Description	Max Positive Error	Zero Error	Max Negative Error
Heat Map			

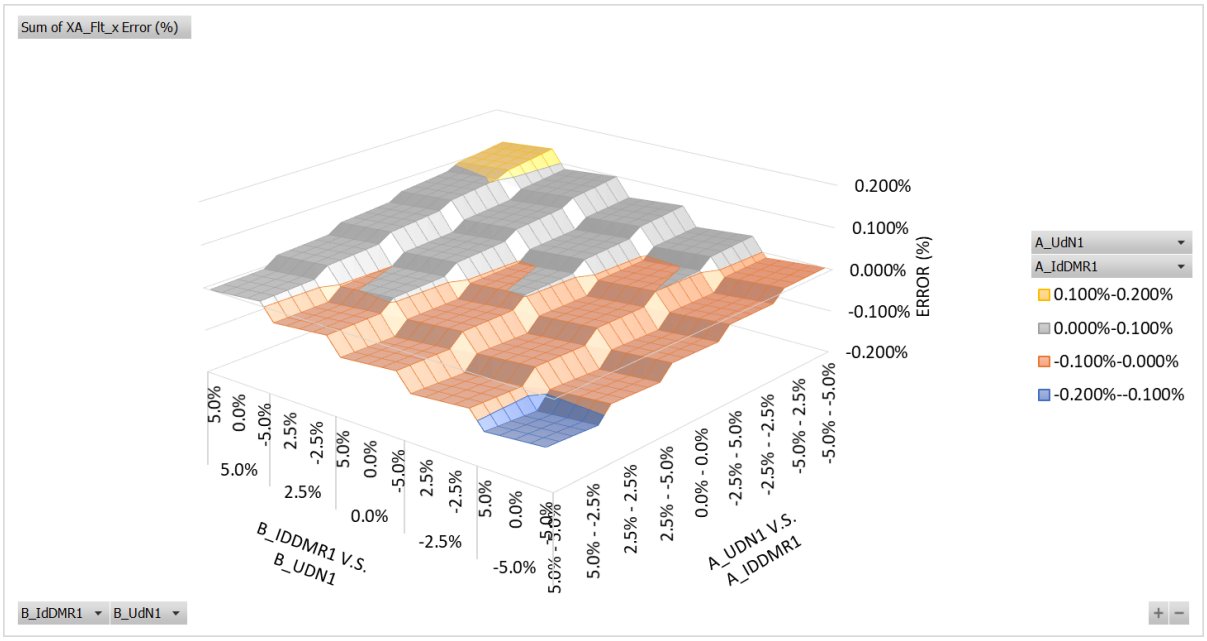

Figure 3-32: Sensitivity of the fault distance ($X_{A\_Flt\_x}$) to changes in the terminal voltages and line currents for a fault at Station A.

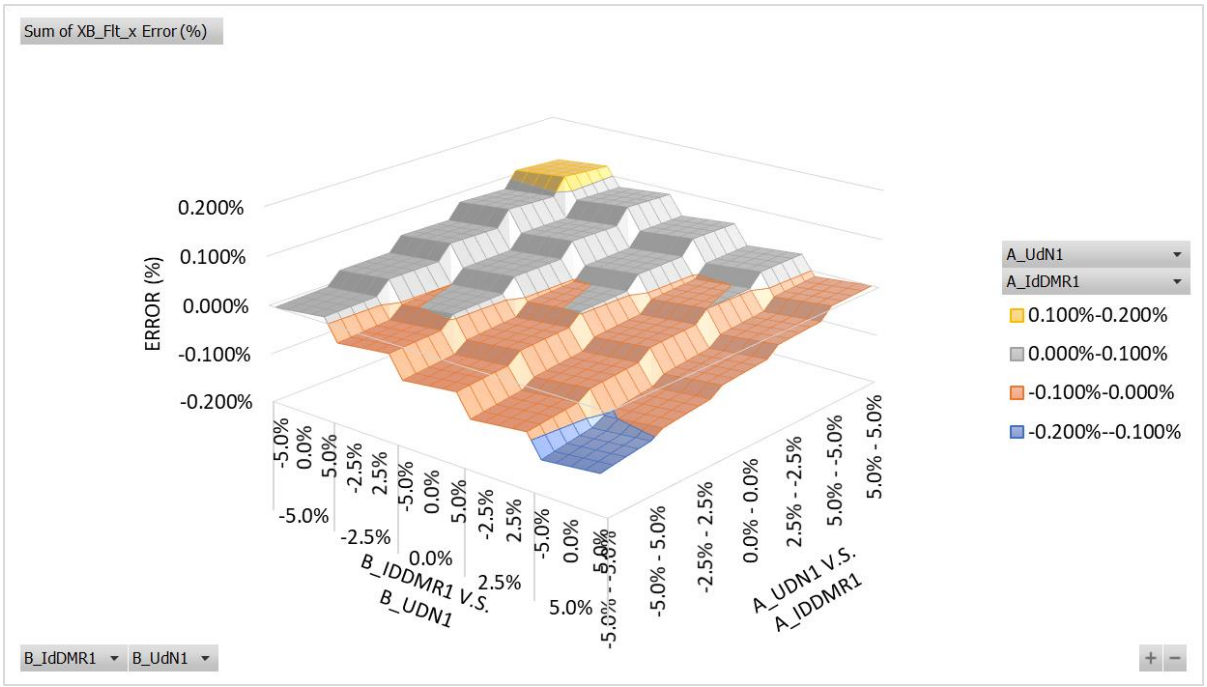

Figure 3-33: Sensitivity of the fault distance ($X_{B\_Flt\_x}$) to changes in the terminal voltages and line currents for a fault at Station A.

3.6 Chapter Summary

This chapter examined the design and implementation of the nLFL algorithm. Specifically, this chapter discussed how the algorithm was used to calculate an accurate line fault location for the HVdc system. The following were investigated:

- The neutral or DMR conductor can only determine a fault location when a voltage and a current of sufficient magnitude is present on the conductor. Hence:
    - Monopolar and Homopolar HVdc schemes can detect a DMR fault during the normal operation of the HVdc system, as the DMR is energized;
    - However, in fully balanced Bipolar point to point or balanced Bipolar Multiterminal HVdc schemes, the DMR carries negligible current and fault detection is a challenge. This problem can be overcome by energising the DMR, when running the HVdc system in an unbalanced state such that the DMR carries a current;
- The following features were incorporated into the design of a successful new nLFL strategy developed for this thesis:
    - The nLFL detects a fault when a transient event exceeds a threshold set for the measured signals, that are filtered to remove the dc component and any high frequency noise;
    - It determines the faulted conductor when the measured current at the two ends of the conductor differ by a specified amount after the fault was detected;

- The fault location algorithm uses the steady state voltages and currents that the HVdc system would have settled into (at $t = \infty$ if protective action had not taken it out of service. For this, the HVdc system can be simplified to a simple electric circuit consisting of resistors and fixed voltage sources. The Fault Distance Equation can be derived from nodal analysis of this simple electric circuit;
- However, the above steady state values are not attained in an actual system as the protection system must operate rapidly to clear the fault. Hence the nLFL algorithm only has access to the available data collected during the transient period prior to the operation of the protection system. Hence, a regression based curve fitting of the pre-protection data, is used to estimate the steady state fault location in the faulted steady-state condition of the HVdc system.
    - The nLFL requires a minimum transient event data period of 650 ms to maintain an accuracy similar to commercial offline fault locator systems whose accuracy is less than 1% error.

Chapter 4: Online Neutral Line Fault Locator (nLFL) Hardware Architecture

This chapter describes the design and the development of the hardware for implementing the proposed novel online Neutral Line Fault Locator (nLFL). It examines the requirements for the nLFL's hardware and discusses the software for the nLFL system. The performance of the nLFL is analyzed in the subsequent chapters.

4.1 Online Neutral Line Fault Locator Implementation

Unlike the online dc Line Fault Locator (dcLFL), which requires high frequency sampling to determine the precise arrival time of the wave front at the station, the nLFL design requires that the system be capable of sampling and capturing data during the pre-protection and transient period. The device developed for this purpose is called the Data Measurement Unit (DMU) shown in Figure 4-1.

Figure 4-1: The Data Measurement Unit (DMU).

The DMU is the real-time data collection system of the nLFL. The nLFL system requires that the measurements from both stations be synchronized, for correlation of the data and calculation of the Fault Distance Equation. Hence, each DMU utilizes a Global Positioning System (GPS) clock to synchronize all measurements collected from each DMU. As discussed in previous sections the accuracy of the measurements is critical to the accuracy of the nLFL. Thus, the Data Acquisition (DAQ) system of the DMU must be as accurate as possible for accurate fault location calculations. Therefore, the DAQ of the DMU must have a sufficiently high resolution that is accurate at the sampling rates used by the DMU.

Since each station's conductor typically has a voltage and a current measurement and there are three conductors plus the electrode ground current, a minimum of seven channels are needed for the DMU's DAQ at each station. However, since many DAQ channels come in powers of two, the DMU will have 8 DAQ channels. To further improved the accuracy of the DMU, every DAQ channel is simultaneously captured, and time stamped by the GPS clock. The DMU uses a LAN connection to communicate with the rest of the nLFL system. The detailed DMU specifications are listed below with several other features and functionalities.

DMU specifications:

- Data Acquisition (DAQ)
    - 8 differential channels
    - 16 bit per channel
    - 1.0 million samples per second per channel (simultaneous)
    - ±10 V input
- Global Positioning System (GPS) Clock
    - Accurate to within ±100 ns, greater than 99.0% of the time
    - Every sampled is timestamped by GPS clock
- 4 Dry Alarm contacts
    - 250 V
    - 8 Amps
    - Alarm Types
        - Major Alarm (Triggered by a GPS failure or a GPS loss of lock detection at the Field Programmable Gate Array (FPGA) level)
        - Minor Alarm (Triggered by the real-time system for communication loss)
        - Line Fault Locator (LFL) Operated (Triggered by the host computer on successful fault location)
        - LFL Self-Test Operated (Triggered by the host computer on a self-test event)
- 2 100 Mbps LAN communication ports
- 1 USB communication port
- All inputs and outputs normally connected for operation are surge protected

To achieve the above design specifications of the DMU, the DMU was designed with three levels as seen in the Figure 4-2. The first level is the protection level, the second level is the FPGA level, and the third level is the real-time operation level.

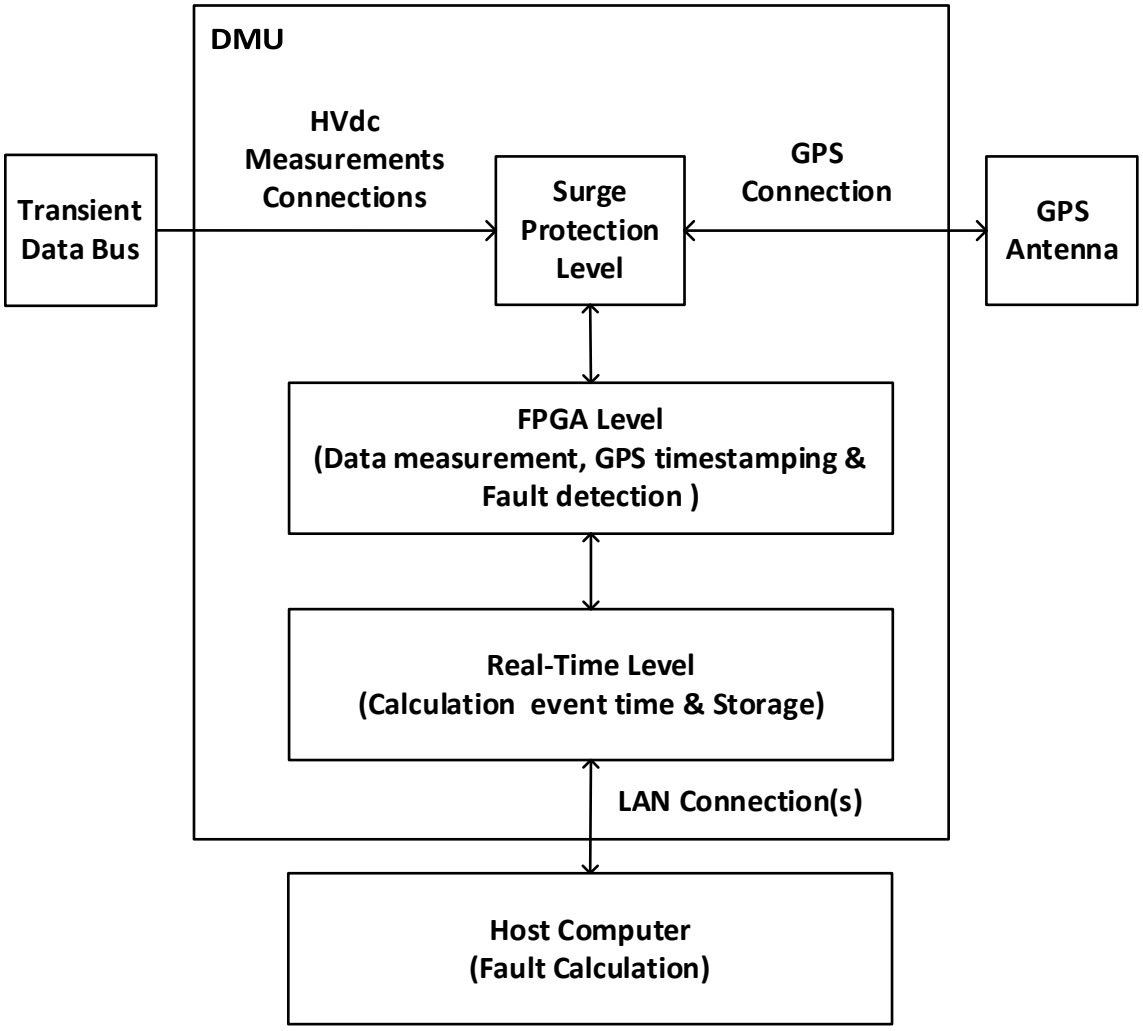

Figure 4-2: DMU design.

4.2 Online Neutral Line Fault Locator Protection System

The protection level contains all the input and the output protection for all the normally connected DMU ports. The analog inputs are protected by an overvoltage protection circuit to 12 V ac/dc and will pass frequencies less that 100 MHz. The dry alarm contacts are protected up to 120 V ac (170 V dc). The GPS clock antenna protection circuit will pass voltages from –1 V to +7 V with frequencies between 1.15 GHz to 1.6 GHz. The Ethernet ports are protected up to 7.5 V with a max data rate of 100 Mbps. The USB port is not surge protected as it is only designed for diagnostic purposes and not for general use.

4.3 Online Neutral Line Fault Locator FPGA System

The FPGA level is responsible for data acquisition and timestamping of the required measurements. The FPGA level is also responsible for detection of the fault. The overall operation of this stage is depicted in Figure 4-3. The FPGA level samples all channels simultaneously in parallel from the Analog to Digital Converter (ADC) and captures the GPS time simultaneously at the specified sample rate. The rate of change between the samples captured and the previous samples captured are compared to the threshold rate of change specified for the sampled signal. If the rate of change is greater than or equal to the specified rate of change the sampled signals and timestamp are tagged to indicate the detection of a transient fault event at the real-time level. The FPGA uses Direct Memory Access (DMA) to store the signal and time reading of the event for the real-time target to read and process. The FPGA level then blocks detection of events, for the pre-specified period of time, to prevent retriggering of the DMU on the same event that was just detected.

The FPGA level also provides auxiliary service information to the real-time target. The FPGA level reports the current GPS status and the current GPS time to the real-time target. The FPGA level also controls the enabling and the disabling of the four alarm contacts on the DMU.

The FPGA system has been designed around the Xilinx Kintex-7 FPGA 7K70T.

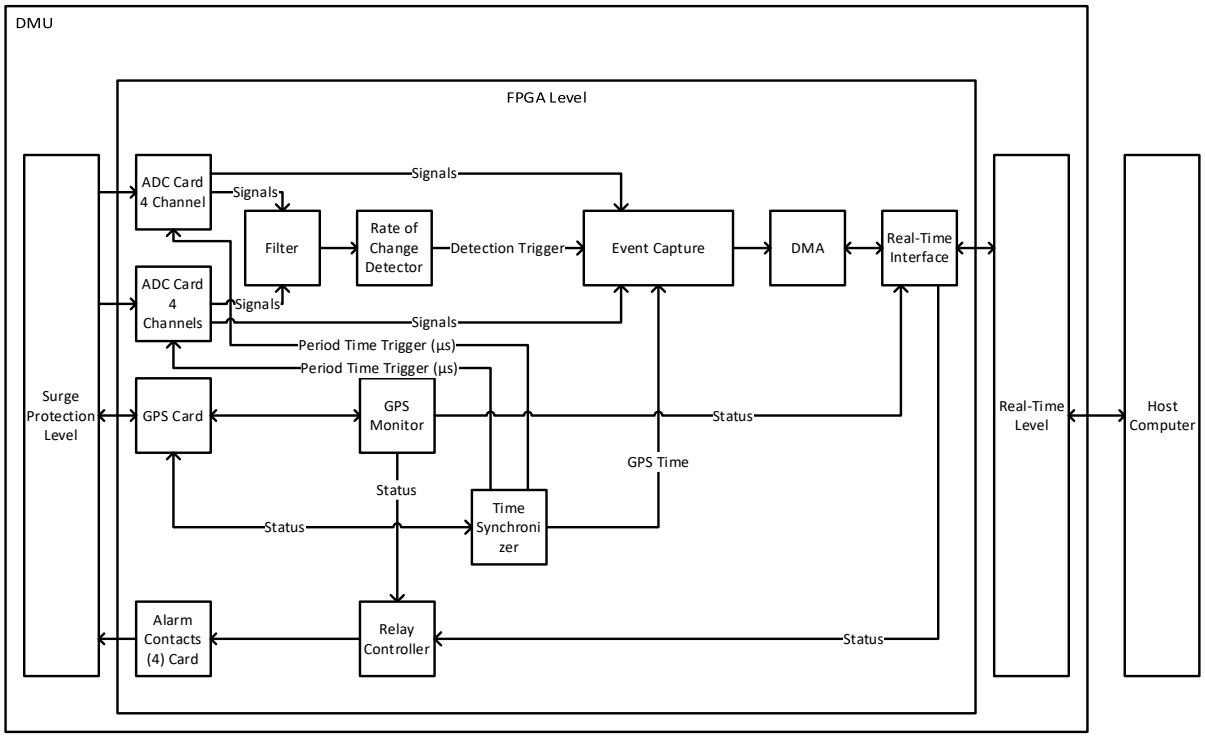

Figure 4-3: DMU FPGA design.

4.4 Online Neutral Line Fault Locator Real-Time System

The real-time level is responsible for calculating the trigger event time and for collecting the analog measurements and timestamps from the time window of the event from the FPGA level. The overall operation of this stage is depicted in Figure 4-4. The real-time level reads the data from the DMA to process the data. If no fault event triggers are detected, the measured voltages and timestamps are stored up to the specified number of pre-sample values. When a trigger event is detected in the DMA data from the FPGA, the real-time software analyzes the measurements to interpolate the precise time that the voltage rate of change has surpassed the rate of change specified for the analog channel. The time of the event is calculated for each of the channels that the trigger event was identified from the DMA data. The calculated trigger event timestamps are stored locally to its local file system and passed to the DMU's host computer via its local LAN connection. Additionally, the pre-trigger event

and the post-trigger event voltages and timestamps are stored up to the specified number of sample values. This collection of pre and post samples are stored locally to its local file system and passed to the DMU's host computer via its local LAN connection.

The axillary signals, that the real-time level, received from the FPGA level are also transferred to the host computer via the LAN. The real-time level also relays alarm signals from the host computer to the FPGA to operate the alarm contacts.

The real-time system of the DMU has been built upon the Intel Atom E3825 1.33 GHz dual-core processor, with 1 GB of random-access memory and 4 GB disk storage memory.

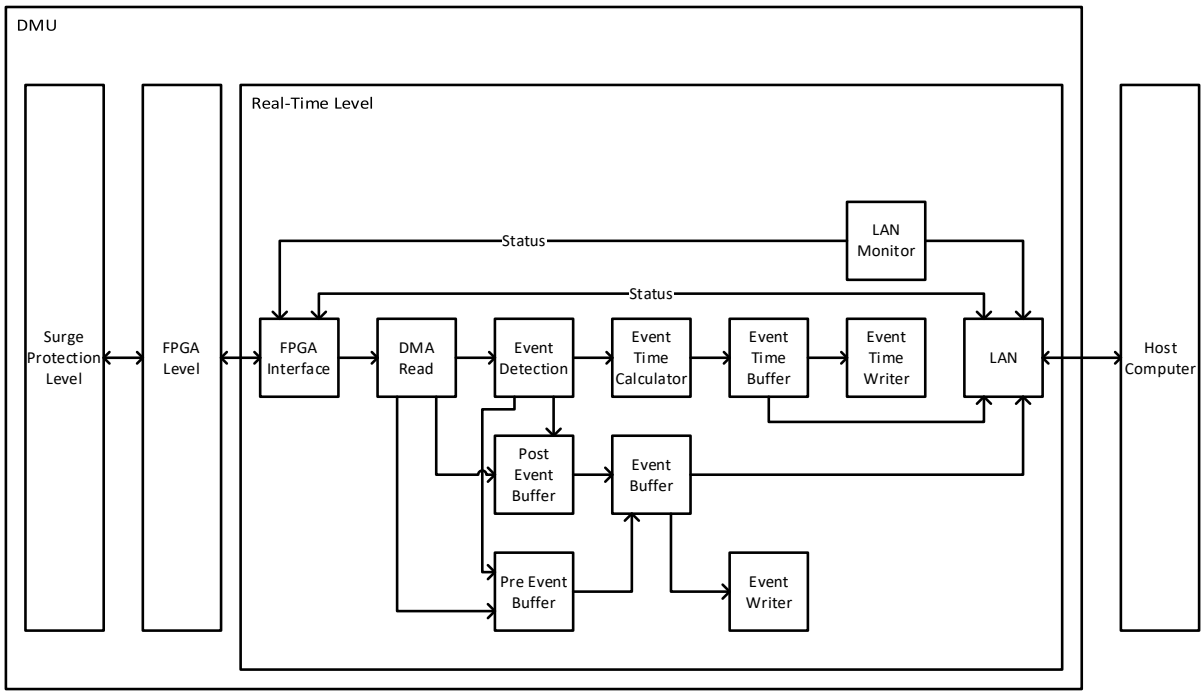

Figure 4-4: DMU real-time design.

4.5 Online Neutral Line Fault Locator Non-Real-Time System

The host computer receives all the messages from the DMU. The messages from the DMU are stored in the host computer's local Structured Query Language (SQL) database. The host computer also hosts a Windows service that processes the line fault data to find the line fault location. The host service uses the data stored on the local and the remote computer to calculate the fault location relative to the location of the host computer at the converter station. The algorithm used for processing the data was discussed further in Section 3.4. On successful detection of a fault the nLFL service will send a message to the DMU to operate the dcLFL operated alarm.

The non-real-time industrial computer has been built upon the Intel dual-core i7 2.0 GHz processor, with 8 GB of random-access memory and 500 GB disk storage memory.

4.5.1 Online Neutral Line Fault Locator Human Machine Interface (HMI)

The host computer also provides a Human Machine Interface (HMI) to view events and interact with the nLFL system. The HMI is a web-based interface that allows for local and remote access to the nLFL's operation and control, without the use of remote desktop services. The HMI includes several pages that can be viewed in Appendix B: Online Neutral Line Fault Locator Webpages.

4.6 Chapter Summary

This chapter looked at the design and implementation of the nLFL system's hardware. Specifically, the chapter first looked at the requirements and the design of the DMU. The DMU is required for detecting and capturing of the faulted waveforms. This is critical as errors in measuring the faulted waveforms can lead to increased errors in the fault location. Secondly,

this chapter looked at the implementation of the software for the nLFL system. The nLFL system software consists of two parts. These are the DMU firmware used for detecting and collecting the fault information and the Windows service running on the computer that calculates the fault location. The overall analysis of the nLFL system will be discussed in the next chapter.

Chapter 5: Online Neutral Line Fault Locator (nLFL) Testing and Performance Analysis

The performance of the nLFL system was evaluated exhaustively using EMT simulation model. Testing was also conducted on an actual hardware implementation. The following tests were performed to discover the accuracy of the system.

5.1 Off-line Simulation studies of the Online Neutral Line Fault Locator

5.1.1 Simulation Based Modeling and Setup of the Online Neutral Line Fault Locator

For testing the nLFL system in a practical test environment, the East Alberta Transmission Link (EATL) HVdc system was modeled in the EMT simulator PSCAD™/EMTDC™. The HVdc converters of the EATL HVdc system were modeled in detail as 12-pulse converter models. The dc yard of the EATL HVdc system, including the dc line reactors and the dc filters, was also modeled in detail. The transmission line was also modeled in the EMT simulator, using frequency dependent parameters, considering the EATL's tower and line geometry. An earth resistivity 5000.0 Ω-m was assumed [15], [59], typical for the area. The ac side includes the ac damped-arm type filters totaling 500 MVar targeting the 11^{th} and 13^{th} harmonics and provides high pass filtering of higher order harmonics. An additional 125 MVar capacitor bank was present for additional reactive compensation. The ac networks are modeled were Thevenin equivalents with an impedance given by a Short Circuit Ratio (SCR) of 2.5 ∠ 84° on the rectifier side and 2.5 ∠ 75° on the inverter side.

The Transient Data Measurement (TDM) and the Analog Interface Module 2 (AIM2) were also modeled by a signal sampler with the appropriate sampling rate and filtering. The schematic of the overall EMT simulation case as modeled in PSCAD™/EMTDC™ is shown in Figure 5-1 below.

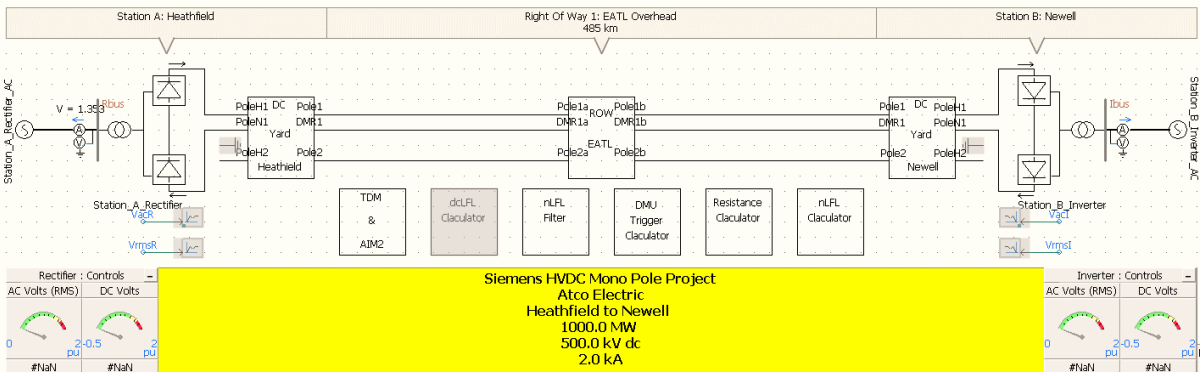

Figure 5-1: PSCAD™/EMTDC™ EATL HVdc system model.

The fault detection algorithm in, the nLFL system uses data captured during a transient postfault period 900 ms, immediately after a fault detection. This is because, typically, 1000 ms is required to clear the DMR 1 or Pole 2 fault by opening the Metallic Return Transfer Breaker (MRTB) or Ground Return Transfer Switch (GRTS).

5.1.2 Simulation Based Testing of the Online Neutral Line Fault Locator

To test the EMT model of the nLFL system, five scenarios of the EMT EATL HVdc system were considered as listed below:

1. With only Pole 1 energized; and the DMR 1 and Pole 2 conductor in parallel providing the current return path together as a parallel return path. Faults were applied to the DMR 1 conductor;

2. The same pre-fault configuration as in 1 above (i.e., Pole 1 energized and DMR 1 + Pole 2 conductors as the current return path). The faults were applied to the Pole 2 conductor;

3. With the same pre-fault configuration as in 1 and 2 above, but with double line-ground faults, i.e., the DMR 1 and the Pole 2 conductor were simultaneously shorted to ground;

4. With Pole 1 energized and just the DMR 1 as return path (i.e., with the Pole 2 conductor out of service) and faults were applied to the DMR 1 conductor;

5. With Pole 1 energized and just the Pole 2 conductor as return path (i.e., DMR 1 out of service), faults were applied to the Pole 2 conductor;

Each of the system scenarios were tested with the following conditions:

- Transmission line length
    - 485.0 km (The length of the EATL HVdc system's transmission line)
    - 1000.0 km (Typical long line length for a 500 kV HVdc system)

- Fault location along the transmission line starting from Station A (Heathfield converter station)
    - 0.0% of the total transmission line length (0.0 km; 0.0 km)
    - 2.0% of the total transmission line length (9.7 km; 20.0 km)
    - 25.0% of the total transmission line length (121.25 km; 250.0 km)
    - 50.0% of the total transmission line length (242.5 km; 500.0 km)
    - 75.0% of the total transmission line length (363.75 km; 750.0 km)
    - 98.0% of the total transmission line length (475.3 km; 980.0 km)
    - 100.0% of the total transmission line length (485.0 km; 1000.0 km)
- Station ground resistance

    - 0.01 Ω (Approximately the resistance of an HVdc system ground)
- Line fault resistance
    - 0.1 Ω (Typical low impedance fault resistance)
- Power order of the HVdc system
    - 100 MW (500 kV, 0.2 kA) (This is the minimum power order of the EATL HVdc system)
    - 1000 MW (500 kV, 2.0 kA) (This is the maximum power order of the EATL HVdc system)

In scenarios 1 and 2, the protection system opens the appropriate breaker to isolate the faulted conductor and let the remaining ground potential conductor carry the return current. This is a favorable operating mode as no current is forced to flow through the earth.

In scenarios 3, 4 and 5, the protection system opens the appropriate breaker to isolate the faulted conductor and the HVdc system has to operate in earth return mode which is an unfavorable operating mode as discussed in earlier chapters. However, the current would be smaller in this conductor as the faulted conductor(s) was the primary return path for all the current in the HVdc system.

In the fault detection approach, there are many possible sources of error. Incorrect fault locations could be reported because of a short transient period, (i.e., insufficient transient event data captured for analysis) and measurement noise. Also, the multiple conversions from analog to digital (the transducers to the TDM bus) and digital to analog (the AIM2 to the DMU) could introduce additional errors in the measurements.

5.1.2.1 Fault Location Error in the Simulated Online Neutral Line Fault Locator Scheme

Table 5-1 and Figure 5-2 show the results of calculating a fault location on the DMR 1 conductor in scenarios 1, 3 and 4 using the nLFL method presented in this thesis. The results showed that the error of the nLFL method for the DMR 1 conductor was less than 0.5% for the entire length of the transmission line, which is within the specified 1% accuracy target. These results confirmed that the nLFL method would accurately calculate a fault location on the DMR 1 conductor using the measurements collected in the transient event data period.

Table 5-1: Error in calculated distance ($X_{A\_Flt\_DMR1}$) for a fault on the DMR 1 conductor in scenarios 1, 3 and 4. station ground resistance = 0.01 Ω; fault resistance = 0.1 Ω.

Fault Distance (%)	Percent Error (%)											
	Scenario 1				Scenario 3				Scenario 4			
	Length = 485 km		Length = 1000 km		Length = 485 km		Length = 1000 km		Length = 485 km		Length = 1000 km	
	Power = 100 MW	Power = 1000 MW	Power = 100 MW	Power = 1000 MW	Power = 100 MW	Power = 1000 MW	Power = 100 MW	Power = 1000 MW	Power = 100 MW	Power = 1000 MW	Power = 100 MW	Power = 1000 MW
0.0%	0.009%	-0.086%	0.071%	-0.007%	-0.001%	0.048%	0.008%	0.065%	0.073%	0.085%	0.085%	-0.009%
2.0%	-0.216%	-0.066%	0.021%	0.021%	0.222%	-0.021%	0.152%	0.096%	0.232%	0.352%	0.278%	0.245%
25.0%	0.242%	0.374%	0.006%	0.069%	-0.104%	0.126%	-0.147%	0.227%	0.152%	0.348%	0.078%	0.134%
50.0%	0.010%	-0.019%	0.096%	0.096%	-0.255%	0.150%	-0.141%	0.109%	-0.101%	0.060%	0.039%	0.005%
75.0%	-0.219%	-0.391%	-0.016%	0.020%	-0.381%	-0.172%	0.128%	-0.012%	-0.362%	-0.225%	-0.142%	-0.114%
98.0%	-0.276%	-0.209%	-0.202%	-0.244%	-0.051%	0.002%	-0.037%	-0.071%	-0.239%	-0.247%	-0.275%	-0.247%
100.0%	-0.001%	-0.003%	0.055%	0.180%	-0.097%	-0.178%	0.247%	-0.067%	-0.190%	0.148%	-0.085%	0.091%

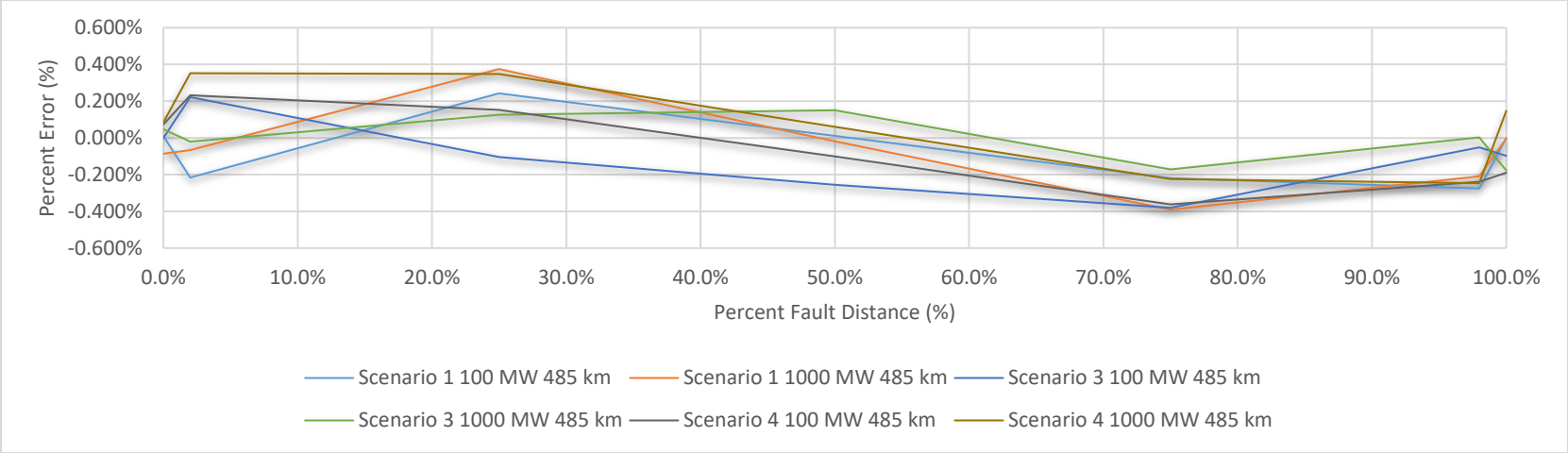

Figure 5-2: Error in calculated distance ($X_{A\_Flt\_DMR1}$) for a fault on the DMR 1 conductor in scenarios 1, 3 and 4. station ground resistance = 0.01 Ω; fault resistance = 0.1 Ω; transmission line length = 485.0 km

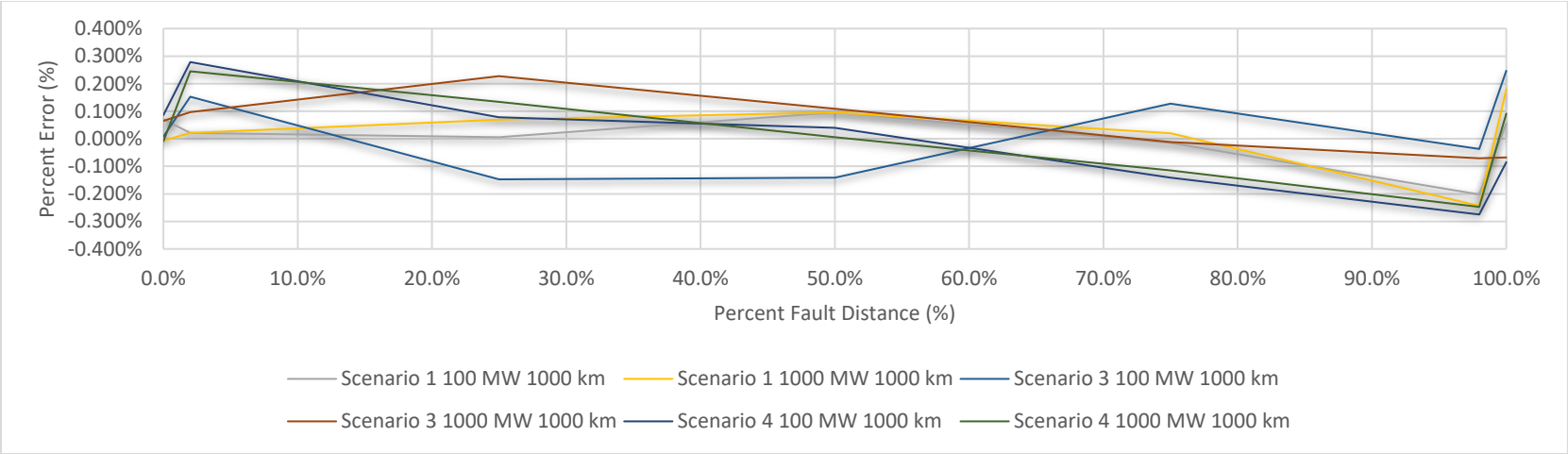

Figure 5-3: Error in calculated distance ($X_{A\_Flt\_DMR1}$) for a fault on the DMR 1 conductor in scenarios 1, 3 and 4. station ground resistance = 0.01 Ω; fault resistance = 0.1 Ω; transmission line length = 1000.0 km

Table 5-2 and Figure 5-4 show the results of calculating a fault location on the Pole 2 conductor in scenarios 2, 3 and 5 using the nLFL method presented in this thesis. These results confirmed that the nLFL method would accurately calculate a fault location on the Pole 2 conductor using the measurements collected in the transient event data period giving a maximum error of 0.5%, which is well within the target level of 1%.

Table 5-2: Error in calculated distance ($X_{A\_Flt\_Pole2}$) for a fault on the Pole 2 conductor in scenarios 2, 3 and 5. station ground resistance = 0.01 Ω; fault resistance = 0.1 Ω.

Fault Distance (%)	Percent Error (%)											
	Scenario 2				Scenario 3				Scenario 5			
	Length = 485 km		Length = 1000 km		Length = 485 km		Length = 1000 km		Length = 485 km		Length = 1000 km	
	Power = 100 MW	Power = 1000 MW	Power = 100 MW	Power = 1000 MW	Power = 100 MW	Power = 1000 MW	Power = 100 MW	Power = 1000 MW	Power = 100 MW	Power = 1000 MW	Power = 100 MW	Power = 1000 MW
0.0%	0.045%	-0.041%	0.000%	0.017%	-0.001%	0.048%	0.008%	0.065%	0.012%	0.015%	-0.099%	-0.029%
2.0%	-0.312%	0.061%	0.369%	0.142%	0.222%	-0.021%	0.152%	0.096%	0.110%	0.227%	0.070%	0.186%
25.0%	0.130%	0.162%	-0.093%	0.017%	-0.104%	0.126%	-0.147%	0.227%	0.287%	0.120%	0.043%	0.110%
50.0%	-0.263%	-0.028%	0.058%	-0.071%	-0.255%	0.150%	-0.141%	0.109%	-0.094%	-0.005%	0.053%	-0.007%
75.0%	-0.358%	-0.109%	-0.060%	-0.117%	-0.381%	-0.172%	0.128%	-0.012%	-0.133%	-0.197%	-0.158%	-0.111%
98.0%	-0.070%	-0.116%	-0.155%	-0.173%	-0.051%	0.002%	-0.037%	-0.071%	-0.114%	-0.121%	-0.216%	-0.155%
100.0%	0.025%	-0.085%	-0.316%	-0.073%	-0.097%	-0.178%	0.247%	-0.067%	0.390%	0.027%	-0.339%	0.013%

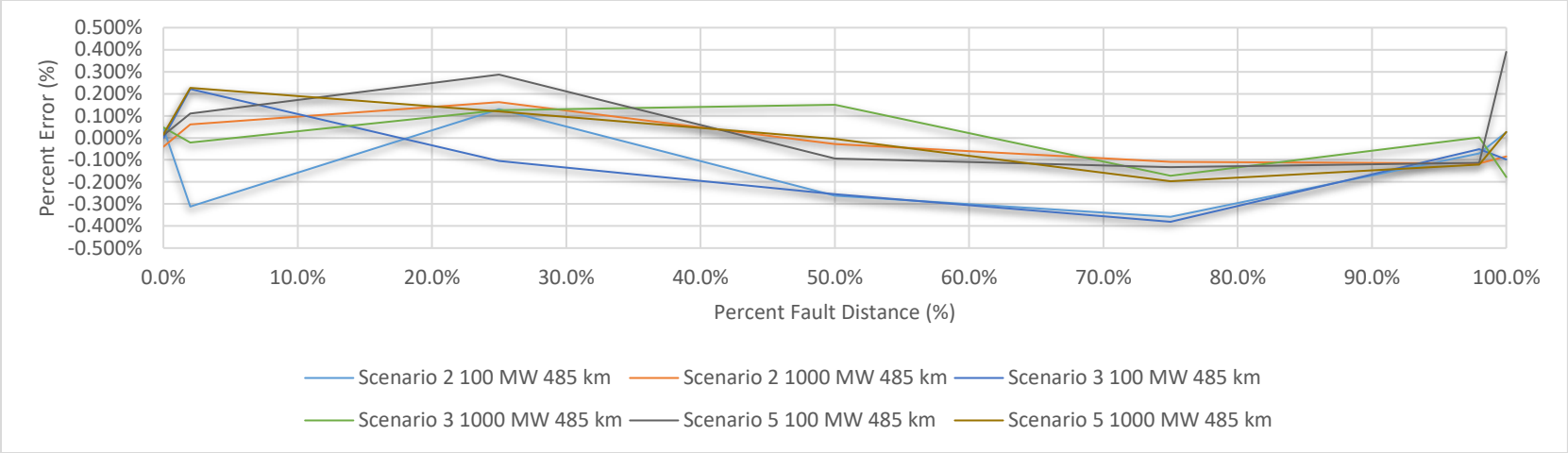

Figure 5-4: Error in calculated distance ($X_{A\_Flt\_Pole2}$) for a fault on the Pole 2 conductor in scenarios 2, 3 and 5. station ground resistance = 0.01 Ω; fault resistance = 0.1 Ω; transmission line length = 485.0 km

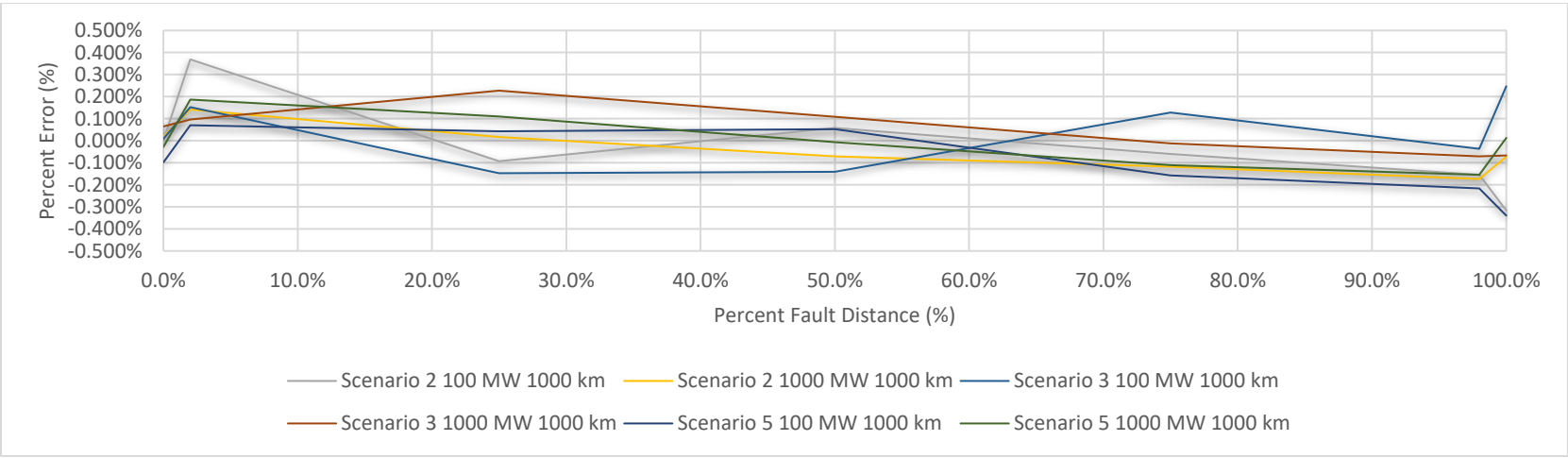

Figure 5-5: Error in calculated distance ($X_{A\_Flt\_Pole2}$) for a fault on the Pole 2 conductor in scenarios 2, 3 and 5. station ground resistance = 0.01 Ω; fault resistance = 0.1 Ω; transmission line length = 1000.0 km

Thus, the above results confirmed the efficacy of the proposed approach in which the steady state values (i.e., without protection operation) are estimated by using regression to extrapolate the collected transient event data to its asymptotic value at time $t \rightarrow \infty$. The key to the success of this algorithm, is the selection of an appropriate curve fitting equation to represent the time varying response of the Fault Distance Equation.

From the results shown in this section, the power order setpoints in the HVdc system ranging from the minimum (100 MW) to the maximum (1000 MW) had negligible impact on the accuracy of the fault location. The error distributions in Figure 5-2 and Figure 5-4 did not appear to have a specific pattern (e.g., monotonic increase towards one line endpoint, or larger errors at the midpoint, etc.). Hence, the only conclusion that could be drawn from all five scenarios, is that all cases gave an acceptable fault calculation error of no more than 0.5% of line length.

5.2 Real-Time Hardware in the Loop Testing of the Online Neutral Line Fault Locator

5.2.1 Real-Time Hardware in the Loop Modeling and Setup of the Online Neutral Line Fault Locator

For testing the nLFL system in a practical real-time test environment, the East Alberta Transmission Link (EATL) HVdc system was modeled in the real-time EMT simulator RTDS™ using the identical models as in the off-line simulation described in Section 5.1 above. However, unlike the purely simulation-based analysis of the previous section, the real-time EMT simulator only modeled the power network. While the measurements from the power network were output to the analog channels of the RTDS™ to the analog interfaces to the actual online Neutral Line Fault Locator (nLFL) devices.

The sampling rate and filtering and scaling of the signals as carried out by the Transient Data Measurement (TDM) system were also modeled to match measurements provided to the Analog Interface Module 2 (AIM2). To simulate the AIM2 for hardware in the loop testing, the Gigabit Transfer Analog Output (GTAO) was used to output the scaled signals from the EMT simulator as the AIM2 does in the actual HVdc system. The outputs of the GTAO card were then wired to the corresponding Data Measurement Units (DMUs) for each station (north end station Heathfield and south end station Newell). The test setup can be seen in the RTDS screen-capture as seen in Figure 5-6. The actual hardware connections between the nLFL and the RTDS racks are shown in Figure 5-7.

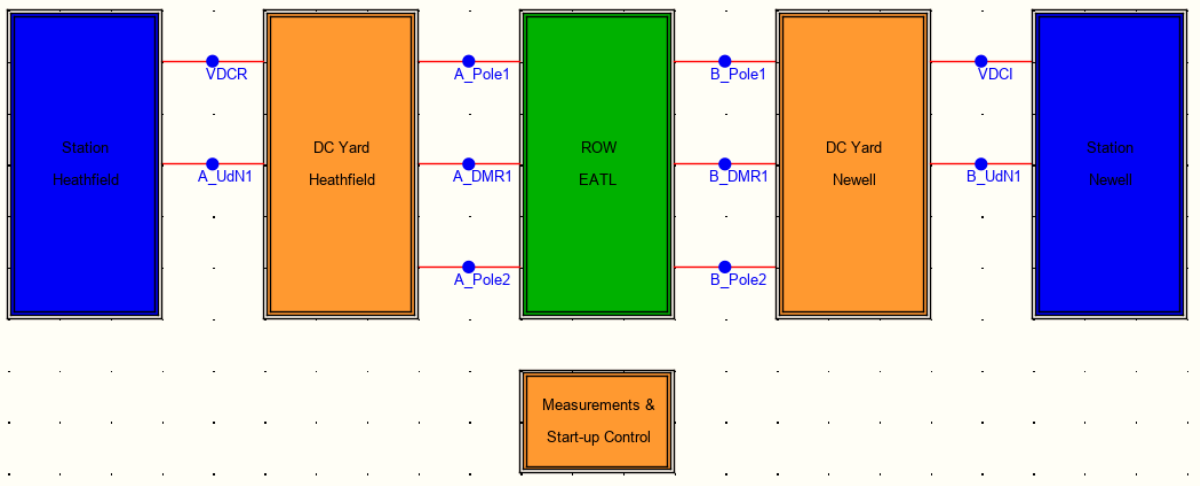

Figure 5-6: RTDS™ EATL HVdc system hardware in the loop draft case.

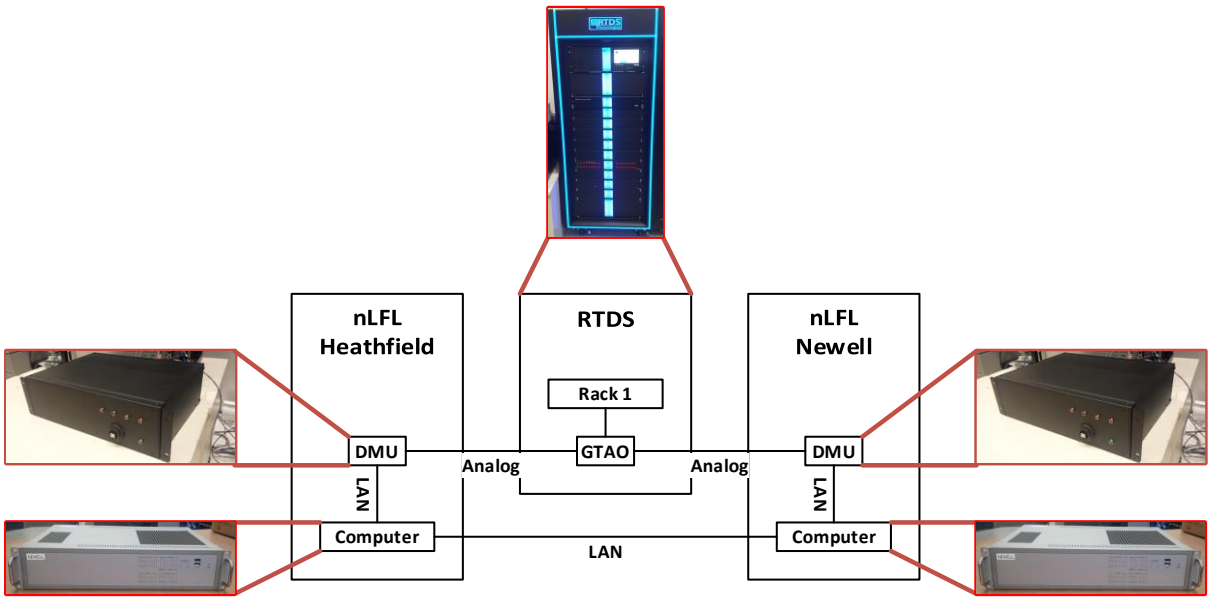

Figure 5-7: RTDS™ EATL HVdc system hardware in the loop configuration.

5.2.2 Real-Time Hardware in the Testing of the Online Neutral Line Fault Locator

The same five scenarios as described in Section 5.1.2 were considered to test the actual nLFL hardware:

1. With only Pole 1 energized; and the DMR 1 and Pole 2 conductor in parallel providing the current return path together as a parallel return path. Faults were applied to the DMR 1 conductor;

2. The same pre-fault configuration as in 1 above (i.e., Pole 1 energized and DMR 1 + Pole 2 conductors as the current return path). The faults were applied to the Pole 2 conductor;

3. With the same pre-fault configuration as in 1 and 2 above, but with double line-ground faults, i.e., the DMR 1 and the Pole 2 conductor were simultaneously shorted to ground;

4. With Pole 1 energized and just the DMR 1 as return path (i.e., with the Pole 2 conductor out of service) and faults were applied to the DMR 1 conductor;

5. With Pole 1 energized and just the Pole 2 conductor as return path (i.e., DMR 1 out of service), faults were applied to the Pole 2 conductor;

Similar to the tests in Section 5.1.2, line lengths of 485.0 km and 1000.0 km and power levels of 100 MW and 1000 MW were considered.

5.2.2.1 Fault Location Error in the Hardware In Loop (HIL) Testing with the Actual Online Neutral Line Fault Locator System

Table 5-3 and Figure 5-8 show the error in fault location identification for faults on the DMR 1 conductor and Table 5-4 and Figure 5-10 show the error for faults on the Pole 2 conductor. The results are similar to those obtained from pure EMT simulation in Section 5.1.2.1 and confirmed that the fault can be identified within an error of 0.5%.

Table 5-3: Error in calculated distance ($X_{A\_Flt\_DMR1}$) for a fault on the DMR 1 conductor in scenarios 1, 3 and 4. station ground resistance = 0.01 Ω; fault resistance = 0.1 Ω.

Fault Distance (%)	Percent Error (%)											
	Scenario 1				Scenario 3				Scenario 4			
	Length = 485 km		Length = 1000 km		Length = 485 km		Length = 1000 km		Length = 485 km		Length = 1000 km	
	Power = 100 MW	Power = 1000 MW	Power = 100 MW	Power = 1000 MW	Power = 100 MW	Power = 1000 MW	Power = 100 MW	Power = 1000 MW	Power = 100 MW	Power = 1000 MW	Power = 100 MW	Power = 1000 MW
0.0%	-0.037%	0.042%	0.011%	-0.040%	-0.098%	0.173%	0.035%	-0.113%	-0.096%	0.024%	0.066%	0.330%
2.0%	0.325%	0.194%	0.224%	0.082%	-0.236%	0.191%	-0.135%	0.096%	0.013%	0.190%	0.203%	0.470%
25.0%	0.315%	0.180%	0.098%	0.110%	-0.230%	-0.348%	-0.348%	-0.168%	-0.146%	0.065%	0.417%	0.349%
50.0%	0.274%	0.266%	0.119%	0.148%	0.213%	-0.326%	0.372%	0.032%	-0.111%	0.226%	0.237%	0.146%
75.0%	-0.056%	0.222%	0.199%	0.125%	0.262%	-0.098%	-0.088%	-0.193%	0.416%	0.289%	0.251%	0.253%
98.0%	-0.205%	-0.269%	0.166%	-0.140%	-0.050%	0.312%	-0.146%	-0.020%	-0.296%	0.089%	-0.024%	-0.150%
100.0%	-0.302%	0.164%	0.143%	0.223%	0.405%	-0.440%	-0.333%	-0.049%	-0.258%	-0.411%	-0.145%	-0.060%

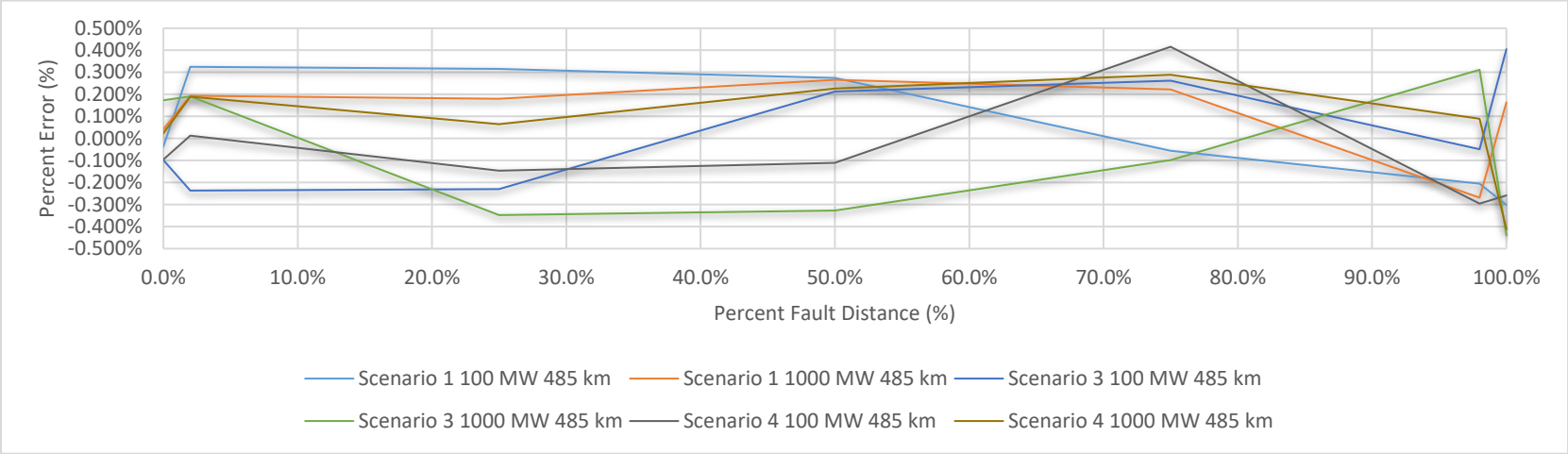

Figure 5-8: Error in calculated distance ($X_{A\_Flt\_DMR1}$) for a fault on the DMR 1 conductor in scenarios 1, 3 and 4. station ground resistance = 0.01 Ω; fault resistance = 0.1 Ω; transmission line length = 485.0 km

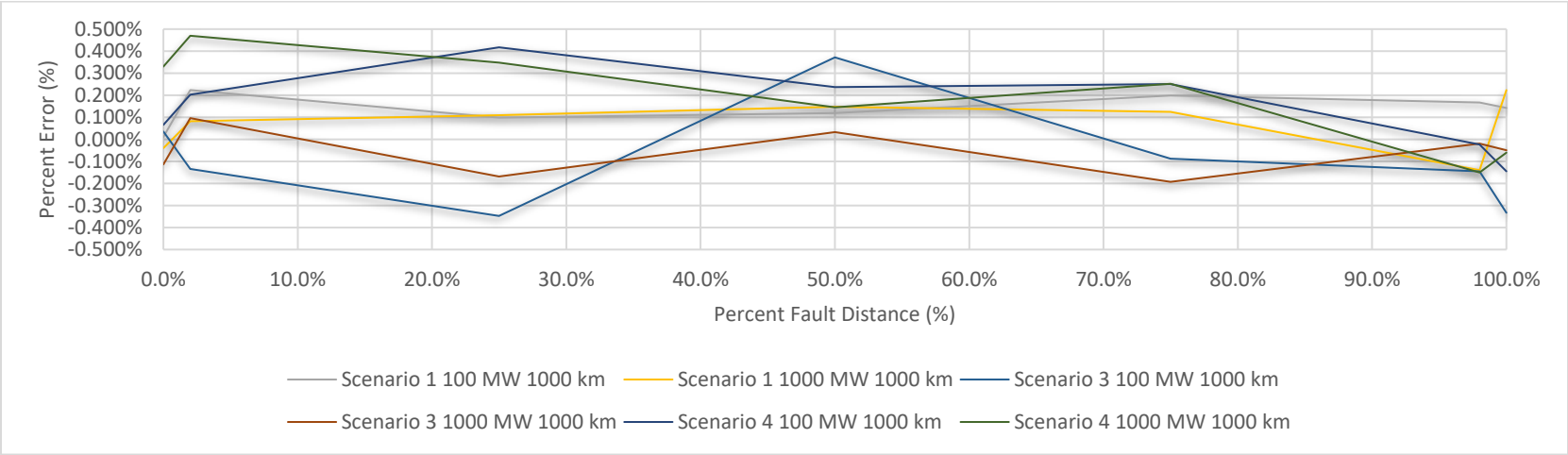

Figure 5-9: Error in calculated distance ($X_{A\_Flt\_DMR1}$) for a fault on the DMR 1 conductor in scenarios 1, 3 and 4. station ground resistance = 0.01 Ω; fault resistance = 0.1 Ω.; transmission line length = 1000.0 km

Table 5-4: Error in calculated distance ($X_{A\_Flt\_Pole2}$) for a fault on the Pole 2 conductor in scenarios 2, 3 and 5. station ground resistance = 0.01 Ω; fault resistance = 0.1 Ω.

Fault Distance (%)	Percent Error (%)											
	Scenario 2				Scenario 3				Scenario 5			
	Length = 485 km		Length = 1000 km		Length = 485 km		Length = 1000 km		Length = 485 km		Length = 1000 km	
	Power = 100 MW	Power = 1000 MW	Power = 100 MW	Power = 1000 MW	Power = 100 MW	Power = 1000 MW	Power = 100 MW	Power = 1000 MW	Power = 100 MW	Power = 1000 MW	Power = 100 MW	Power = 1000 MW
0.0%	0.093%	0.050%	0.084%	0.017%	-0.098%	0.173%	0.035%	-0.113%	0.073%	0.053%	-0.078%	-0.069%
2.0%	0.133%	0.126%	0.342%	0.142%	-0.236%	0.191%	-0.135%	0.096%	-0.070%	0.077%	0.144%	0.028%
25.0%	0.143%	0.036%	0.148%	0.017%	-0.230%	-0.348%	-0.348%	-0.168%	-0.040%	0.085%	0.282%	0.104%
50.0%	0.035%	0.220%	-0.144%	-0.071%	0.213%	-0.326%	0.372%	0.032%	-0.301%	0.104%	0.008%	-0.098%
75.0%	0.387%	0.286%	0.195%	-0.117%	0.262%	-0.098%	-0.088%	-0.193%	0.123%	0.170%	0.308%	0.120%
98.0%	0.074%	0.214%	0.040%	-0.173%	-0.050%	0.312%	-0.146%	-0.020%	0.316%	0.256%	-0.050%	0.073%
100.0%	-0.260%	-0.159%	-0.339%	-0.073%	0.405%	-0.440%	-0.333%	-0.049%	-0.426%	-0.492%	0.034%	0.144%

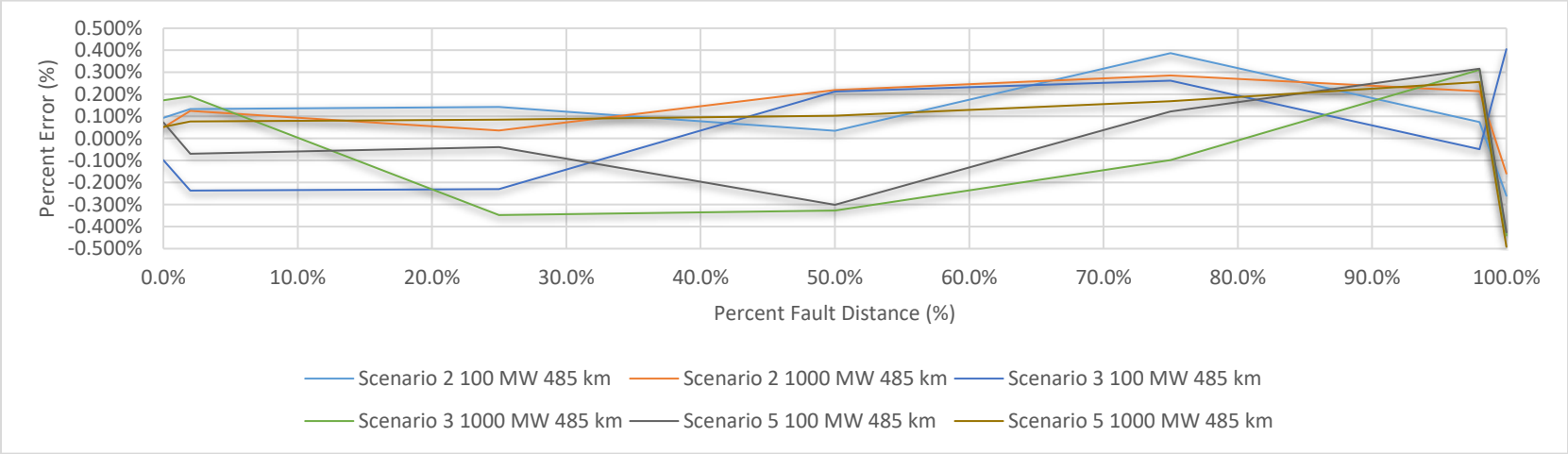

Figure 5-10: Error in calculated distance ($X_{A\_Flt\_Pole2}$) for a fault on the Pole 2 conductor in scenarios 2, 3 and 5. station ground resistance = 0.01 Ω; fault resistance = 0.1 Ω; transmission line length = 485.0 km

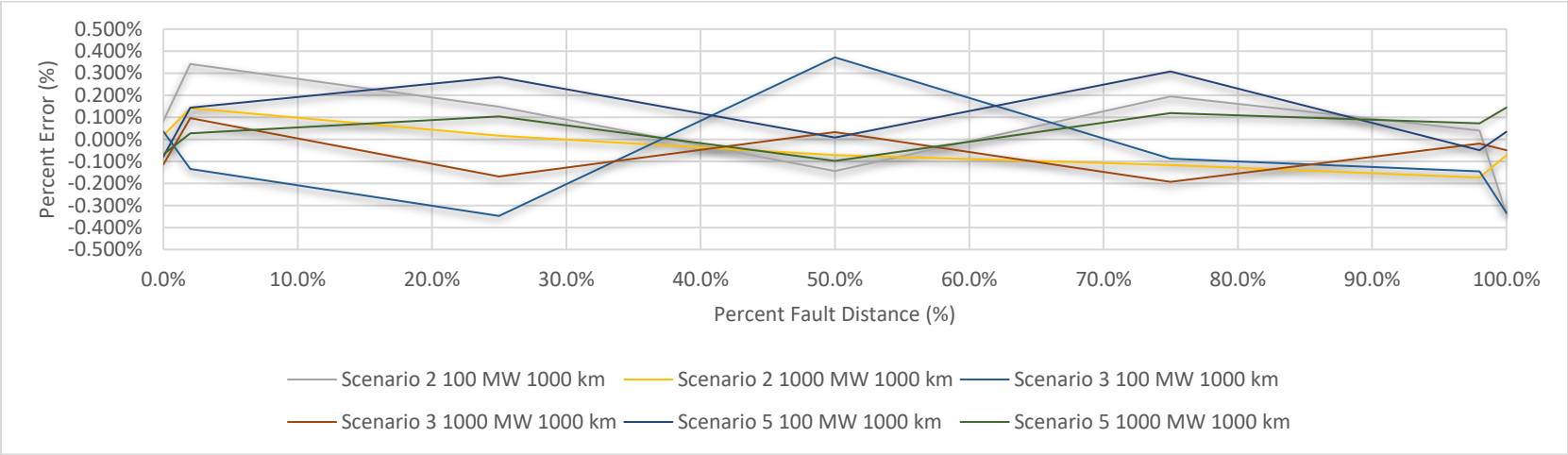

Figure 5-11: Error in calculated distance ($X_{A\_Flt\_Pole2}$) for a fault on the Pole 2 conductor in scenarios 2, 3 and 5. station ground resistance = 0.01 Ω; fault resistance = 0.1 Ω; transmission line length = 1000.0 km

5.3 Real World Testing of the Online Neutral Line Fault Locator

5.3.1 EATL Setup of the Online Neutral Line Fault Locator

To further determine the capacity of the nLFL system, live testing on the EATL HVdc system with the nLFL system installed in the EATL HVdc system were conducted. The testing, the setup and the installation were done in collaboration with Atco Electric (The owner of the EATL HVdc system), Siemens (The builder of the EATL HVdc system), MHI and the University of Manitoba (The developers of the nLFL technology).

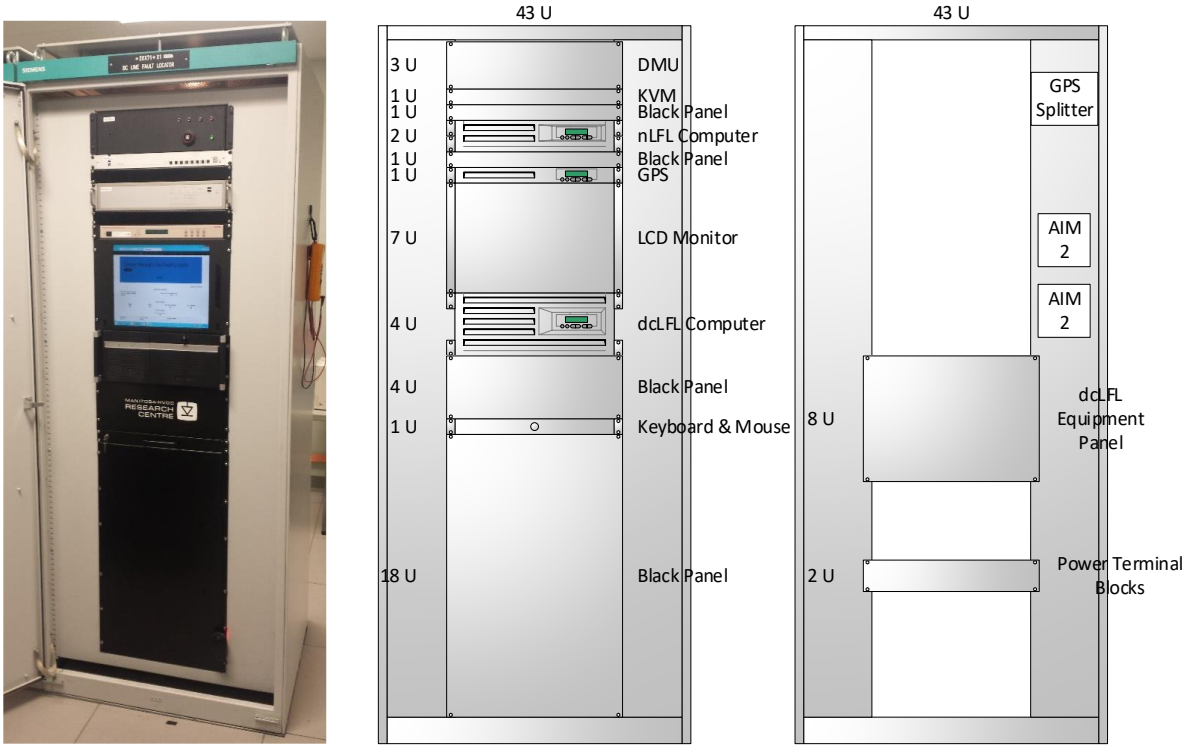

Figure 5-12: Fault location cabinet layout.

The nLFL system was installed at each station in the EATL HVdc system. Each station had its own nLFL hardware, which consisted of a DMU, an AIM2 and a computer. The AIM2 extracted the required measurements from the TDM bus and converted them to analog signals to be read by the DMU. The nLFL equipment was installed in the existing dcLFL cubicle and

laid out as seen in Figure 5-12. A Keyboard Video Mouse (KVM) switch was also installed to facilitate the use the existing keyboard, video, and mouse in the cabinet for both the dcLFL and the nLFL systems. The additional equipment added to the cabinet were all powered by the existing power system in the cabinet. The GPS signal coming to the cabinet was split with a 2-way coaxial splitter to provide the GPS signal to both the dcLFL and the nLFL. The nLFL computer was also tied into the interstation network for interstation communication of the two nLFL stations. The overall configuration is shown in Figure 5-13 below.

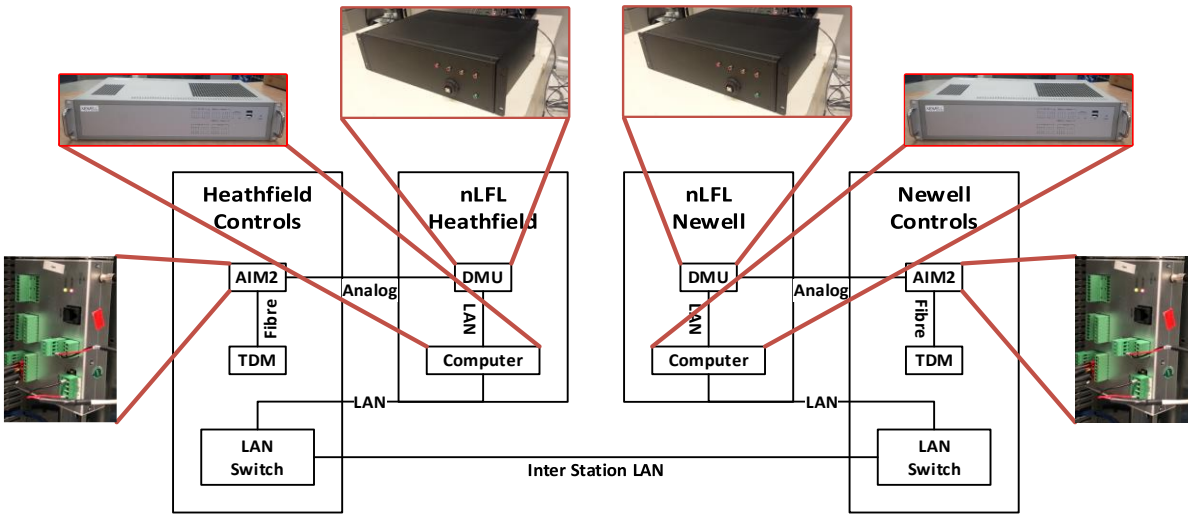

Figure 5-13: Overall nLFL installation layout.

5.3.2 EATL Testing of the Online Neutral Line Fault Locator

Due to the practical limitations imposed at the site, such as access to conductors, licenses for flying Unmanned Aerial Vehicles (UAV) to apply faults, etc., only two scenarios of the five in Sections 5.1 and 5.2 were tested.

1. With only Pole 1 energized; and the DMR 1 and Pole 2 conductor in parallel providing the current return path together as a parallel return path. Faults were applied to the DMR 1 conductor;

2. The same pre-fault configuration as in 1 above (i.e., Pole 1 energized and DMR 1 + Pole 2 conductors as the current return path). The faults were applied to the Pole 2 conductor;

Each of the system scenarios were tested with the following conditions:

As this was the physical line of length 485.0 km, no parametric studies with different line lengths were carried out. The testing was done at four power levels, 150 MW, 250 MW, 500 MW and 1000 MW. Also, the fault could only be applied at the 0.0% location at Newell station due to the fact that permission was pending from Air Traffic Control and ATCO to do faults at other locations.

These scenarios were selected because if one of the return conductors was faulted the EATL HVdc system would clear the fault by opening the coinciding breaker from the conductor bundle. This act would clear the fault on the EATL HVdc system and allow the system to operate without any substantial impact to the system's operation or the system's power delivery.

An Dro (UAV) was deployed to apply line faults. First, a ground wire of sufficient length to reach the conductor bundles on the tower and of sufficient gauge to carry the fault current was connected to the tower ground. Secondly, the opposite end of the cable was fastened to an insulating rope that would isolate the UAV from the conducting ground fault wire. Thirdly, the opposite end of the rope was connected to the UAV such that the UAV could fly the grounding wire into the conductor. Figure 5-14 shows a visual representation of the setup and Figure 5-15 shows the application of the fault at the EATL HVdc station

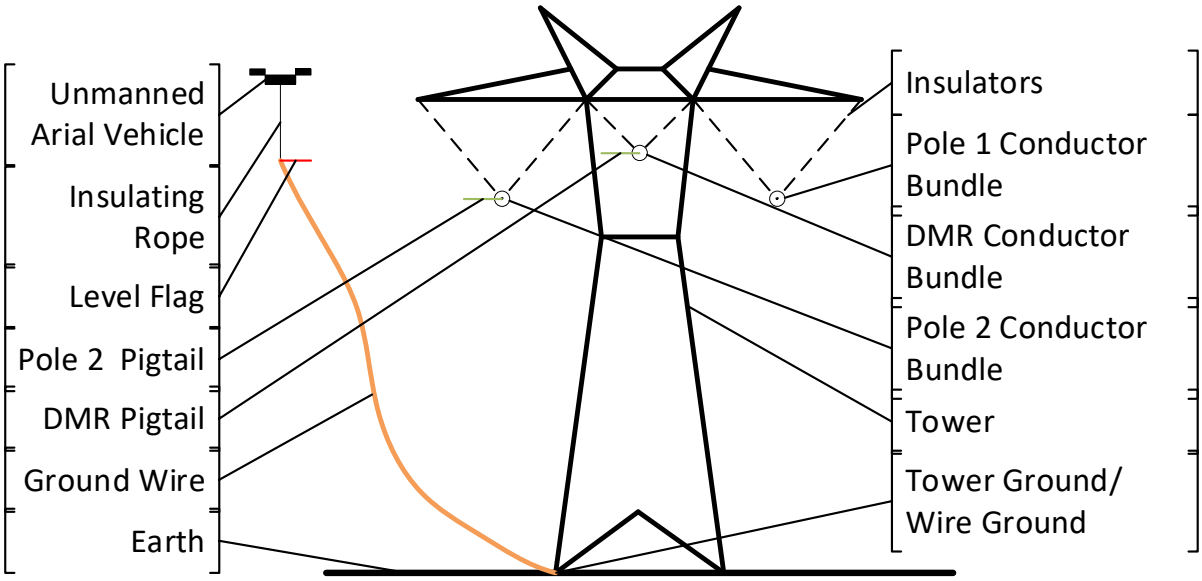

Figure 5-14 UAV Fault application configuration.

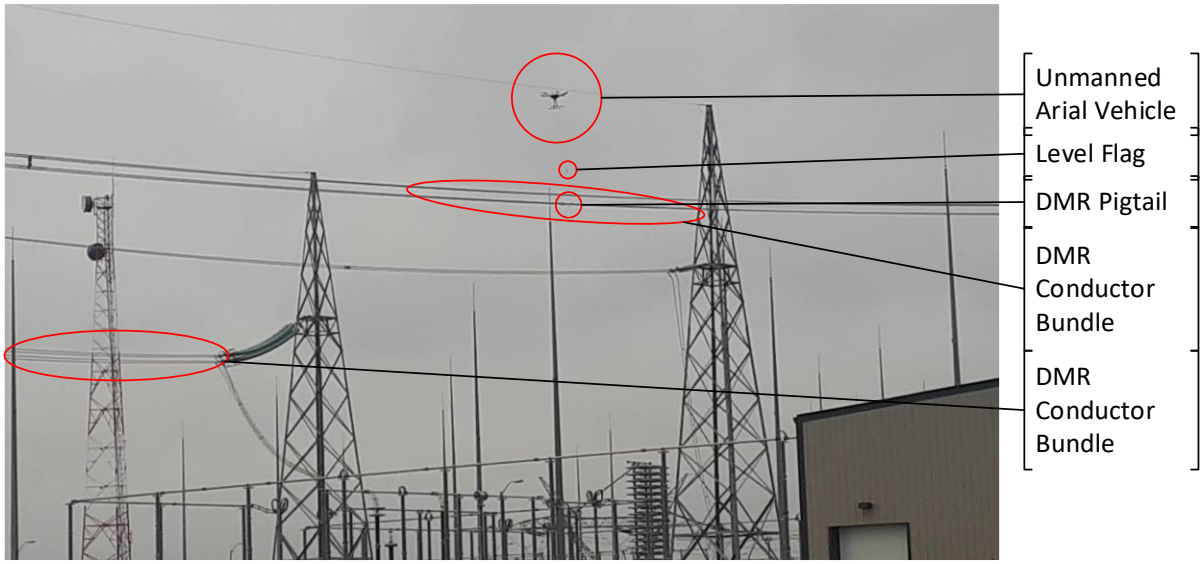

Figure 5-15: UAV fault application.

On the commencement of the test, the UAV flew the grounded conductor wire into the conductor bundle (Pole 2 or DMR 1) to be faulted. This created a line to ground fault. The EATL HVdc system cleared the faulted conductor bundle (Pole 2 or DMR 1) by opening the breaker associated with the conductor bundle isolating the conductor bundle from the rest of the system, this essentially took the conductor bundle out of service. After this was completed,

the UAV landed, thereby removing the fault from the conductor bundle. Then the faulted conductor bundle was brought back into service and the next test was started. (The UAV as seen in Figure 5-16 was owned and operated by AeroVision Canada Inc..)

Owing to logistics and permitted flight plans, the live line test was restricted to the set of tests outlined above. The potential risk of the UAV colliding with the line and causing significant damage to the transmission line dictated the limited number of tests that could be performed. Also, at the time of writing this thesis, permission had not been granted to apply the faults outside the station at other line locations.

Figure 5-16: UAV used for fault application.

In the fault detection approach, there are many possible sources of error. Incorrect fault locations could be reported because of a short transient period, (i.e., insufficient transient event data captured for analysis) or due to noise in measurements and sensitivity of the measured quantities at different locations along the line. Also, the multiple conversions from analog to digital (the transducers to the TDM bus) and digital to analog (the AIM2 to the DMU) could introduce additional errors in the measurements.

5.3.2.1 Fault Location Error in the Actual Online Neutral Line Fault Locator Scheme

Table 5-5 shows the results of calculating a fault location on the DMR 1 conductor and Pole 2 conductor in scenarios 1 and 2 using the actual nLFL. As before, the field tests confirmed the acceptable accuracy of the nLFL giving an error under 0.5% for faults at the beginning of the transmission line.

Table 5-5: EATL HVdc system DMR 1 and Pole 2 fault location results for scenarios 1 and 2 for transmission line length of 485.0 km (Actual fault location: 0.0 km from Heathfield converter station).

Faulted Conductor	Fault Distance (%)	Percent Error (%)			
		150 MW	250 MW	500 MW	1000 MW
DMR 1	0%	0.290%	-0.296%	-0.390%	-0.432%
Pole 2	0%	0.182%	-0.286%	-0.296%	-0.411%

5.4 Chapter Summary

This chapter examined the testing and verification of the capabilities of the nLFL system. The nLFL tests were conducted to determine the capacity of the nLFL to accurately detect and locate faults on the DMR 1 and Pole 2 conductor of the HVdc system. Three testing scenarios were used:

1. A detailed EMT simulation of the HVdc system and a model of the nLFL algorithm, including sampling rates etc.
2. Hardware in Loop testing with the actual nLFL connected to a real-time EMT simulator.
3. Field Testing of the nLFL.

The EMT model confirmed that the nLFL system is capable of accurately detecting and locating faults across the entire length of the line, with different power orders and conductor lengths, in several HVdc operating scenarios. The hardware in the loop testing of the nLFL

system with the RTDS™ confirmed that the physical implementation of the nLFL system performed as it was designed to in the PSCAD™/EMTDC™ simulation. Finally, the deployment of the nLFL system at the EATL HVdc system confirmed that practical implementation of the nLFL system was successful in detecting and locating the faults during the live tests conducted on the EATL HVdc system.

Chapter 6: Contributions and Conclusions and Recommendations

This thesis proposed a novel online Neutral Line Fault Locater (nLFL) system for fault location on the neutral/return conductors (DMR 1 and Pole 2) of an HVdc system. The nLFL is a passive double ended fault location algorithm that utilizes regression, of the time-based response of the Fault Distance Equation and the transient fault data from the HVdc system, to determine the neutral conductors' fault location.

6.1 Contributions and Conclusions

The salient contributions of this thesis are as follows:

- The thesis presented a comprehensive evaluation of existing HVdc line fault locator technologies. It also presented the limitations of these technologies for return conductors, with a view to improving on them. These include the following:
    - The main difficulty of fault location on the Dedicated Metallic Return (DMR) conductor is that the nominal operating voltage of this conductor is near zero during balanced operation of the system and one end of the return conductor is grounded. Thus, a fault to ground makes a very small change in the DMR voltage, making it a challenge to use this voltage for traveling wave fault detection at the station(s);
    - Another difficulty for fault location on the HVdc system, is the rapid control and protection capabilities of the HVdc system. This prevents

the HVdc system from reaching the faulted steady state period needed for fault location based on impedance.

- Existing HVdc line fault locator technologies, are either based on traveling waves or impedance measurements and have the following drawbacks:
  - Fault location based on traveling waves uses the arrival of a wave front(s) at the station from a fault to determine the fault location. However, this process will not work on return conductors since the detection of a wavefront on a zero voltage or grounded conductor is not possible;
  - Fault location based on impedance uses a ratio of the apparent resistance of the faulted conductor to the unfaulted conductor to determine the fault location. This method does not work well for return conductors since the required calculations have to be done at the faulted steady state and the HVdc control and protection system will operate to prevent the HVdc system from reaching the faulted steady state.

- The proposed nLFL system overcomes the drawbacks of existing fault location technologies. It uses a fault location technique based on impedance (dc resistance of the transmission line). It is able to assess the dc resistance value even before the faulted steady state is reached by using regression analysis to extrapolate the data, to estimate the steady state impedance. Hence, even if

protection opens the line before the faulted steady state is reached, the dc resistance value can be accurately determined.

    - The Fault Distance Equation is derived from nodal analysis of the equivalent circuit of the HVdc system in the faulted steady state. Here the system is simplified to a simple electric circuit consisting of resistors and fixed voltage sources.

- To locate a fault on a DMR conductor, the nLFL requires a voltage and a current of sufficient magnitude to perform its analysis:
    - Monopolar and Homopolar HVdc schemes can detect a return conductor fault during the normal operation of the HVdc system, because the return conductor is energized;
    - Bipolar and Bipolar Multiterminal HVdc schemes can only detect faults when running in an unbalanced operating mode or in a metallic return mode (Monopolar mode) where the return conductor is energized.
- The new nLFL strategy was implemented in hardware using two principal components that are located at each of the stations:
    - The Data Measurement Unit (DMU) that is responsible for detecting and capturing the data from the event for processing;
    - The industrial computer that is responsible for storing the event data, for processing the nLFL algorithm to locate the fault.
- The new nLFL strategy incorporates the following features into the design:

- The nLFL detects a fault when a transient event exceeds a threshold set for the measured signals. The measured signals are filtered to remove the dc component and any high frequency noise;
- The nLFL determines the faulted conductor when the measured current, at the two ends of the conductor, differ by a specified amount after the fault was detected;
- The fault location algorithm formulates the time domain response of the fault distance formula ($X_{A\_Flt\_x}$) by using the transient fault data (Voltages and currents measurements from the HVdc system) collected from the inception of the fault to the clearing of the fault by the HVdc protection system. It then uses regression to find the asymptotic value of $X_{A\_Flt\_x}$ at $t = \infty$, which gives the fault distance assuming that the values of voltage and current used in it had converged to the faulted steady state values (i.e., as if protective action had not taken the line out of service):
  - The nLFL measures data over a minimum transient interval of 900 ms to maintain an error of less than 1%.

- Sensitivity analysis was conducted on simulations of the measured quantities. It was determined that using regression to determine the faulted steady state values of currents (A_I_{dx} and B_I_{dx}) and voltages (A_U_{dx} and B_U_{dx}) at stations A and B resulted in less accurate results. Instead, the analysis showed that it is preferable to estimate the asymptotic values of the Fault Distance Equation, which is a combination of the measured voltages, currents, and conductor

resistance (R_x). To do this, $X_{A\_Flt\_x}$ is calculated at each instant in the transient period, and its asymptotic value is determined by regression.

- The performance of the nLFL system was evaluated using offline EMT studies, real-time hardware in the loop testing of the nLFL hardware when it was connected to a real-time EMT simulator and with real world testing at the EATL HVdc system:
    - The EMT simulation studies' results showed that it is possible to accurately detect and predict the fault location on the return conductors of a Monopolar HVdc scheme where the return path contains both the DMR 1 conductor and/or the Pole 2 conductor.
    - The real-time hardware in the loop tests, once again confirmed that the actual real-time hardware accurately detects and predicts the fault location on the return conductors for a Monopolar HVdc scheme where the return path contains both the DMR 1 conductor and/or the Pole 2 conductor.
    - The nLFL device was installed and tested on the East Alberta Transmission Line (EATL) HVdc system for limited on-site testing.
    - The accuracy of the nLFL system was shown to be within 0.5% of the total line length for both simulated tests, hardware in the loop tests and real-world transient events.

6.2 Recommendations for Future Work

The actual testing has shown that the nLFL is capable of accurately detecting and calculating the fault location on the HVdc return conductors. However, further research into

the system could prove to be valuable in improving the reliability of future energy projects. For instance, the thesis has shown that regression can be used to accurately predict the location of faults in an HVdc system. However, further research into regression techniques could introduce better models to predict the future values of the system and to improve the accuracy of the nLFL system. This could lead to more accurate dispatch of the resources needed for repair of HVdc systems and thereby reduce the down times of the HVdc system and improve the reliability of the power supply for the public.

As was previously discussed, at the time of completion of this thesis, official permission for further fault testing along the length of the EATL HVdc transmission line had not been approved. It recommended that further fault testing be done along the length of the transmission line outside of the Heathfield station where testing had been done. These tests will further confirm the testing perform in the offline EMT studies and real-time EMT hardware in the loop tests.

Further development of the nLFL system can be conducted to accommodate line to line faults on the HVdc transmission system. This research will expand the capabilities of the nLFL system and thus the reliability of the HVdc system as a whole.

As it is not feasible to break the conductor for practical testing of the nLFL the impact of conductor falling was not explicitly investigated. Therefore, further investigations should be conducted to observe the impact of conductor falling or breaking on the nLFL system.

The asymmetric sigmoidal function has been verified and has been shown to be accurate for the nLFL system in typical HVdc schemes. However, it is possible for the filters or other shunt elements to impact the characteristic response of the transmission line.

Therefore, further investigations should be done to observe how the asymmetric sigmoidal function would model the characteristic transient response of the faulted transmission line with additional filters or shunt devices.

The growing use of Multiterminal HVdc schemes, would benefit from the nLFL algorithm. The nLFL algorithm could be further enhanced to optimize the number of measurements needed from each station to calculate a fault location. Optimizing the number of measurements devices would help to reduce the overall costs to the HVdc system.

Furthermore, the principles employed in the nLFL algorithm to calculate the fault location in the HVdc system could be expanded to the ac fault location domain as well. The growing use of power electronic controlled devices, in the ac system, has reduced the accuracy of traditional fault location technologies. The power electronic devices can respond faster to transient events than can the traditional ac systems, to mitigate events. Power electronic devices, in the ac system, cause fault locations systems based on impedance to be less accurate in the identification of the fault location. The techniques employed by the nLFL could improve the accuracy of the ac fault location systems that have power electronic systems integrated in them, and by extensions improve the reliability of the ac system.

Overall, a commitment by the power transmission industries to provide further research into the Online Neutral Line Fault Locater's technology could benefit the power transmission industries.

References

[1] A. Kalair, N. Abas and N. Khan, "Comparative study of HVAC and HVDC transmission systems," *Renewable and Sustainable Energy Reviews*, vol. 59, no. 1, pp. 1653-1675, Feb 2016.

[2] B. Bose, "Global Warming: Energy, Environmental Pollution, and the Impact of Power Electronics," *IEEE Industrial Electronics Magazine*, vol. 4, no. 1, pp. 6-17, March 2010.

[3] S. Kumar and R. Madlener, "Energy systems and COP21 Paris climate agreement targets in Germany: an integrated modeling approach," in *2018 7th International Energy and Sustainability Conference (IESC)* , Cologne, May 2018.

[4] R. Serrano, M. R. Carvalho, J. C. Araneda, O. Alamos, L. Barroso, D. Bayma, R. Ferreira and R. Moreno, "Fighting Against Wildfires in Power Systems: Lessons and Resilient Practices From the Chilean and Brazilian Experiences," *IEEE Power & Energy Magazine*, vol. 20, no. 1, pp. 38-51, 2022.

[5] Mohibullah, Imdadullah and I. Ashraf, "Estimation of CO2 Mitigation Potential through Renewable Energy Generation," in *2006 IEEE International Power and Energy Conference*, Putra Jaya, Nov. 2006.

[6] G. M. Masters, Renewable and Efficient Electric Power Systems, 2 ed., Hoboken, New Jersey: John Wiley & Sons, Incorporated, 2013.

[7] M. Fiorelli, E. R. Sanseverino, F. Massaro, S. Favuzza, M. Ippolito and G. Zizzo, "The Energy Market Impact of Climate Change on Electricity Generation in Europe," in *2018 IEEE International Conference on Environment and Electrical Engineering and 2018 IEEE Industrial and Commercial Power Systems Europe (EEEIC / I&CPS Europe)*, Palermo, 2018.

[8] A. Grid, C. Barker, C. Davidson, J. Gold and N. Kirby, HVDC Connection to the Future, Levallois-Perret, Cedex: Alstom Grid, 2010, pp. 378-421.

[9] D. Marshall, P. Goosen and S. Boshoff, "Hydro generation and HVDC vs. fossil fired generation and HVAC," in *IEEE 3D Africon Conference. Africon '92 Proceedings (Cat. No.92CH3215)*, Johannesburg, 1992.

[10] R. G. Arrabé, C. A. Platero, F. Á. Gómez and E. R. López, "New Differential Protection Method for Multiterminal HVDC Cable Networks," *MDPI Energies*, vol. 11, no. 1, pp. 3386-3387, 2018.

[11] A. L. Figueroa-Acevedo, M. S. Czahor and D. E. Jahn, "A comparison of the technological, economic, public policy, and environmental factors of HVDC and HVAC interregional transmission," *AIMS Energy,* vol. 3, no. 1, pp. 144-161, Sep 2014.

[12] S. Liu, J. Daniel and J. Pan, "Offshore Wind Delivery System Technology Assessments and Performance Evaluation," in *2014 IEEE PES General Meeting | Conference & Exposition*, National Harbor, 2014.

[13] S. Naik and E. Koley, "Fault Detection and Classification scheme using KNN for AC/HVDC Transmission Lines," in *2019 International Conference on Communication and Electronics Systems (ICCES)*, Coimbatore, July 2019.

[14] J. Arrillaga, "High Voltage Direct Current Transmission," in *DC versus AC transmission*, 2 ed., The Institution of Engineering and Technology, 1998, pp. 253-278.

[15] Canadian Association of Petroleum, "Influence of High Voltage DC Power Lines on Metallic Pipelines," Canadian Association of Petroleum Producers, Calgary, Oct. 2014.

[16] J. Hu, Convenor, B. McLeod, Secretary, R. Ahmed, B. Bisewski, M. Dalzell, F. Exl, G. Georgel, L. Hidalgo, J. Jardini, T. Magg, M. Marzinotto, J. McNichol, P. Naidoo, S. Nyberg, G. Olguin, J. D. Rayo, M. Reynolds, H. Thunehed and K. Z. CN, "General Guidelines for HVdc Electrode Design," CIGRE, 2017.

[17] C. M. Franck, "HVDC Circuit Breakers: A Review Identifying Future Research Needs," *IEEE Transactions on Power Delivery*, vol. 26, no. 2, pp. 998-1007, April 2011.

[18] D. Jovcic, High Voltage Direct Current Transmission: Converters, Systems and DC Grids, John Wiley & Sons Ltd., 2019.

[19] J. Mooney and R. Cunico, "IEEE Guide for Determining Fault Location on AC Transmission and Distribution Lines," IEEE, New York, 2014.

[20] D. Guillen, C. Salas, L. F. Sanchez-Gomez and L. M. Castro, "Enhancement of dynamic phasor estimation based fault location algorithms for AC transmission lines," *IET Generation, Transmission & Distribution,* vol. 14, no. 1, pp. 1091-1103, 2019.

[21] T. Peng, D. Tzelepis, A. Dysko and I. Glesk, "Assessment of Fault Location Techniques in Voltage Source Converter based HVDC systems," in *2017 IEEE Texas Power and Energy Conference (TPEC)*, College Station, Feb. 2017.

[22] N. R. Warson and J. D. Watson, "An Overview of HVDC Technology," *MDPI Energies 2020,* vol. 13, 2020.

[23] R. Iravani, Voltage-Sourced Converters in Power Systems, Hoboken, New Jersey: John Wiley & Sons, Inc, 2010.

[24] N. Flourentzou, V. G. Agelidis and G. D. Demetriades, "VSC-Based HVDC Power Transmission Systems: An Overview," vol. 24, no. 3, p. IEEE Transactions on Power Electronics, March 2009.

[25] S. Allebrod, R. Hamerski and R. Marquardt, "New transformless, scalable modular multilevel converters for HVDC transmission," in *IEEE Power Electronics Specialists Conference – PESC 2008*, Rhodes, Greece, 2008.

[26] M. Davies, M. Dommaschk, J. Dorn, J. Lang, D. Retzmann and D. Soerangr, "HVDC Plus – basics and principle of operation," Siemens Energy Sector, 2008.

[27] A. Marzouki, F. Fnaiech and M. Hamouda, "A Review of PWM Voltage Source Converters Based Industrial Applications," in *2015 International Conference on Electrical Systems for Aircraft, Railway, Ship Propulsion and Road Vehicles (ESARS)*, Aachen, 2015.

[28] Siemens, "High Voltage Direct Current - Proven Technology for Power Exchange," Siemens AG, Erlangen, Germany.

[29] I. Takei, "Sakuma Frequency Converter Project," *IEEE Transactions on Power Apparatus and Systems*, vol. 84, pp. 411-415, 1965.

[30] G. Migliavacca, Advanced Technologies for Future Transmission Grids, Power Systems, London: Springer-Verlag, 2013.

[31] Z. Dai, X. Liu, C. Zhang and H. Zhu, "Protection scheme for DC lines in AC/DC hybrid distribution grids with MMCs," in *2018 International Conference on Power System Technology (POWERCON)*, Guangzhou, Nov. 2018.

[32] D. Naidoo and N. M. Ijumba, "HVDC line protection for the proposed future HVDC systems," in *2004 International Conference on Power System Technology*, Singapore, 2004.

[33] C. Kim, V. Sood, J. G., S. Lim and L. Lee, HVDC Transmission, John Wiley & Sons (Asia) Pte Ltd, 2009.

[34] K. Nanayakkara, Line Fault Location in Emerging HVDC Transmission Systems, Winnipeg,: University of Manitoba, 2014.

[35] H. Rao, "IEEE Guide for Establishing Basic Requirements for High-Voltage Direct-Current Transmission Protection and Control Equipment," IEEE, Piscataway, 2017.

[36] M. M. Saha, J. Izykowski and E. Rosolowski, Fault Location on Power Networks, New York: Springer-Verlag London Limited, 2010.

[37] M. R., Raza, A., Hussain, M. R., Abbas, G., Ahmed, I., Qayyum, M., Rasool, M. A., Khaleel and M. A., "MT–HVdc Systems Fault Classification and Location Methods

Based on Traveling and Non-Traveling Waves—A Comprehensive Review," *MDPI Applied Sciences*, vol. 9, no. 22, 2019.

[38] S. Lin, L. Liu, P. Sun, Y. Lei, Y. Teng and X. Li, "Fault Location Algorithm Based on Characteristic- Harmonic Measured Impedance for HVdc Grounding Electrode Lines," *IEEE Transactions on Instrumentation and Measurement*, vol. 69, no. 12, pp. 9578-9585, Dec. 2020.

[39] C. Zhang, Y. Teng, X. Li, Q. Huang, Z. Zhang and F. Li, "A Novel Location Method for Grounding Electrode Line Fault Caused by Unipolar Fault of the HVDC Transmission System," in *2018 International Conference on Smart Grid and Clean Energy Technologies (ICSGCE)*, 2018.

[40] S. Govindarajan, An Online Monitoring and Fault Location Methodology for Underground Power Cables, Arizona: Arizona State University , 2016.

[41] C. F. Jensen, Online Location of Faults on AC Cables in Underground Transmission Systems, Aalborg: Springer, 2014.

[42] M. Gilany, D. k. Ibrahim and E. S. T. Eldin, "Traveling-Wave-Based Fault-Location Scheme for Multiend-Aged Underground Cable System," in *IEEE Transactions on Power Delivery*, 2007.

[43] A. Ghaderi, H. A. Mohammadpour and H. Ginn, "Active Fault Location in Distribution Network using Time-Frequency Reflectometry," in *2015 IEEE Power and Energy Conference at Illinois*, Champaign, 2015.

[44] Y. Holbert and K. E. Kim, "New Passive Methodology for Online Power Cable Diagnosis by Frequency Analysis," in *2015 IEEE Power & Energy Society General Meeting*, Denver, 2015.

[45] P. Chen, B. Xu and J. Li, "A Traveling Wave Based Fault Locating System for HVDC Transmission Lines," in *2006 International Conference on Power System Technology*, Chongqing, 2006.

[46] J. Ammon, *A new Electrode Line Monitoring System for HVDC Applications.*

[47] A. Hermansson, "Simulation of line fault locator on HVDC Light electrode line," in *University West, Department of Engineering Science,*, Trollhättan, 2010.

[48] V. Pathirana, U. Gnanarathna and O. Nanayakkara, *Protection Strategy for HVDC Systems with Dedicated Metallic Return (DMR) Conductors*, PARIS: CIGRE, 2015.

[49] F. Chunju, D. Xiuhua, L. Shengfang and Y. Weiyong, "An Adaptive Fault Location Technique Based on PMU for Transmission Line," in *2007 IEEE Power Engineering Society General Meeting*, Tampa, FL, USA, 2007.

[50] A. H. Al-Mohammed and M. A. Abido, "Fault Location Based on Synchronized Measurements: A Comprehensive Survey," *Scientific World Journal,* vol. 2014, 2014.

[51] DVN, "Smart Cable Guard," DVN, 2020. [Online]. Available: https://www.dnv.com/power-renewables/services/scg/technology.html. [Accessed 2020].

[52] K. Gopalan, R. N. Biswas and S. Gupta, "A Cable Fault Locator Using Pulse Echo Measurement," *IETE Journal of Research,* vol. 23, no. 6, pp. 377-380, 1977.

[53] C. Yulin, Z. Jianfeng, Y. Xiaoyang, Z. X. and Z. Jie, "A Novel Fault Monitoring and Location System for HVDC Electrode Line," in *International Conference on Power System Technology,* Guangzhou, China, 2018.

[54] P. D. Bruyne and B. Currat, "Temperature and frequency effects on cable resistance Snapshots on multi-materials power cable linear resistance," 2015.

[55] P. Molfino, M. Nervi and S. Malgarotti, "On the choice of the right HVDC Electrode type," in *2019 AEIT HVDC International Conference (AEIT HVDC)*, Florence, 2019.

[56] C. Weber, "HVDC Divider: Compensated voltage divider for HVDC transmission systems," Trench, Saint Louis Cedex, 2012.

[57] D. Tzelepis, V. Psaras, E. Tsotsopoulou, S. Mirsaeidi, A. Dyśko, Q. Hong, X. Dong, S. M. Blair, V. C. Nikolaidis, V. Papaspiliotopoulos, G. Fusiek, G. M. Burt, P. Niewczas and C. D. Booth, "Voltage and Current Measuring Technologies for High Voltage Direct Current Supergrids: A Technology Review Identifying the Options for Protection, Fault Location and Automation Applications," *IEEE ACCESS,* pp. 203398-203428, 15 10 2020.

[58] M. Takahashi, K. Sasaki, Y. Hirata, T. Murao, H. Takeda, Y. Nakamura, T. Ohtsuka, T. Sakai and N. Nosaka, "Field test of DC optical current transformer for HVDC Link," in *IEEE PES General Meeting*, Minneapolis, 2010.

[59] P. Liu and V. Dinavahi, "Finite-Difference Relaxation for Parallel Computation of Ionized Field of HVDC," *IEEE Transactions on Power Delivery,* vol. 33, no. 1, pp. 119-129, Jan 2017.

[60] D. Festo, Electricity and New Energy Overcurrent and Overload Protection Using Protective Relays, Quebec, Quebec: Festo Didactic Ltée/Ltd, 2015.

[61] F. Didactic, Overcurrent and Overload Protection, Quebec,: Festo Didactic Ltée/Ltd, Nov. 2016.

[62] M. Ltd., "MyCurveFit," MyAssays Ltd., 2020. [Online]. Available: https://www.mycurvefit.com/. [Accessed 2020].

[63] B. W. Group, "General Guidelines For HVdc Electrode Design," CIGRE, 2017.

[64] D. Naidoo and N. Ijumba, "HVDC line protection for the proposed future HVDC systems," in *2004 International Conference on Power System Technology, 2004. PowerCon 2004.*, Singapore, Nov. 2004.

[65] ABB, Medium voltage products technical guide Protection criteria for medium voltage networks, Via Friuli: ABB, 2016.

Appendix A: Monopolar Fault Location Calculation

Parameter list:

A_U_{dH1}	Station A voltage for Pole 1
A_U_{dN1}	Station A voltage for Neutral 1
A_I_{dLH1}	Station A current for Pole 1
A_I_{dLH2}	Station A current for Pole 2
A_I_{dLN1}	Station A current for Neutral 1
A_I_{dDMR1}	Station A current for DMR 1
B_U_{dH1}	Station B voltage for Pole 1
B_U_{dN1}	Station B voltage for Neutral 1
B_I_{dLH1}	Station B current for Pole 1
B_I_{dLH2}	Station B current for Pole 2
B_I_{dLN1}	Station B current for Neutral 1
B_I_{dDMR1}	Station B current for DMR 1
B_I_{dSG}	Station B current for ground electrode
$D_{A\_Flt\_Pole1}$	Distance from Station A to the fault location for conductor Pole 1
$D_{A\_Flt\_Pole2}$	Distance from Station A to the fault location for conductor Pole 2
$D_{A\_Flt\_DMR1}$	Distance from Station A to the fault location for conductor DMR 1
$D_{B\_Flt\_Pole1}$	Distance from Station B to the fault location for conductor Pole 1
$D_{B\_Flt\_Pole2}$	Distance from Station B to the fault location for conductor Pole 2
$D_{B\_Flt\_DMR1}$	Distance from Station B to the fault location for conductor DMR 1
I_{Flt_Pole1}	Fault Current on conductor Pole 1
I_{Flt_Pole2}	Fault Current on conductor Pole 2

I_{Flt_DMR1}	Fault Current on conductor DMR 1
L_{Pole1}	Total length for conductor Pole 1
L_{Pole2}	Total length for conductor Pole 2
L_{DMR1}	Total length for conductor DMR 1
$R_{//}$	Resistance of Pole 2 and DMR 1 in parallel
R_{Pole1}	Total resistance for conductor Pole 1
R_{Pole2}	Total resistance for conductor Pole 2
R_{DMR1}	Total resistance for conductor DMR 1
R_{GND}	Resistance of the ground electrode
R_{Flt_Pole1}	Resistance of the fault on conductor Pole 1
R_{Flt_Pole2}	Resistance of the fault on conductor Pole 2
R_{Flt_DMR1}	Resistance of the fault on conductor DMR 1
$R_{A\_Flt\_Pole1}$	Resistance from Station A to the fault location for conductor Pole 1
$R_{A\_Flt\_Pole2}$	Resistance from Station A to the fault location for conductor Pole 2
$R_{A\_Flt\_DMR1}$	Resistance from Station A to the fault location for conductor DMR 1
$R_{B\_Flt\_Pole1}$	Resistance from Station B to the fault location for conductor Pole 1
$R_{B\_Flt\_Pole2}$	Resistance from Station B to the fault location for conductor Pole 2
$R_{B\_Flt\_DMR1}$	Resistance from Station B to the fault location for conductor DMR 1
$U_{//}$	Voltage across conductors Pole 2 and DMR 1 in parallel
U_{Flt_Pole1}	Fault voltage on conductor Pole 1
U_{Flt_Pole2}	Fault voltage on conductor Pole 2
U_{Flt_DMR1}	Fault voltage on conductor DMR 1
$X_{A\_Flt\_Pole1}$	Percentage of total line length from Station A to the fault location for conductor Pole 1
$X_{A\_Flt\_Pole2}$	Percentage of total line length from Station A to the fault location for conductor Pole 2
$X_{A\_Flt\_DMR1}$	Percentage of total line length from Station A to the fault location for conductor DMR 1

$X_{B\_Flt\_Pole1}$	Percentage of total line length from Station B to the fault location for conductor Pole 1
$X_{B\_Flt\_Pole2}$	Percentage of total line length from Station B to the fault location for conductor Pole 2
$X_{B\_Flt\_DMR1}$	Percentage of total line length from Station B to the fault location for conductor DMR 1

Pre-Fault Equivalent

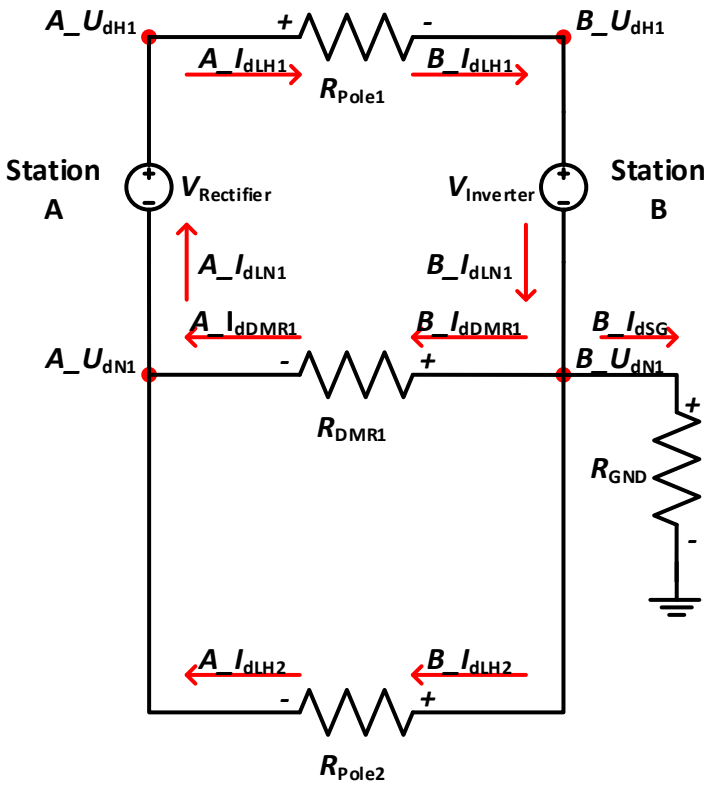

Figure A-1: Pre-Fault equivalent circuit schematic.

Assumptions:

$$A\_I_{\mathrm{dLH1}} = B\_I_{\mathrm{dLH1}}$$
$$A\_I_{\mathrm{dLH1}} = A\_I_{\mathrm{dLN1}}$$
$$A\_I_{\mathrm{dDMR1}} = B\_I_{\mathrm{dDMR1}}$$
$$A\_I_{\mathrm{dLH2}} = B\_I_{\mathrm{dLH2}}$$
$$B\_I_{\mathrm{dLH1}} = B\_I_{\mathrm{dLN1}}$$

Node A_U_{dH1}:

$$A\_I_{\mathrm{dLH1}} = \frac{A\_U_{\mathrm{dH1}} - B\_U_{\mathrm{dH1}}}{R_{\mathrm{Pole1}}}$$

Node B_U_{dH1}:

$$B\_I_{\mathrm{dLH1}} = \frac{A\_U_{\mathrm{dH1}} - B\_U_{\mathrm{dH1}}}{R_{\mathrm{Pole1}}}$$

Node A_U_{dN1}:

$$A\_I_{\mathrm{dLN1}} = A\_I_{\mathrm{dLH2}} + A\_I_{\mathrm{dDMR1}}$$

Node B_U_{dN1}:

$$B\_I_{\mathrm{dLN1}} = B\_I_{\mathrm{dLH2}} + B\_I_{\mathrm{dDMR1}} + B\_I_{\mathrm{dSG}}$$

Fault Parameters and Equations

Unknown:

B_U_{dN1}

U_{Flt_Pole1}
U_{Flt_Pole2}
U_{Flt_DMR1}

I_{Flt_Pole1}
I_{Flt_Pole2}
I_{Flt_DMR1}

R_{Pole1}
R_{Pole2}
R_{DMR1}

R_{GND}

R_{Flt_Pole1}
R_{Flt_Pole2}
R_{Flt_DMR1}

$R_{A\_Flt\_Pole1}$
$R_{A\_Flt\_Pole2}$
$R_{A\_Flt\_DMR1}$
$R_{B\_Flt\_Pole1}$
$R_{B\_Flt\_Pole2}$
$R_{B\_Flt\_DMR1}$

$D_{A\_Flt\_Pole1}$
$D_{A\_Flt\_Pole2}$
$D_{A\_Flt\_DMR1}$
$D_{B\_Flt\_Pole1}$
$D_{B\_Flt\_Pole2}$
$D_{B\_Flt\_DMR1}$

$X_{A\_Flt\_Pole1}$
$X_{A\_Flt\_Pole2}$
$X_{A\_Flt\_DMR1}$
$X_{B\_Flt\_Pole1}$
$X_{B\_Flt\_Pole2}$
$X_{B\_Flt\_DMR1}$

Measured:

A_U_{dH1}
A_U_{dN1}
A_I_{dLH1}
A_I_{dLH2}
A_I_{dLN1}
A_I_{dDMR1}

B_U_{dH1}
B_I_{dLH1}
B_I_{dLH2}
B_I_{dLN1} (Not Recorded)
B_I_{dDMR1}
B_I_{dSG}
B_I_{dSGHR}

Assumptions:

$$100\% = X_{A\_Flt\_Pole1} + X_{B\_Flt\_Pole1}$$
$$100\% = X_{A\_Flt\_Pole2} + X_{B\_Flt\_Pole2}$$
$$100\% = X_{A\_Flt\_DMR1} + X_{B\_Flt\_DMR1}$$

$$L_{Pole1} = D_{A\_Flt\_Pole1} + D_{B\_Flt\_Pole1}$$
$$L_{Pole2} = D_{A\_Flt\_Pole2} + D_{B\_Flt\_Pole2}$$
$$L_{DMR1} = D_{A\_Flt\_DMR1} + D_{B\_Flt\_DMR1}$$

$$R_{Pole1} = R_{A\_Flt\_Pole1} + R_{B\_Flt\_Pole1}$$
$$R_{Pole2} = R_{A\_Flt\_Pole2} + R_{B\_Flt\_Pole2}$$
$$R_{DMR1} = R_{A\_Flt\_DMR1} + R_{B\_Flt\_DMR1}$$

$$U_{Flt\_Pole1} = I_{Flt\_Pole1} \times R_{Flt\_Pole1}$$
$$U_{Flt\_Pole2} = I_{Flt\_Pole2} \times R_{Flt\_Pole2}$$
$$U_{Flt\_DMR1} = I_{Flt\_DMR1} \times R_{Flt\_DMR1}$$

$$B\_U_{dN1} = B\_I_{dSG} \times R_{GND}$$

$$R_{Pole1} \cong R_{Pole2}$$

$$R_{Pole1} = \frac{A\_U_{dH1} - B\_U_{dH1}}{A\_I_{dLH1}}$$
$$R_{Pole2} = \frac{A\_U_{dN1} - B\_U_{dN1}}{A\_I_{dLH2}}$$
$$R_{DMR1} = \frac{A\_U_{dN1} - B\_U_{dN1}}{A\_I_{dDMR1}}$$

Known:

L_{Pole1} = 485.0 km
L_{Pole2} = 485.0 km
L_{DMR1} = 485.0 km

DMR 1 Fault Equivalent

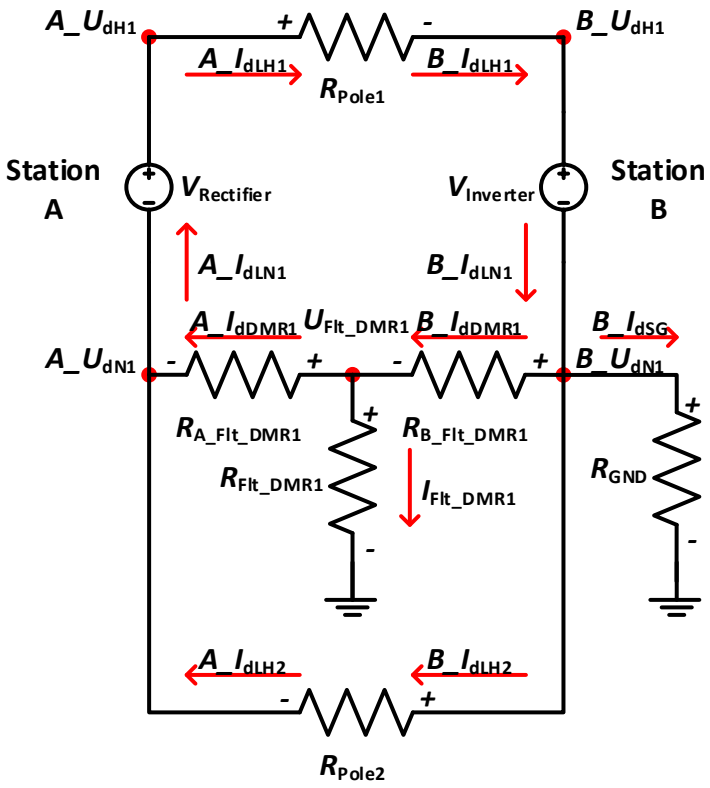

Figure A-2: DMR 1 fault equivalent circuit schematic.

Assumptions:

$$A\_I_{\mathrm{dLH1}} = B\_I_{\mathrm{dLH1}}$$
$$A\_I_{\mathrm{dLH1}} \cong A\_I_{\mathrm{dLN1}}$$
$$A\_I_{\mathrm{dDMR1}} \neq B\_I_{\mathrm{dDMR1}}$$
$$A\_I_{\mathrm{dLH2}} = B\_I_{\mathrm{dLH2}}$$
$$B\_I_{\mathrm{dLH1}} \cong B\_I_{\mathrm{dLN1}}$$

Node A_U_{dH1}:

$$A\_I_{\mathrm{dLH1}} = \frac{A\_U_{\mathrm{dH1}} - B\_U_{\mathrm{dH1}}}{R_{\mathrm{Pole1}}}$$

Node B_U_{dH1}:

$$B\_I_{\mathrm{dLH1}} = \frac{A\_U_{\mathrm{dH1}} - B\_U_{\mathrm{dH1}}}{R_{\mathrm{Pole1}}}$$

Node A_U_{dN1}:

$$A\_I_{\mathrm{dLN1}} = A\_I_{\mathrm{dLH2}} + A\_I_{\mathrm{dDMR1}}$$

Node B_U_{dN1}:

$$B\_I_{\mathrm{dLN1}} = B\_I_{\mathrm{dLH2}} + B\_I_{\mathrm{dDMR1}} + B\_I_{\mathrm{dSG}}$$

Node $U_{\text{Flt\_DMR1}}$:

$$B\_I_{\text{dDMR1}} = A\_I_{\text{dDMR1}} + I_{\text{Flt\_DMR1}}$$

DMR 1 Fault Equivalent from Station A

Equation 1: DMR 1 fault current from Station A.

$$A\_I_{\text{dDMR1}} = \frac{U_{\text{Flt\_DMR1}} - A\_U_{\text{dN1}}}{\left(X_{\text{A\_Flt\_DMR1}} \times R_{\text{DMR1}}\right)}$$
$$\left(A\_I_{\text{dDMR1}} \times X_{\text{A\_Flt\_DMR1}} \times R_{\text{DMR1}}\right) = U_{\text{Flt\_DMR1}} - A\_U_{\text{dN1}}$$
$$U_{\text{Flt\_DMR1}} = A\_U_{\text{dN1}} + \left(X_{\text{A\_Flt\_DMR1}} \times A\_I_{\text{dDMR1}} \times R_{\text{DMR1}}\right)$$

Equation 2: DMR 1 fault current from Station B.

$$B\_I_{\text{dDMR1}} = \frac{B\_U_{\text{dN1}} - U_{\text{Flt\_DMR1}}}{\left(\left(100\% - X_{\text{A\_Flt\_DMR1}}\right) \times R_{\text{DMR1}}\right)}$$
$$B\_I_{\text{dDMR1}} \times \left(\left(100\% - X_{\text{A\_Flt\_DMR1}}\right) \times R_{\text{DMR1}}\right) = B\_U_{\text{dN1}} - U_{\text{Flt\_DMR1}}$$
$$\left(100\% \times B\_I_{\text{dDMR1}} \times R_{\text{DMR1}}\right) - \left(X_{\text{A\_Flt\_DMR1}} \times B\_I_{\text{dDMR1}} \times R_{\text{DMR1}}\right) = B\_U_{\text{dN1}} - U_{\text{Flt\_DMR1}}$$
$$\left(B\_I_{\text{dDMR1}} \times R_{\text{DMR1}}\right) - \left(X_{\text{A\_Flt\_DMR1}} \times B\_I_{\text{dDMR1}} \times R_{\text{DMR1}}\right) = B\_U_{\text{dN1}} - U_{\text{Flt\_DMR1}}$$
$$U_{\text{Flt\_DMR1}} = B\_U_{\text{dN1}} - \left(B\_I_{\text{dDMR1}} \times R_{\text{DMR1}}\right) + \left(X_{\text{A\_Flt\_DMR1}} \times B\_I_{\text{dDMR1}} \times R_{\text{DMR1}}\right)$$

DMR 1 solved for $X_{\text{A\_Flt\_DMR1}}$.

$$A\_U_{\text{dN1}} + \left(X_{\text{A\_Flt\_DMR1}} \times A\_I_{\text{dDMR1}} \times R_{\text{DMR1}}\right) = B\_U_{\text{dN1}} - \left(B\_I_{\text{dDMR1}} \times R_{\text{DMR1}}\right) + \left(X_{\text{A\_Flt\_DMR1}} \times B\_I_{\text{dDMR1}} \times R_{\text{DMR1}}\right)$$
$$A\_U_{\text{dN1}} - B\_U_{\text{dN1}} + \left(B\_I_{\text{dDMR1}} \times R_{\text{DMR1}}\right) = -\left(X_{\text{A\_Flt\_DMR1}} \times A\_I_{\text{dDMR1}} \times R_{\text{DMR1}}\right) + \left(X_{\text{A\_Flt\_DMR1}} \times B\_I_{\text{dDMR1}} \times R_{\text{DMR1}}\right)$$
$$A\_U_{\text{dN1}} - B\_U_{\text{dN1}} + \left(B\_I_{\text{dDMR1}} \times R_{\text{DMR1}}\right) = X_{\text{A\_Flt\_DMR1}} \times R_{\text{DMR1}} \times \left(-A\_I_{\text{dDMR1}} + B\_I_{\text{dDMR1}}\right)$$
$$X_{\text{A\_Flt\_DMR1}} = \frac{A\_U_{\text{dN1}} - B\_U_{\text{dN1}} + \left(B\_I_{\text{dDMR1}} \times R_{\text{DMR1}}\right)}{R_{\text{DMR1}} \times \left(-A\_I_{\text{dDMR1}} + B\_I_{\text{dDMR1}}\right)}$$

DMR 1 Fault Equivalent from Station B

Equation 1: DMR 1 fault current from Station A.

$$A\_I_{\mathrm{dDMR1}} = \frac{U_{\mathrm{Flt\_DMR1}} - A\_U_{\mathrm{dN1}}}{\left(\left(100\% - X_{\mathrm{B\_Flt\_DMR1}}\right) \times R_{\mathrm{DMR1}}\right)}$$

$$A\_I_{\mathrm{dDMR1}} \times \left(\left(100\% - X_{\mathrm{B\_Flt\_DMR1}}\right) \times R_{\mathrm{DMR1}}\right) = U_{\mathrm{Flt\_DMR1}} - A\_U_{\mathrm{dN1}}$$

$$(100\% \times A\_I_{\mathrm{dDMR1}} \times R_{\mathrm{DMR1}}) - \left(X_{\mathrm{B\_Flt\_DMR1}} \times A\_I_{\mathrm{dDMR1}} \times R_{\mathrm{DMR1}}\right) = U_{\mathrm{Flt\_DMR1}} - A\_U_{\mathrm{dN1}}$$

$$(A\_I_{\mathrm{dDMR1}} \times R_{\mathrm{DMR1}}) - \left(X_{\mathrm{B\_Flt\_DMR1}} \times A\_I_{\mathrm{dDMR1}} \times R_{\mathrm{DMR1}}\right) = U_{\mathrm{Flt\_DMR1}} - A\_U_{\mathrm{dN1}}$$

$$U_{\mathrm{Flt\_DMR1}} = A\_U_{\mathrm{dN1}} + (A\_I_{\mathrm{dDMR1}} \times R_{\mathrm{DMR1}}) - \left(X_{\mathrm{B\_Flt\_DMR1}} \times A\_I_{\mathrm{dDMR1}} \times R_{\mathrm{DMR1}}\right)$$

Equation 2: DMR 1 fault current from Station B.

$$B\_I_{\mathrm{dDMR1}} = \frac{B\_U_{\mathrm{dN1}} - U_{\mathrm{Flt\_DMR1}}}{\left(X_{\mathrm{B\_Flt\_DMR1}} \times R_{\mathrm{DMR1}}\right)}$$

$$\left(B\_I_{\mathrm{dDMR1}} \times X_{\mathrm{B\_Flt\_DMR1}} \times R_{\mathrm{DMR1}}\right) = B\_U_{\mathrm{dN1}} - U_{\mathrm{Flt\_DMR1}}$$

$$U_{\mathrm{Flt\_DMR1}} = B\_U_{\mathrm{dN1}} - \left(X_{\mathrm{B\_Flt\_DMR1}} \times B\_I_{\mathrm{dDMR1}} \times R_{\mathrm{DMR1}}\right)$$

DMR 1 solved for $X_{\mathrm{B\_Flt\_DMR1}}$.

$$B\_U_{\mathrm{dN1}} - \left(X_{\mathrm{B\_Flt\_DMR1}} \times B\_I_{\mathrm{dDMR1}} \times R_{\mathrm{DMR1}}\right) = A\_U_{\mathrm{dN1}} + (A\_I_{\mathrm{dDMR1}} \times R_{\mathrm{DMR1}}) - \left(X_{\mathrm{B\_Flt\_DMR1}} \times A\_I_{\mathrm{dDMR1}} \times R_{\mathrm{DMR1}}\right)$$

$$B\_U_{dN1} - A\_U_{dN1} - (A\_I_{dDMR1} \times R_{DMR1}) = \left(X_{\mathrm{B\_Flt\_DMR1}} \times B\_I_{\mathrm{dDMR1}} \times R_{\mathrm{DMR1}}\right) - \left(X_{\mathrm{B\_Flt\_DMR1}} \times A\_I_{\mathrm{dDMR1}} \times R_{\mathrm{DMR1}}\right)$$

$$B\_U_{\mathrm{dN1}} - A\_U_{\mathrm{dN1}} - (A\_I_{\mathrm{dDMR1}} \times R_{\mathrm{DMR1}}) = X_{\mathrm{B\_Flt\_DMR1}} \times R_{\mathrm{DMR1}} \times (-A\_I_{\mathrm{dDMR1}} + B\_I_{\mathrm{dDMR1}})$$

$$X_{\mathrm{B\_Flt\_DMR1}} = \frac{B\_U_{\mathrm{dN1}} - A\_U_{\mathrm{dN1}} - (A\_I_{\mathrm{dDMR1}} \times R_{\mathrm{DMR1}})}{R_{\mathrm{DMR1}} \times (-A\_I_{\mathrm{dDMR1}} + B\_I_{\mathrm{dDMR1}})}$$

Pole 2 Fault Equivalent

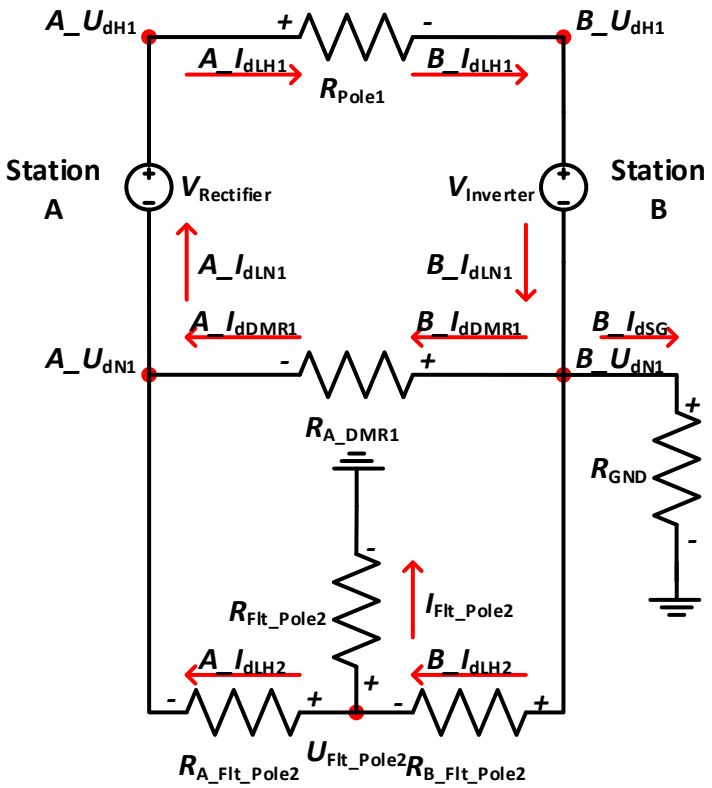

Figure A-3: Pole 2 fault equivalent circuit schematic.

Assumptions:

$$A\_I_{\mathrm{dLH1}} = B\_I_{\mathrm{dLH1}}$$
$$A\_I_{\mathrm{dLH1}} \cong A\_I_{\mathrm{dLN1}}$$
$$A\_I_{\mathrm{dDMR1}} = B\_I_{\mathrm{dDMR1}}$$
$$A\_I_{\mathrm{dLH2}} \neq B\_I_{\mathrm{dLH2}}$$
$$B\_I_{\mathrm{dLH1}} \cong B\_I_{\mathrm{dLN1}}$$

Node A_U_{dH1}:

$$A\_I_{\mathrm{dLH1}} = \frac{A\_U_{\mathrm{dH1}} - B\_U_{\mathrm{dH1}}}{R_{\mathrm{Pole1}}}$$

Node B_U_{dH1}:

$$B\_I_{\mathrm{dLH1}} = \frac{A\_U_{\mathrm{dH1}} - B\_U_{\mathrm{dH1}}}{R_{\mathrm{Pole1}}}$$

Node A_U_{dN1}:

$$A\_I_{\mathrm{dLN1}} = A\_I_{\mathrm{dLN2}} + A\_I_{\mathrm{dDMR1}}$$

Node B_U_{dN1}:

$$B\_I_{\mathrm{dLN1}} = B\_I_{\mathrm{dLN2}} + B\_I_{\mathrm{dDMR1}} + B\_I_{\mathrm{dGR}}$$

Node $U_{\text{Flt\_Pole2}}$:

$$B\_I_{\text{dLH2}} = A\_I_{\text{dLH2}} + I_{\text{Flt\_Pole2}}$$

Pole 2 Fault Equivalent from Station A

Equation 1: Pole 2 fault current from Station A.

$$A\_I_{\text{dLH2}} = \frac{U_{\text{Flt\_Pole2}} - A\_U_{\text{dN1}}}{\left(X_{\text{A\_Flt\_Pole2}} \times R_{\text{Pole2}}\right)}$$
$$\left(A\_I_{\text{dLH2}} \times X_{\text{A\_Flt\_Pole2}} \times R_{\text{Pole2}}\right) = U_{\text{Flt\_Pole2}} - A\_U_{\text{dN1}}$$
$$U_{\text{Flt\_Pole2}} = A\_U_{\text{dN1}} + \left(X_{\text{A\_Flt\_Pole2}} \times A\_I_{\text{dLH2}} \times R_{\text{Pole2}}\right)$$

Equation 2: Pole 2 fault current from Station B.

$$B\_I_{\text{dLH2}} = \frac{B\_U_{\text{dN1}} - U_{\text{Flt\_Pole2}}}{\left(\left(100\% - X_{\text{A\_Flt\_Pole2}}\right) \times R_{\text{Pole2}}\right)}$$
$$B\_I_{\text{dLH2}} \times \left(\left(100\% - X_{\text{A\_Flt\_Pole2}}\right) \times R_{\text{Pole2}}\right) = B\_U_{\text{dN1}} - U_{\text{Flt\_Pole2}}$$
$$\left(100\% \times B\_I_{\text{dLH2}} \times R_{\text{Pole2}}\right) - \left(X_{\text{A\_Flt\_Pole2}} \times B\_I_{\text{dLH2}} \times R_{\text{Pole2}}\right) = B\_U_{\text{dN1}} - U_{\text{Flt\_Pole2}}$$
$$\left(B\_I_{\text{dLH2}} \times R_{\text{Pole2}}\right) - \left(X_{\text{A\_Flt\_Pole2}} \times B\_I_{\text{dLH2}} \times R_{\text{Pole2}}\right) = B\_U_{\text{dN1}} - U_{\text{Flt\_Pole2}}$$
$$U_{\text{Flt\_Pole2}} = B\_U_{\text{dN1}} - \left(B\_I_{\text{dLH2}} \times R_{\text{Pole2}}\right) + \left(X_{\text{A\_Flt\_Pole2}} \times B\_I_{\text{dLH2}} \times R_{\text{Pole2}}\right)$$

Pole 2 solved for $X_{\text{A\_Flt\_Pole2}}$.

$$A\_U_{\text{dN1}} + \left(X_{\text{A\_Flt\_Pole2}} \times A\_I_{\text{dLH2}} \times R_{\text{Pole2}}\right) = B\_U_{\text{dN1}} - \left(B\_I_{\text{dLH2}} \times R_{\text{Pole2}}\right) + \left(X_{\text{A\_Flt\_Pole2}} \times B\_I_{\text{dLH2}} \times R_{\text{Pole2}}\right)$$
$$A\_U_{\text{dN1}} - B\_U_{\text{dN1}} + \left(B\_I_{\text{dLH2}} \times R_{\text{Pole2}}\right) = -\left(X_{\text{A\_Flt\_Pole2}} \times A\_I_{\text{dLH2}} \times R_{\text{Pole2}}\right) + \left(X_{\text{A\_Flt\_Pole2}} \times B\_I_{\text{dLH2}} \times R_{\text{Pole2}}\right)$$
$$A\_U_{\text{dN1}} - B\_U_{\text{dN1}} + \left(B\_I_{\text{dLH2}} \times R_{\text{Pole2}}\right) = X_{\text{A\_Flt\_Pole2}} \times R_{\text{Pole2}} \times \left(-A\_I_{\text{dLH2}} + B\_I_{\text{dLH2}}\right)$$
$$X_{\text{A\_Flt\_Pole2}} = \frac{A\_U_{\text{dN1}} - B\_U_{\text{dN1}} + \left(B\_I_{\text{dLH2}} \times R_{\text{Pole2}}\right)}{R_{\text{Pole2}} \times \left(-A\_I_{\text{dLH2}} + B\_I_{\text{dLH2}}\right)}$$

Pole 2 Fault Equivalent from Station B

Equation 1: Pole 2 fault current from Station A.

$$A\_I_{\mathrm{dLH2}} = \frac{U_{\mathrm{Flt\_Pole2}} - A\_U_{\mathrm{dN1}}}{\left(\left(100\% - X_{\mathrm{B\_Flt\_Pole2}}\right) \times R_{\mathrm{Pole2}}\right)}$$

$$A\_I_{\mathrm{dLH2}} \times \left(\left(100\% - X_{\mathrm{B\_Flt\_Pole2}}\right) \times R_{\mathrm{Pole2}}\right) = U_{\mathrm{Flt\_Pole2}} - A\_U_{\mathrm{dN1}}$$

$$(100\% \times A\_I_{\mathrm{dLH2}} \times R_{\mathrm{Pole2}}) - \left(X_{\mathrm{B\_Flt\_Pole2}} \times A\_I_{\mathrm{dLH2}} \times R_{\mathrm{Pole2}}\right) = U_{\mathrm{Flt\_Pole2}} - A\_U_{\mathrm{dN1}}$$

$$(A\_I_{\mathrm{dLH2}} \times R_{\mathrm{Pole2}}) - \left(X_{\mathrm{B\_Flt\_Pole2}} \times A\_I_{\mathrm{dLH2}} \times R_{\mathrm{Pole2}}\right) = U_{\mathrm{Flt\_Pole2}} - A\_U_{\mathrm{dN1}}$$

$$U_{\mathrm{Flt\_Pole2}} = A\_U_{\mathrm{dN1}} + (A\_I_{\mathrm{dLH2}} \times R_{\mathrm{Pole2}}) - \left(X_{\mathrm{B\_Flt\_Pole2}} \times A\_I_{\mathrm{dLH2}} \times R_{\mathrm{Pole2}}\right)$$

Equation 2: Pole 2 fault current from Station B.

$$B\_I_{\mathrm{dLH2}} = \frac{B\_U_{\mathrm{dN1}} - U_{\mathrm{Flt\_Pole2}}}{\left(X_{\mathrm{B\_Flt\_Pole2}} \times R_{\mathrm{Pole2}}\right)}$$

$$\left(B\_I_{\mathrm{dLH2}} \times X_{\mathrm{B\_Flt\_Pole2}} \times R_{\mathrm{Pole2}}\right) = B\_U_{\mathrm{dN1}} - U_{\mathrm{Flt\_Pole2}}$$

$$U_{\mathrm{Flt\_Pole2}} = B\_U_{\mathrm{dN1}} - \left(X_{\mathrm{B\_Flt\_Pole2}} \times B\_I_{\mathrm{dLH2}} \times R_{\mathrm{Pole2}}\right)$$

Pole 2 solve for $X_{\mathrm{B\_Flt\_Pole2}}$.

$$B\_U_{\mathrm{dN1}} - \left(X_{\mathrm{B\_Flt\_Pole2}} \times B\_I_{\mathrm{dLH2}} \times R_{\mathrm{Pole2}}\right) = A\_U_{\mathrm{dN1}} + (A\_I_{\mathrm{dLH2}} \times R_{\mathrm{Pole2}}) - \left(X_{\mathrm{B\_Flt\_Pole2}} \times A\_I_{\mathrm{dLH2}} \times R_{\mathrm{Pole2}}\right)$$

$$B\_U_{\mathrm{dN1}} - A\_U_{\mathrm{dN1}} - (A\_I_{\mathrm{dLH2}} \times R_{\mathrm{Pole2}}) = \left(X_{\mathrm{B\_Flt\_Pole2}} \times B\_I_{\mathrm{dLH2}} \times R_{\mathrm{Pole2}}\right) - \left(X_{\mathrm{B\_Flt\_Pole2}} \times A\_I_{\mathrm{dLH2}} \times R_{\mathrm{Pole2}}\right)$$

$$B\_U_{\mathrm{dN1}} - A\_U_{\mathrm{dN1}} - (A\_I_{\mathrm{dLH2}} \times R_{\mathrm{Pole2}}) = X_{\mathrm{B\_Flt\_Pole2}} \times R_{\mathrm{Pole2}} \times (-A\_I_{\mathrm{dLH2}} + B\_I_{\mathrm{dLH2}})$$

$$X_{\mathrm{B\_Flt\_Pole2}} = \frac{B\_U_{\mathrm{dN1}} - A\_U_{\mathrm{dN1}} - (A\_I_{\mathrm{dLH2}} \times R_{\mathrm{Pole2}})}{R_{\mathrm{Pole2}} \times (-A\_I_{\mathrm{dLH2}} + B\_I_{\mathrm{dLH2}})}$$

DMR 1 Resistance Equation

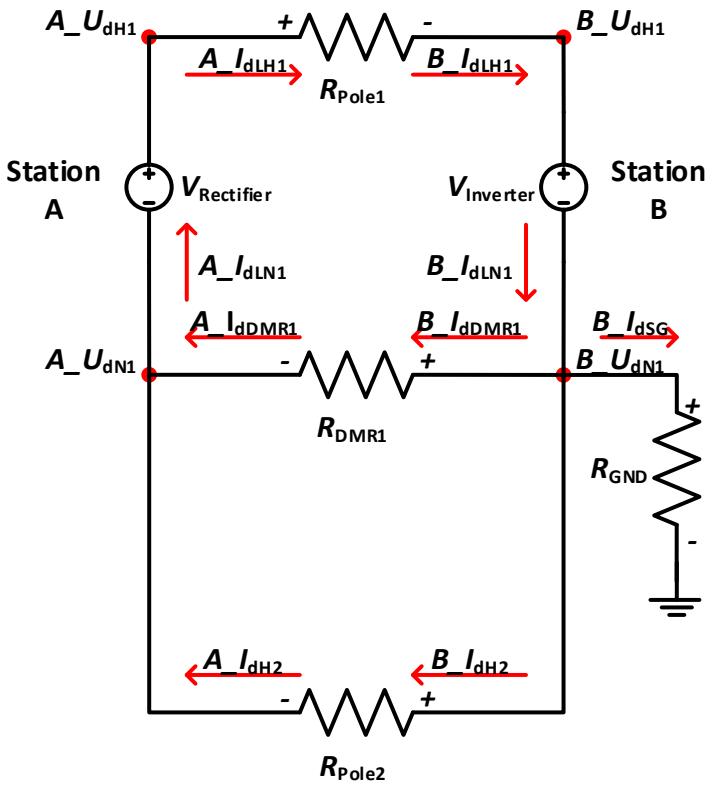

Figure A-4: Pre-Fault equivalent circuit schematic.

Assumptions:

$$A\_I_{\mathrm{dLH1}} = B\_I_{\mathrm{dLH1}}$$
$$A\_I_{\mathrm{dLH1}} = A\_I_{\mathrm{dLN1}}$$
$$A\_I_{\mathrm{dDMR1}} = B\_I_{\mathrm{dDMR1}}$$
$$A\_I_{\mathrm{dLH2}} = B\_I_{\mathrm{dLH2}}$$
$$B\_I_{\mathrm{dLH1}} = B\_I_{\mathrm{dLN1}}$$
$$R_{//} = \frac{R_{\mathrm{Pole1}} \times R_{\mathrm{DMR1}}}{R_{\mathrm{Pole1}} + R_{\mathrm{DMR1}}}$$
$$R_{//} = \frac{U_{//}}{A\_I_{\mathrm{dLN1}}}$$

Equation 1: Solve for R_{DMR1} from $R_{//}$.

$$R_{//} = \frac{R_{\mathrm{Pole2}} \times R_{\mathrm{DMR1}}}{R_{\mathrm{Pole2}} + R_{\mathrm{DMR1}}}$$
$$R_{//} \times (R_{\mathrm{Pole2}} + R_{\mathrm{DMR1}}) = (R_{\mathrm{Pole2}} \times R_{\mathrm{DMR1}})$$
$$(R_{//} \times R_{\mathrm{Pole2}}) + (R_{//} \times R_{\mathrm{DMR1}}) = (R_{\mathrm{Pole2}} \times R_{\mathrm{DMR1}})$$
$$(R_{//} \times R_{\mathrm{Pole2}}) = (R_{\mathrm{Pole2}} \times R_{\mathrm{DMR1}}) - (R_{//} \times R_{\mathrm{DMR1}})$$
$$(R_{//} \times R_{\mathrm{Pole2}}) = R_{\mathrm{DMR1}} \times (R_{\mathrm{Pole2}} - R_{//})$$

$$R_{\mathrm{DMR1}} = \frac{\left(R_{\mathrm{Pole2}} \times R_{//}\right)}{\left(R_{\mathrm{Pole2}} - R_{//}\right)}$$

Equation 2: Solve for $R_{//}$ from system voltages and currents.

$$R_{//} = \frac{U_{//}}{A\_I_{\mathrm{dLN1}}}$$

$$R_{//} = \frac{A\_U_{\mathrm{dN1}} - B\_U_{\mathrm{dN1}}}{A\_I_{\mathrm{dLN1}}}$$

$$R_{//} = \frac{A\_U_{\mathrm{dN1}} - (B\_I_{\mathrm{dSG}} \times R_{\mathrm{GND}})}{A\_I_{\mathrm{dLN1}}}$$

Solve for R_{DMR1}.

$$R_{\mathrm{DMR1}} = \frac{R_{\mathrm{Pole2}} \times \left(\frac{A\_U_{\mathrm{dN1}} - (B\_I_{\mathrm{dSG}} \times R_{\mathrm{GND}})}{A\_I_{\mathrm{dLN1}}}\right)}{R_{\mathrm{Pole2}} - \left(\frac{A\_U_{\mathrm{dN1}} - (B\_I_{\mathrm{dSG}} \times R_{\mathrm{GND}})}{A\_I_{\mathrm{dLN1}}}\right)}$$

$$R_{DMR1} = \frac{R_{\mathrm{Pole2}} \times \left(A\_U_{\mathrm{dN1}} - (B\_I_{\mathrm{dSG}} \times R_{\mathrm{GND}})\right)}{(R_{\mathrm{Pole2}} \times A\_I_{\mathrm{dLN1}}) - \left(A\_U_{\mathrm{dN1}} - (B\_I_{\mathrm{dSG}} \times R_{\mathrm{GND}})\right)}$$

Appendix B: Online Neutral Line Fault Locator Webpages

Main page (Figure B-1) – This displays the general status of the nLFL including the last known fault location, current GPS status and current alarm status.

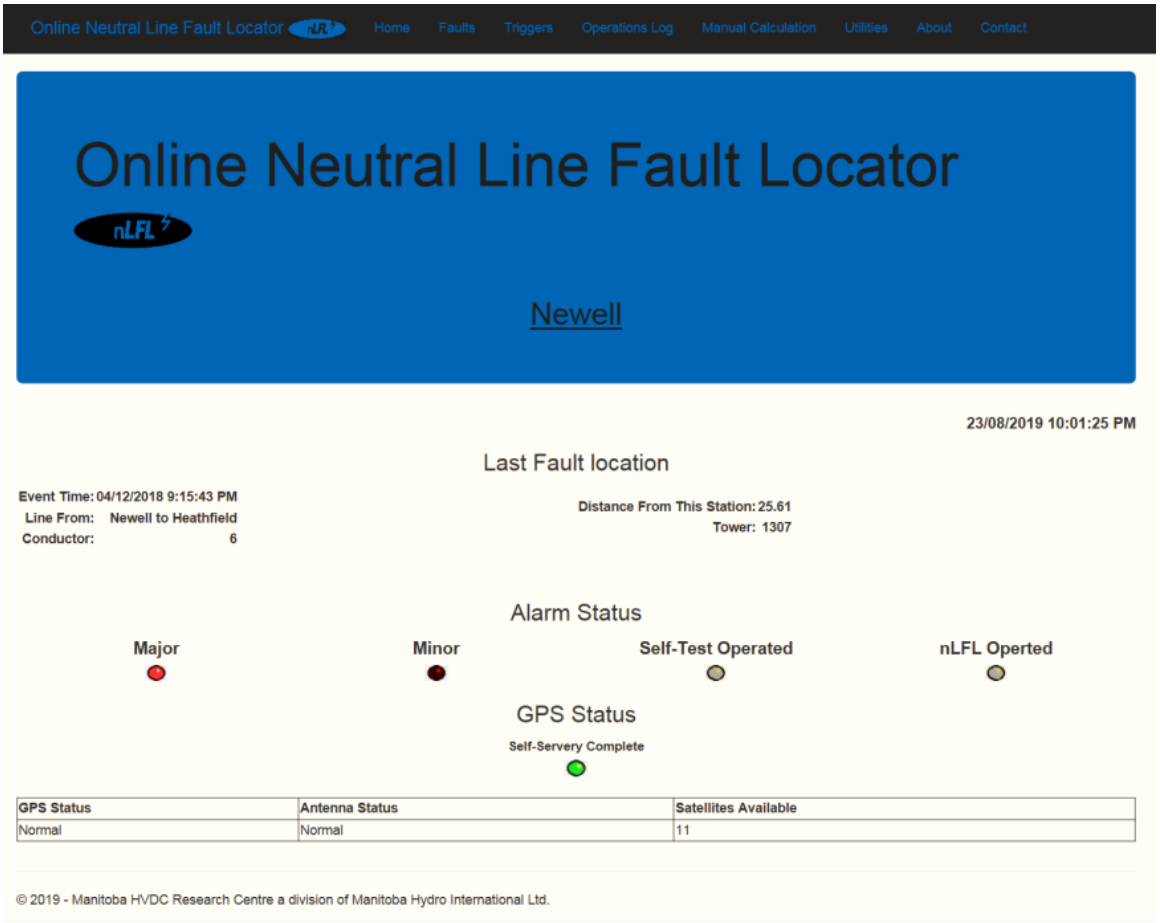

Figure B-1: Main Page.

Fault List Page (Figure B-2) – This displays a historical list of all fault events detected by the system for the selected day.

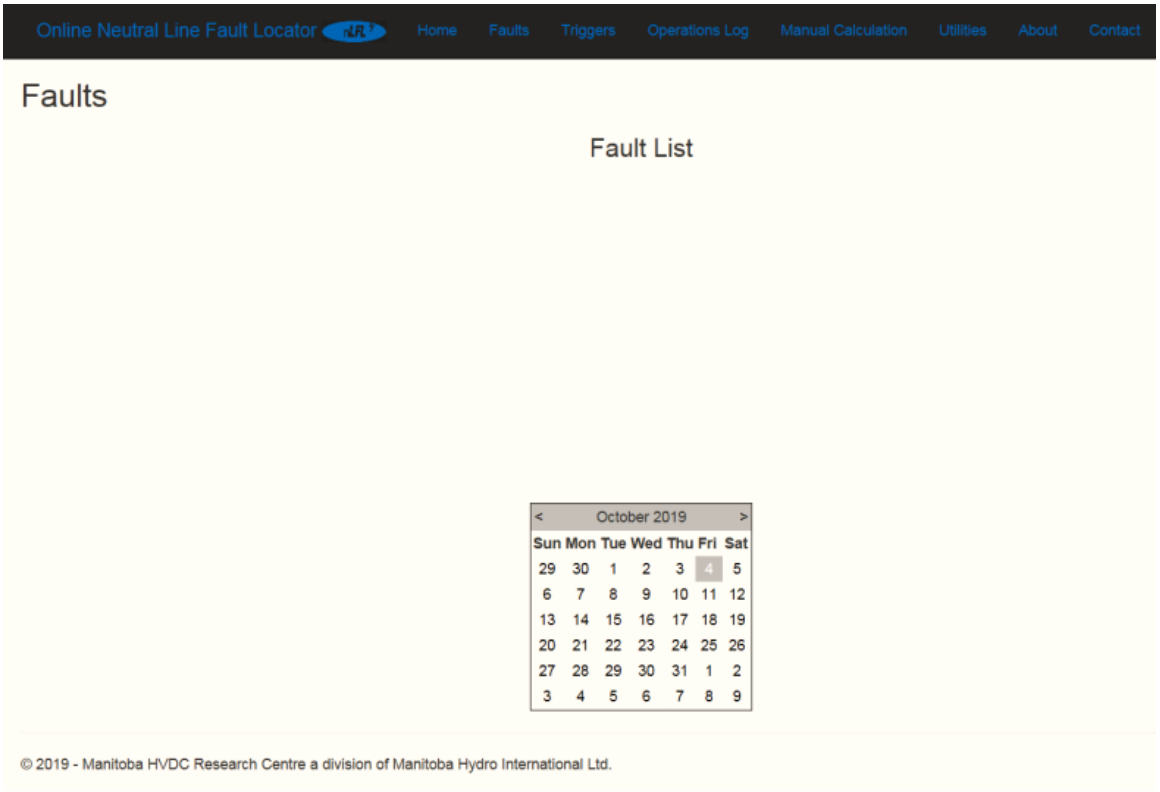

Figure B-2: Fault List Page.

Trigger List Page (Figure B-3) – This displays a historical list of all trigger events detected by the system for the selected day.

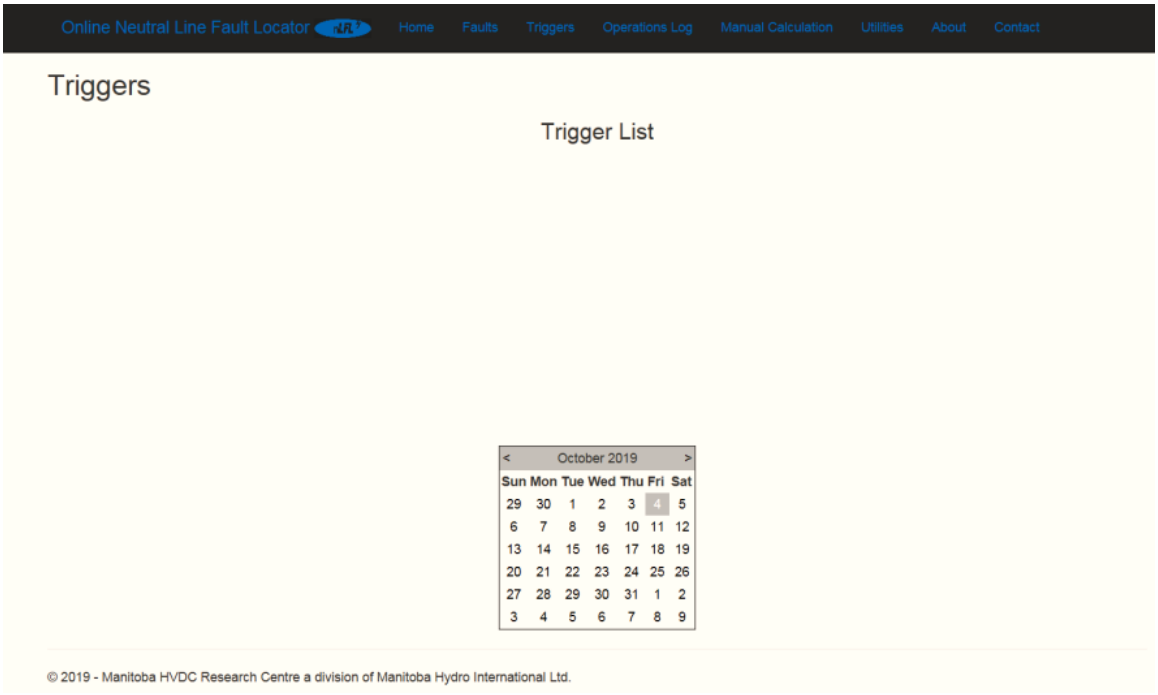

Figure B-3: Trigger List Page.

Operations Log Page (Figure B-4) – This displays a historical list of all recorded operations of the system for the selected day.

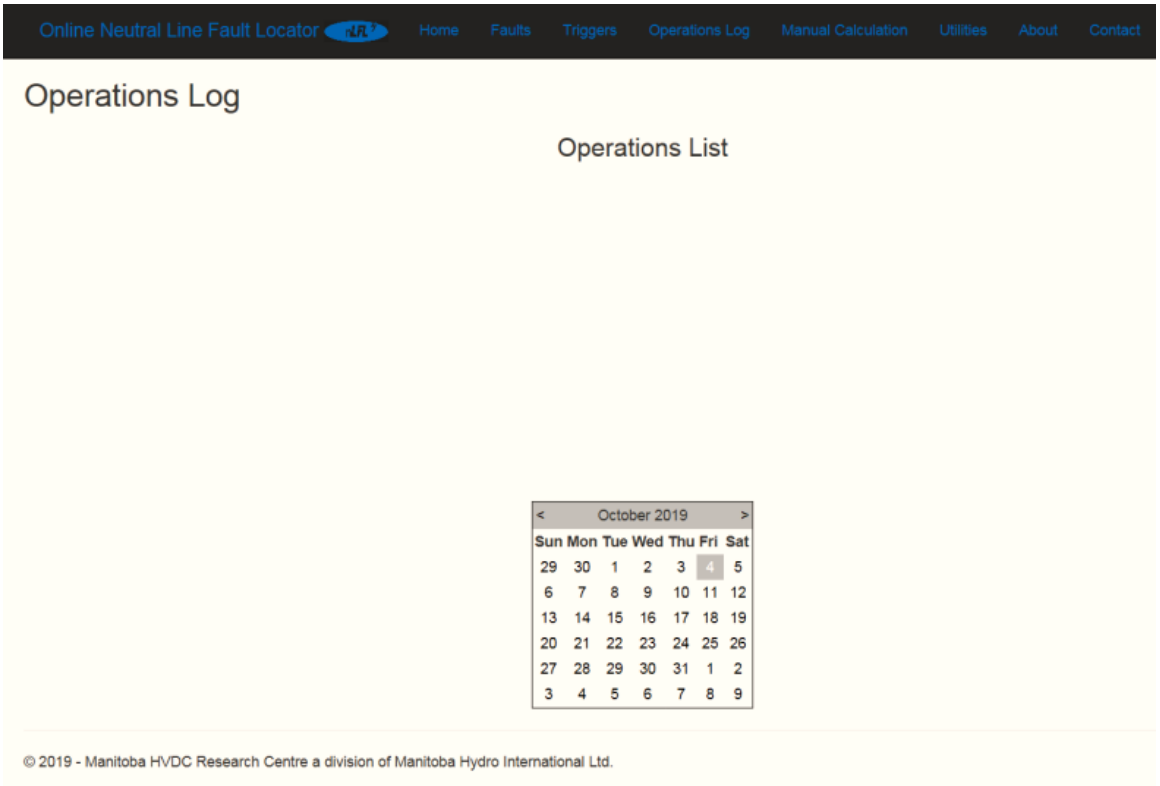

Figure B-4: Operations Log Page.

Utilities Page (Figure B-5) – This provides a control interface for diagnostic testing of the system. It includes Self-Test and Pulse Per Minute (PPM) testing. Self-test is used for instantaneous testing of the system, while PPM is used for synchronous testing of the entire system.

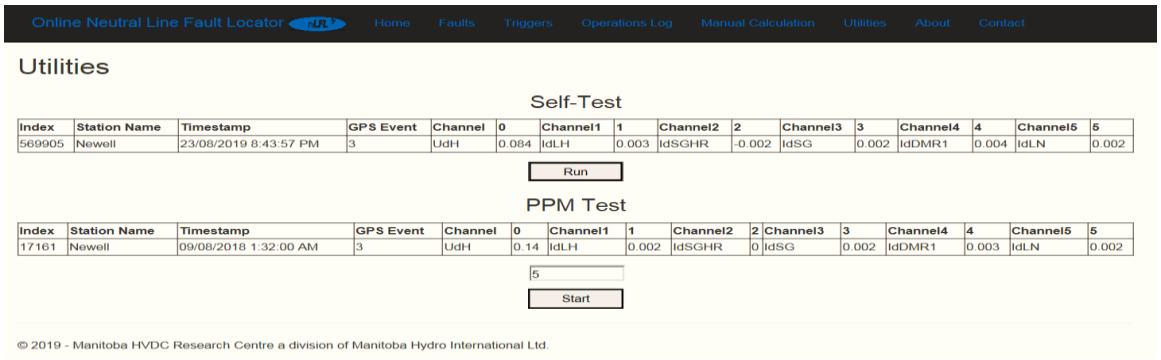

Figure B-5: Utilities Page.